University of Stavanger

FACULTY OF SCIENCE AND TECHNOLOGY

MASTER'S THESIS

Study programme: **Marine and Offshore Technology**	Spring semester, 2021 **Open**
Author: **Torstein Bakkan Vika (No.251692)**	Torstein Bakkan Vika …… (Author's signature)

Faculty supervisor:
Associate Prof. Lin Li
Co Supervisor:
Filippos Kalofotias

Thesis title:

Optimization of Spar-Buoy Foundation for Offshore Wind Turbines Using Open-Source Programs

Credits(ECTS):
30

Keywords: Open-source programs; Offshore wind turbine; Spar-buoy; Salome; Nemoh; Integrated automation	Number of pages: 74 Stavanger, July 12, 2021

Optimization of Spar-Buoy Foundation for Offshore Wind Turbines Using Open-Source Programs

Author: Torstein Bakkan Vika

Supervisor: Associate Prof. Lin Li

Co-Supervisor: Filippos Kalofotias

University of Stavanger

Faculty of Science and Technology

Department of Mechanical and Structural Engineering and Material Science

Master of Science Thesis, Spring 2021

Abstract

Low carbon and renewable energy are paramount to tackle climate change and supply the increasing energy demand in a sustainable way. In recent years, the offshore wind industry has attracted growing attention for its floating wind turbines as a competitive new renewable energy source. By utilising deep-water sites, offshore wind has the potential to become a major contributor to the global energy market.

In this thesis an optimization study on Spar-Buoy foundations is performed using the open-source software's Salome, Nemoh and Python. An automated procedure is created to simulate the hydrodynamic properties for a large number of geometries with different variables. The procedure generates the mesh models, calculates the hydrostatic properties, and uses the results as input to simulate the hydrodynamic properties. Further the geometries are subjected to four performance criteria's considering the static heeling angle, metacentric height $\overline{GM}$, 3-hour maximum pitch angle and acceleration at the nacelle. The geometries are evaluated in five different environmental conditions, considering cut-in, rated, close to cut-out and cut-out wind speeds as well as 50-year extreme wave conditions. Lastly the geometries are optimized by two objective functions, one is a cost function and the other one is a stability function considering the $\overline{GM}$. These are then evaluated by applying the weighted sum method, creating a combined objective function where weight's w_1 and w_2 is applied to the objective functions. The optimum geometry is then found by analysing the different optimums.

The results imply that a larger Spar-Buoy have larger hydrodynamic responses, whereas the static stability is improved. The combined objective function imply that a tall slender geometry would provide the best trade-off between cost and static stability. Whereas, the automated simulation procedure provides a foundation for optimisation study's using open-source software's.

Acknowledgments

I would like to thank my supervisor Associate Prof. Lin Li, for her consistent guidance and help through this thesis. She has given valuable input, guided me in the right directions and inspired me to do my best. I sincerely appreciate the quick responses and follow up's whenever I have needed it.

I would also like to express my gratitude to co-Supervisor Filippos Kalofotias for his positive attitude and motivation. He has provided valuable knowledge on the open-source programs and provided help whenever needed.

Table of Contents

List of Figures

List of Tables

1 Introduction

This chapter aims to briefly describe the background and motivation, the current status of offshore floating wind turbines as well as the aim, scope and outline of this thesis.

1.1 Background and Motivation

Wind power is a fast-growing renewable energy resource with promising potential. However, the commercial development of onshore and offshore bottom fixed wind farms has its limitations. Onshore wind is limited by wind speeds, space, noise, visual pollution, environmental interventions, and growing public dissatisfaction. Furthermore, bottom fixed offshore wind power is limited to water depths of 60 meters. This limitation causes restrictions for larger markets such as Japan and the USA to develop offshore wind farms where there are limited shallow water sites. Thus, several countries are looking towards floating offshore wind farms to be used in deeper, more remote waters. The use of floating offshore wind farms would solve many issues constraining the wind industry today, thus engaging development and markets to invest in offshore wind energy [1].

Figure 1-1 – Illustration of Hywind Scotland [2]

The offshore wind market is expected to grow significantly over the next three decades, increasing from a total installed offshore wind capacity of 23 GW in 2018 to 228 GW in 2030 to nearly 1000 GW in 2050. Offshore wind would represent between 10-15% of the expected installed global wind capacity in 2050 [3]. The cumulative installed capacity with respect to historical and predicted data is shown in figure 1-2.

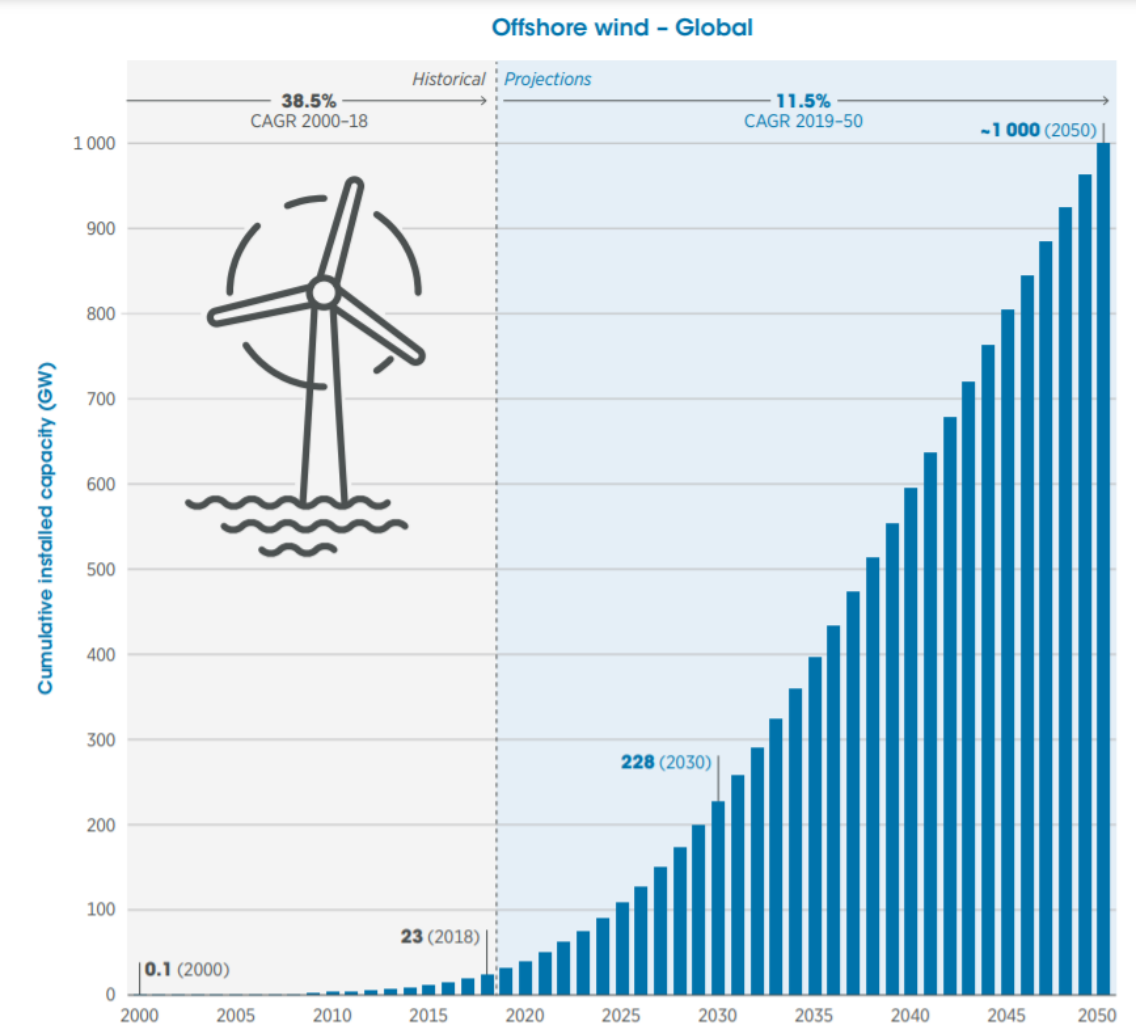

Figure 1-2 - Historical and predicted renewable capacity statistics from IRENA[3]

The development of offshore wind farms has been driven by the technological improvement of wind turbines, grid connection, installation and foundations. These advancements have caused cost reduction, a decline in project risk, and a reduction of levelized cost of electricity (LCOE). Advancement in floater technology is considered a key factor in order to develop new markets for offshore wind, in relation to the predictions shown in figure 2, it is estimated that offshore wind could cover 5-15% of the global offshore wind installed capacity by 2050 [1].

The world's first operative commercial-scale floating windfarm was Equinor's Hywind Scotland, which was successfully commissioned in 2017 with a total capacity of 30 MW, operating at only 65% of its maximum theoretical capacity. By the end of 2018, there were nine

floating wind installations, five in Europe and four in Japan with a cumulative installed capacity of 50 MW. While offshore wind is projected to grow significantly towards 2050, technological development on floating wind power is essential for the projected development. For the floating offshore wind market, it is especially the floating foundation which needs technological development and optimization [1] [4].

1.2 Floating Wind Turbine Concepts

An offshore floating wind turbine is an offshore wind turbine connected to a floating foundation which allows for offshore wind farms to be developed at water depths larger than 60 meters. Floating offshore wind was first proposed as a large scale potential energy source in 1972 by Professor William E. Heronemus at the University of Massachusetts. However, it was not until the 1990s that research on floating offshore wind was resumed after onshore wind power was well established. Furthermore, the basic mechanics of offshore floaters are well understood from the oil and gas industry. In 2015, there where over 30 floating support structure concepts for floating offshore wind turbines covering a broad range of possible prospects. However the floaters can be divided into three categories which describes the stabilizing mechanism of the structure [5].

- *Ballast Stabilized:* Large ballast at the bottom of the structure causes the centre of gravity (CoG) to be far lower than the centre of buoyancy (CoB). This leads to a large righting moment or metacentric height ($\overline{GM}$) which counteracts large rotational displacements.
- *Waterline/buoyancy Stabilized:* The waterline area is the largest contributor to the restoring moments, hence a large waterline area gives a large second moment of inertia with respect to the rotational axis of the floater. This is usually done by having smaller cross-sectional areas (columns) placed at a distance from the rotational axis.
- *Mooring stabilized:* Mooring stabilized structures are stabilized by having high tension mooring lines connected to the floater which counteracts and stabilizes the motion response.

From the three categories mentioned above, three prominent designs are under development and being tested. The three main designs are *spar-buoys, semi-submersibles and tension-leg platforms (TLP's)*, all of which utilizes one of the stabilization mechanisms mentioned above. The three main designs are described in the following section.

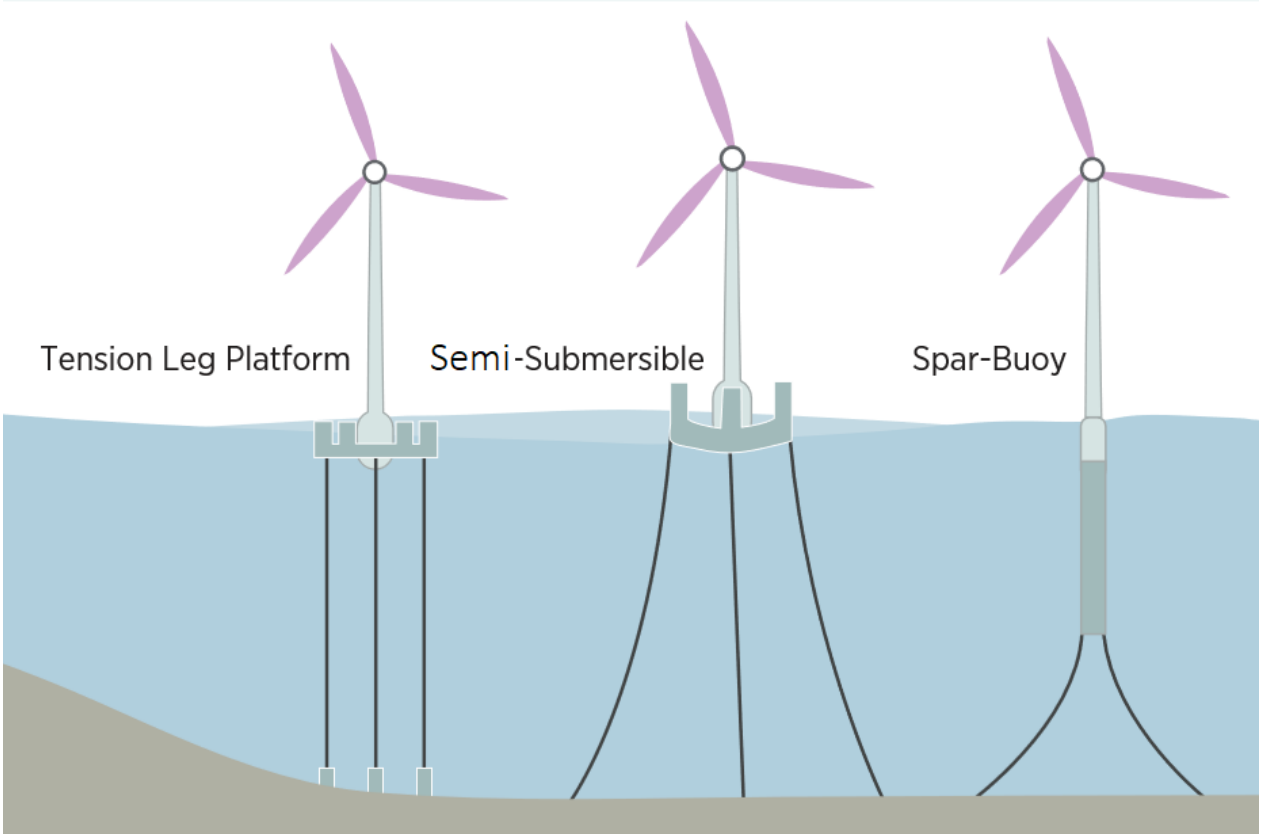

Figure 1-3 - Main floater concepts

TLP's are mooring stabilized, hence the structure is permanently moored to the seabed using tethers or tendons grouped at each corner of the floater. The structure usually consists of three legs with a central column where the wind turbine is mounted. This allows for a smaller structure of the floater, i.e. reduced cost [6]. However technological advancement is needed in order to create a successful design. The main pros and cons are listed table 1-1:

Pros:	Cons:
• Small floater structure, i.e. lower cost of the floater • Limited rotational motion • Limited vertical motion • Suitable in water depths from 50 m • Stable tow-out	• Lack of stability during installation • Total loss if one mooring line fails • Reliant on seabed condition's(advanced anchoring) • Needs development of low-cost tension mooring system • Challenging operation for onshore maintenance

Table 1-1 Pros & cons for TLP

Semi-Submersibles

Semi-Submersibles are waterline stabilized, and consists of three or four columns in a triangle or square. The wind turbine is mounted on one of the semi-sub's corners or on an additional cylinder in the middle. The main pros and cons are listed in table 1-2:

Pros:	Cons:
• Proven design • Stable without mooring lines • Suitable at water depths from 50 m • Cheap and simple mooring system • Heave plates for reduced heave motion	• Large motion response • Higher impact on turbine due to motion response • Large seabed footprint • Large and complex structure

Table 1-2 Pros & cons of Semi-Submersibles

Spar-Buoy

Spar-Buoys are ballast stabilized, consisting of a long slender structure with a high draft, this allows for large ballast fitted at the bottom of the structure causing the CoG to be well below the CoB. The wind turbine is mounted on top of the upper cylinder of the spar. The main pros and cons are listed in table 1-3:

Pros:	Cons:
• Suitable for high sea states • Simple structure • Inherently stable • Cheap and easy mooring system	• Complex and expensive tow out • Suitable only at larger water depths, over 150 m • Long and heavy structure • Only suitable assembly at deeper waters (example fjords)

Table 1-3 Pros & cons of Spar-Buoys

1.3 Aim and Scope

As mentioned, one of the problems with offshore floating wind farms is the floating foundation, this needs to be optimized in order to develop profitable commercial-scale offshore floating wind farms. Large amounts of research is done in this field to obtain projected target goals and a profitable industry. Unlike platforms used in oil and gas, wind turbines are long slender structures, hence the relative motion response for the system is different, such as the velocities and accelerations at the nacelle [5].

As stated earlier, there is a lot of optimization potential regarding floating foundations. However, one of the main hurdles for the industry, is to focus its research on the best prospects. According to a survey conducted by Leimeister et.al [5], the industry needs less diversity and more focused study's. In the survey, industry experts concluded that advanced spar-buoys are the most preferable, and classic spar-buoys are the second most preferable technology available on the market [5]. The thesis is a continuation of a project assignment written in the fall of 2020 as a preparation for this master thesis. The project assignment investigated the critical response, i.e. displacement, velocity, and acceleration at the nacelle of the NREL OC3 and OC4 floating foundations, in two separate sea states. However, the objective of this study is to perform a hydrostatic analysis, hydrodynamic analysis and design optimization of a classic floating Spar-Buoy design over a grid of different geometries using open-source programs. The study will investigate how changes in the geometry influences different performance criteria and motion responses in different sea states.

The optimization will be performed using the OC3 Spar-Buoy mounted with the NREL 5 MW Reference Offshore Wind Turbine as baseline design. The geometries vary with two variables, namely the height and radius of the lower cylinder. The properties of the baseline and modified system is explained in chapter 3. The modelling design, hydrodynamic simulation and post processing will be performed using open-source programs. The objective of this thesis is the following:

- Create an automated simulation and analysis process using open-source programs
- Analyse the hydrostatic performance of the geometries
- Analyse the hydrodynamic performance of the geometries

- Find the optimum design based on objective functions and constraints

1.4 Outline of Thesis

A shot description of the chapters in this thesis is presented below:

Chapter 1 is an introduction to the potential of offshore wind, the current status of floating offshore wind as well as it presents the aim, scope and structure of this thesis.

Chapter 2 presents the relevant theory for hydrostatics, hydrodynamics and wave statistics used to calculate the results in this thesis.

Chapter 3 presents the baseline design and methods used to perform the analysis. It also presents which open-source programs that are used and how they are applied in order to create an automated optimization procedure.

Chapter 4 presents the results which are obtained from the analyses and optimization.

Chapter 5 provides a conclusion of the work as well as a recommendation for future work on the subject.

2 Theory

This chapter explains in simple terms, the theory used on linear wave theory, sea environment, hydrostatic stability, hydrodynamic loads, and the motion response of floating structures in waves.

2.1 Hydrostatic Stability

This subchapter aims to describe the theory for the stability calculations which are required for hydrostatic stability. A floating structure is in the state of vertical equilibrium when the resultant forces and relative moments are zero, then Archimedes law states that:

$$F_{\nabla} = pg\nabla \tag{2.1}$$

Where:

$$F_{\nabla} = buoyancy\ force \tag{2.2}$$

$$pg\nabla = Waterdensity \cdot Gravity \cdot Submerged\ volume\ of\ the\ body \tag{2.3}$$

Hence the buoyancy force F_{∇} is equivalent to the gravitational force of the body $pg\nabla$, thus to achieve vertical static equilibrium, Archimedes principle holds that the gravitational force, mass m multiplied by gravity g can be denoted as:

$$mg = pg\nabla \tag{2.4}$$

The hydrostatic stability of a floating structure is calculated by the hypothetical points the centre of gravity (CoG), the centre of buoyancy (CoB) and the metacentric radius $\overline{BM}$. The CoG is defined as the point where the gravitational force g acts around. Hence it can be described as the point where the combined mass of the body is concentrated. The CoB is defined as the centre of volume of the submerged part of the floating structure. Moreover, the metacentric radius $\overline{BM}$ is expressed as the relation between second moment of the waterline area I_w and the buoyancy force F_{∇}. These properties are used to calculate the metacentric height $\overline{GM}$ between the metacentre *M* and the CoG of the structure. The metacentre is defined as the point where a vertical line drawn from the original CoB would intersect a vertical line drawn from a heeled CoB, see figure 2-1 [7]. The metacentric height $\overline{GM}$, CoG, CoB and $\overline{BM}$ and the length between the keel and the CoG, the $\overline{KG}$, can be expressed as:

$$\overline{GM} = \overline{KB} + \overline{BM} - \overline{KG} \tag{2.5}$$

$$CoG = \frac{\sum m_n z_n}{\sum m_n} \tag{2.6}$$

$$CoB = \frac{\sum \rho g \nabla_n z_n}{\sum \rho g \nabla_n} \tag{2.7}$$

$$\overline{BM} = \frac{I_w}{\nabla} \tag{2.8}$$

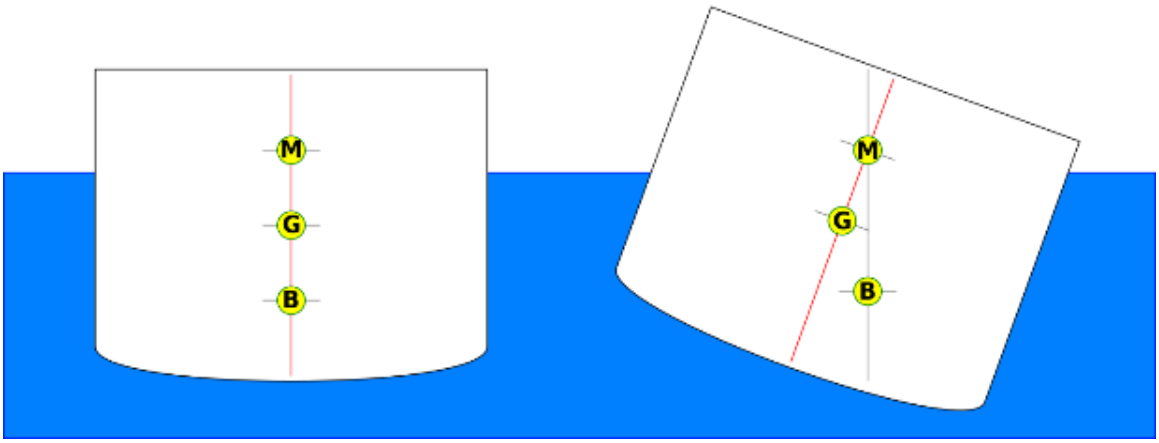

Figure 2-1 Metacentric Height of a Floating Structure

2.2 Linear Wave Theory

This subchapter aims to give a brief introduction to Linear Wave Theory (LWT). LWT is a simplification of the Navier-Stokes equation's, which describes the dynamics of fluid flow. In LWT, it is assumed that the flow is *irrotational*, *inviscid* and that the fluid is *incompressible*, hence solutions obtained for this class of flow are thus an approximation of the full Navier-Stokes solutions, this simplification is called potential flow theory.

Irrotational and inviscid flow

Water particles have a kinematic viscosity of $\mu = 10^{-6}$, small enough to assume zero rotation thus allowing for potential flow theory to be used. Hence, the assumption of *irrotational* flow allows a vector identity to be introduced, concerning the curl of the gradient of any scalar function φ and hence the curl of any vector $\vec{V}$ is always zero from vector calculus. The vector identity can be written:

$$\vec{\nabla} x \vec{\nabla} \varphi = 0, thus\ if\ \vec{\nabla} x \vec{V} = 0, then\ \vec{V} = \vec{\nabla} \varphi \tag{2.9}$$

Thus, if the curl of a vector is zero, the vector can be defined as the gradient of the scalar function φ, called the velocity potential function. Where $\vec{V}$ is the velocity vector field, the velocities for each direction is simply the derivative of the potential function in each direction, and can be written in Cartesian coordinates as:

$$u = \frac{\partial \varphi}{\partial x}, \qquad v = \frac{\partial \varphi}{\partial y}, \qquad w = \frac{\partial \varphi}{\partial z} \tag{2.10}$$

Incompressible flow

In LWT it is also assumed that the flow is incompressible $\left(\frac{dp}{dt} = 0\right)$ this way the continuity equation can be written as:

$$\frac{\partial u}{\partial x} + \frac{\partial v}{\partial y} + \frac{\partial w}{\partial z} = 0 \tag{2.11}$$

Substituting equation (2.8) into equation (2.9) gives the linear Laplace equation:

$$\frac{\partial^2 \varphi}{\partial x^2} + \frac{\partial^2 \varphi}{\partial y^2} + \frac{\partial^2 \varphi}{\partial z^2} = \Delta\varphi = \nabla^2 = 0 \tag{2.12}$$

The velocity potential function exists for irrotational, inviscid and incompressible flow, this type of flow is what's called potential flow [8]. Furthermore, ocean surface waves with small amplitude in relation to its wavelength H/$\lambda \leq 0.03$, can be approximated as potential flow. The solutions of the Laplace equations are harmonic functions, which introduces the superposition principle, the principle state that solutions of linear systems can be added together and being a possible solution of the system [9]. Hence if $\phi_1$and ϕ_2 are solutions to the Laplace equation then $\phi_1 + \phi_2$ is also a solution, thus simple flows can be added together. Furthermore, ocean surface waves can be described as sinusoidal functions, in LWT a harmonic regular wave progressing in x-direction is defined by a sinusoidal function:

$$\zeta = \zeta_a \cdot \cos(kx - \omega t) \tag{2.13}$$

Where:

$\zeta_a = Wave\ amplitude\ (m)$

$\omega = Circular\ wave\ frequency\ \left(\frac{rad}{s}\right)$

$t = time\ (s)$

$k = \frac{2\pi}{\lambda} Wave\ Number\ \left(\frac{rad}{s}\right)$

$\lambda = Wave\ length\ (m)$

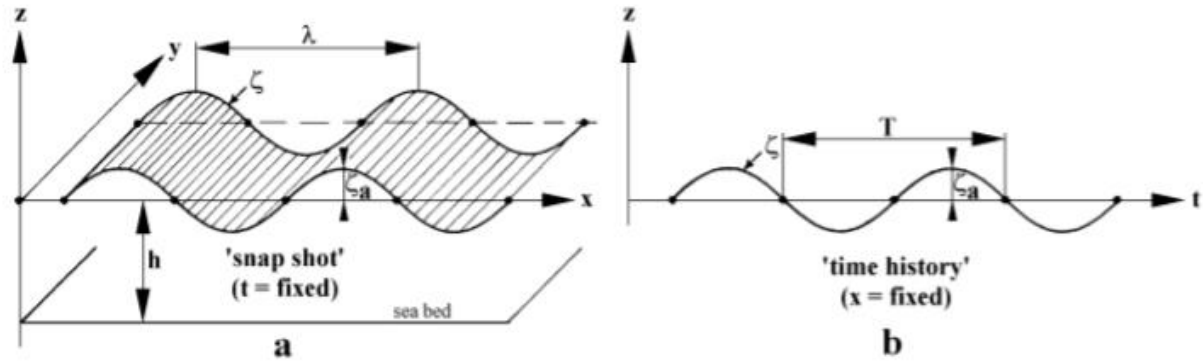

Figure 2-2 Harmonic Wave

Boundary conditions

The first boundary condition states that the velocity perpendicular to the bottom is zero. Hence the Bottom boundary condition is:

$$\frac{\partial \varphi}{\partial z} = w_{z=-h} = 0 \tag{2.14}$$

The second boundary condition states that a particle on the surface will stay on the surface, I.e. the Free Surface Kinematic boundary condition is:

$$\frac{\partial \zeta}{\partial t} + u\frac{\partial \zeta}{\partial x} - w = \frac{\partial \zeta}{\partial t} + \frac{\partial \varphi}{\partial x}\frac{\partial \zeta}{\partial x} - \frac{\partial \zeta}{\partial z} = 0 \tag{2.15}$$

The Free Surface Kinematic boundary condition can be further simplified due to the assumption that the wave amplitude is much smaller than the wavelength $u\frac{\partial \zeta}{\partial x} = 0$, thus the simplified Free Surface Kinematic boundary condition can be written:

$$\frac{\partial z}{\partial t} = \frac{\partial \zeta}{\partial t} = 0, for\ z = \zeta \tag{2.16}$$

The third boundary condition, the Free Surface Dynamic Boundary Condition states that the pressure on the free surface is constant and equal to atmospheric pressure.

$$\frac{\partial \varphi}{\partial t} + g\zeta = 0 \tag{2.17}$$

The velocity potential φ must satisfy the Laplace equation as well as the boundary conditions, furthermore the wave amplitude needs to be small relative to the wavelength in order to apply LWT. By applying these boundary conditions, analytical solutions for the velocity components, pressure and the dispersion relationship is derived [7].

The dispersion relationship states:

$$\omega^2 = gk \tanh kh,\ \omega^2 = gk\ (deep\ water)\ h = water\ depth \tag{2.18}$$

For velocities in the x-z plane the velocities are obtained by the velocity potentials:

$$\begin{aligned} u(x,z,t) &= \frac{\partial \varphi}{\partial x} = \zeta_a \frac{kg}{\omega} \frac{\cosh k(h+z)}{\cosh kh} \cos(kx - \omega t) \\ w(x,z,t) &= \frac{\partial \varphi}{\partial z} = \zeta_a \frac{kg}{\omega} \frac{\sinh k(h+z)}{\cosh kh} \sin(kx - \omega t) \end{aligned} \tag{2.19}$$

2.3 Wave Spectrum

This subchapter introduces the statistics and theory used to calculate the sea environment in this report. Real surface ocean waves can be analysed using the superposition principle, adding a number of regular waves with different frequencies, phase angles and amplitudes into statistical models. It is assumed an instantaneous wave elevation follows a Gaussian/normal distribution with zero mean. Where the wave amplitudes ζ_{a_n} can be found using Fourier analysis, thus the mean square value of the amplitude can be found. The sea state can be described by a wave spectrum $S_\zeta(\omega_n)$, defining the distribution of wave energy for different frequencies and properties. A wave spectrum's properties are defined by the spectral moments, the spectral moments give definitions to significant wave height, significant wave amplitude, water surface elevation and spectral crossing period. Hence a wave spectrum defines the energy of a sea state at a certain frequency. The wave surface elevation $\zeta(t)$ of a number of waves *N* moving in x-direction is described as:

$$\zeta(t) = \sum_{n=1}^{N} \zeta_{amp} cos\ (k_n x - \omega_n t + \epsilon_t) \tag{2.20}$$

Where:

$\zeta_{amp} = wave\ amplitude\ component\ (m)$

$\omega_n = circular\ frequency\ component\ (rad/s)$

$k_n = wave\ number\ component\ (rad/m)$

$\varepsilon_n = random\ phase\ angle\ component\ (rad)$

2.3.1 JONSWAP Spectrum

In 1968 to 1969 the Joint North Sea Wave Observation Project (JONSWAP) was an extensive wave measurement program which was carried out in the North Sea. Analysis of the data yielded in the generation of the JONSWAP spectrum, a wave spectrum suitable for the North Sea [7]. The JONSWAP spectrum is used to calculate the response spectrum in this report.

The JONSWAP spectra is expressed as:

$$S_\zeta(\omega) = \frac{320 \cdot {H^2}_{1/3}}{T_p^4} \cdot \omega^{-5} \cdot exp\left\{\frac{-1950}{T_p^4} \cdot \omega^{-4}\right\} \cdot \gamma^A \tag{2.21}$$

Where:

$H_{1/3} = \ Significant\ Wave\ height$

$T_p = \ Peak\ Period$

$\gamma = \ 3.3\ Preakness\ Factor$

$$A = exp\left\{-\left(\frac{\frac{\omega}{\omega_p} - 1}{\sigma\sqrt{2}}\right)^2\right\}$$

$\omega_p = \frac{2\pi}{T_p} = \ (Circular\ Frequency\ at\ Spectral\ Peak)$

$$\sigma = \begin{cases} 0.07, for\ \ \omega < \omega_p \\ 0.09, for\ \ \omega > \omega_p \end{cases}$$

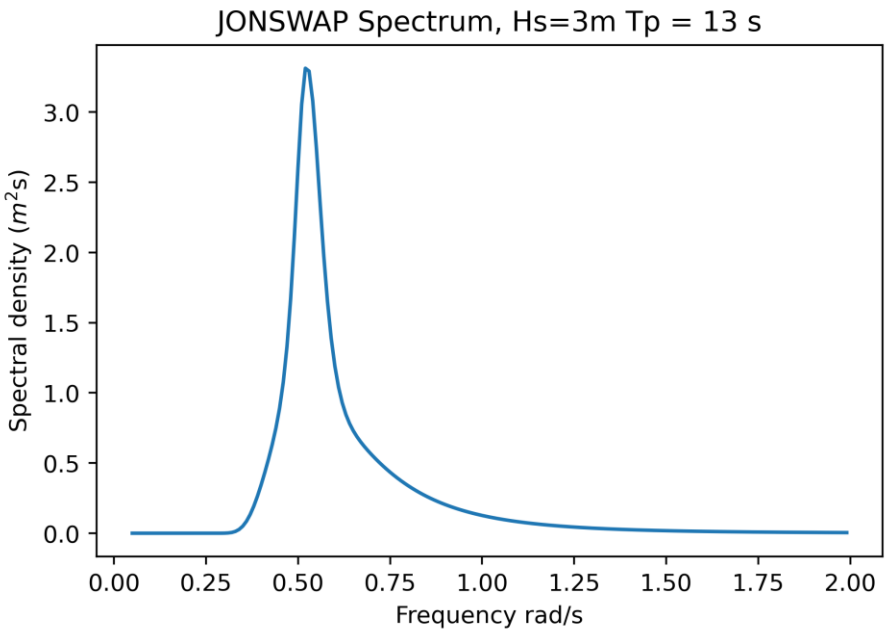

Figure 2-3 Example of a JONSWAP Spectrum

2.3.2 Short Term Wave Statistics

A stationary process for linear waves follows a Gaussian distribution which has the probability density function:

$$f_{\Xi}(\xi) = \frac{1}{\sigma_{\Xi}\sqrt{2\pi}} exp^{\left\{\frac{1}{2}*\left(\frac{\xi}{\sigma_{\Xi}}\right)^2\right\}} \tag{2.22}$$

With mean $E[\Xi(t)] = 0$, variance $Var[\Xi(t)] = \sigma_{\Xi}^2 = \int_0^{\infty} s_{\Xi\Xi}(\omega)d\omega = m_{\Xi,0}$ (area under the wave spectrum). The distribution of global maxima C_G follow a Rayleigh distribution with cumulative density function where the standard deviation is σ_{Ξ} which equals to the square root of the variance σ_{Ξ}^2 [10]:

$$F_{C_G}(c) = 1 - exp^{\left\{-\frac{1}{2}\left(\frac{c}{\sigma_{\Xi}}\right)^2\right\}} \tag{2.23}$$

And probability density function:

$$f(x) = \frac{c}{\sigma_{\Xi}^2} \cdot e^{\frac{-c^2}{2\sigma_{\Xi}^2}} \tag{2.24}$$

From this the second order moment m_2 can be calculated:

$$m_{\Xi,2} = \int_0^{\infty} s_{\Xi\Xi}(\omega)d\omega \tag{2.25}$$

Further the zero-up crossing period can be calculated by:

$$T_{2z} = 2\pi \cdot \sqrt{\frac{m_{\Xi,0}}{m_{\Xi,2}}} \tag{2.26}$$

The distribution function of the 3-hour maximum response amplitude is expressed as:

$$F_{X_{3h}} = \left[1 - exp\left\{\frac{1}{2}\left(\frac{x}{\sigma_x}\right)^2\right\}\right]^{n_{3h}} \tag{2.27}$$

The expected number of occurrences in a 3-hour sea state can then be calculated from the zero-up crossing period T_{2z} as:

$$\bar{n}_{3h} = \frac{3 \cdot 3600s}{T_{2z}} \tag{2.28}$$

By assuming a Rayleigh distribution, the largest global maximum crest height in a 3-hour period can be expressed as:

$$\bar{c}_{3h} = \sigma_{\Xi}\sqrt{2l\,n(\bar{n}_{3h})} \tag{2.29}$$

2.4 Motion Response in Waves

This subchapter introduces, in simple terms the motion response, wave loads and hydrodynamic properties of a floating structure.

2.4.1 Vessel Motion

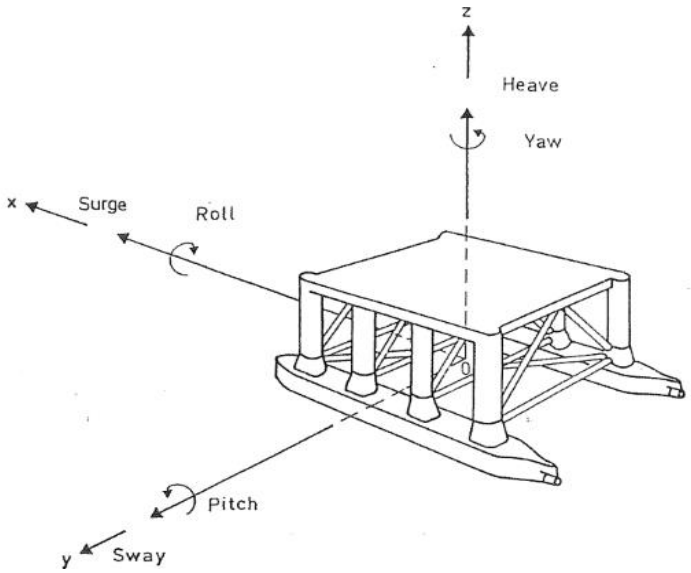

Figure 2-4 System with Six Degrees of Freedom

A vessel, ship or offshore structure in the ocean have six motional degrees of freedom. These are usually given in a right handed coordinates system with the origin O(x, y, z) at the centre of gravity (CoG), as shown in the figure 2-3. The vessel is experiencing three translational motions and three rotational motions denotes as in table 2-1:

Notation	Vessel motion
η_1	Surge
η_2	Sway
η_3	Heave
η_4	Roll
η_5	Pitch
η_6	Yaw

Table 2-1 A floating system's Six Degrees of Freedom

Where η_1, η_2, η_3 represents the translational motion's for the structure and η_4, η_5, η_6 represents the rotational motions.

The loads on a floating object can be constant in time, transient or harmonic, the motion response for these loads are fundamentally different. In early design phases, the use of linear approximation allows random or irregular loads to be treated as a superposition of harmonic loads. Commonly the linear mass spring system (LMSS) is used to calculate the motion responses of a floating structure with six degrees of freedom for LWT. For simplicity, this approach is illustrated using a system with a single degree of freedom. The forces can be derived using newton's second law of motion:

$$F = ma \tag{2.30}$$

The components of the equation and its derivation for one degree of freedom is the Linear Wave-Body Interaction problem and is derived in the following paragraph. The forces acting on a floating body is divided in to two separate problems, the Excitation problem and Radiation problem [11].

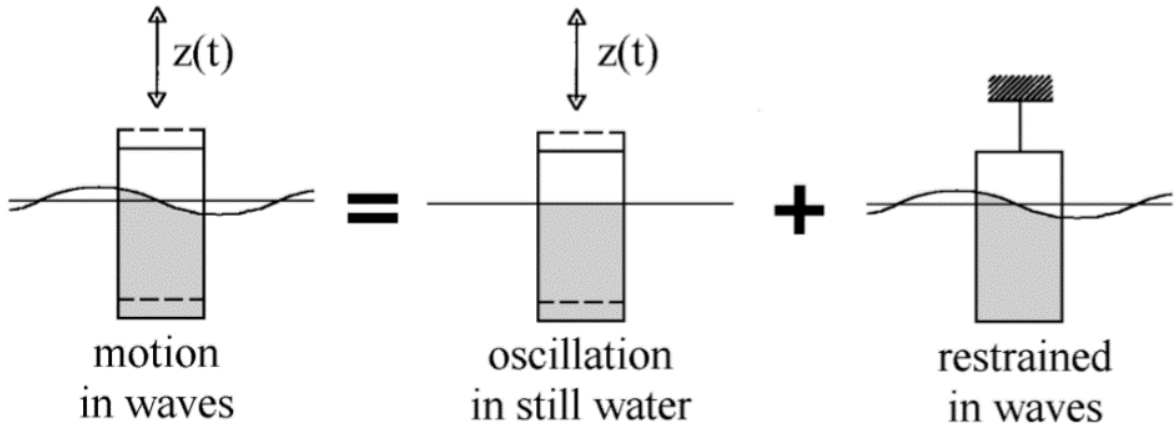

Figure 2-5 Excitation Problem and Radiation Problem [7]

Excitation problem

The excitation problem describes the excitation forces acting on the body in a fixed position, denoted as F_{exc}. As waves hit the body, the pressure field surrounding the body is disrupted causing a disturbance from the hydrostatic state, this is the *Diffraction force*. Furthermore, the integration of the pressure on the body in undisturbed waves are the *Froude-Krylov force*.

Together these make up the total non-viscous forces acting on the body in regular waves. These Forces are the excitation forces which are derived from the open-source program Nemoh.

Radiation problem

The radiation problem describes the hydrodynamic forces acting on the body induced by vertical oscillations. The hydromechanical loads and solid mass of the cylinder determine the vertical motions. The loads can be divided into: F_{rad}, F_{add} and F_{res}.

Added Mass Coefficient

When a body is accelerated in water, the water particles surrounding the body is accelerated as well. The increase in mass inertia is called "added mass" or hydrodynamic mass, the force caused by this acceleration is proportional to the acceleration of the body in a linear system. Where a is the added mass coefficient with the dimension of kg for heave. The added mass force is:

$$F_{add} = -a \cdot \ddot{x} \tag{2.31}$$

Radiation Coefficient

When a floating body experiences oscillation, the movement of the body creates waves to radiate away along the water surface. This results in an energy loss of the body equal to the energy in the waves it radiates. This introduces hydrodynamic or radiation damping, which is proportional to the vertical velocity $\dot{x}$ of the body in a linear system. Where b is the damping coefficient with the dimension of mass per unit of time (for heave). The radiation force is:

$$F_{rad} = -b \cdot \dot{x} \tag{2.32}$$

Restoring Spring Coefficient

When a body in water is oscillating, it displaces water equal to the amount of the submerged volume of the body, this is proportionate to the magnitude of the buoyancy force $F_{boyancy} = pg\nabla$ in terms of Archimedes law. Hence as the body is oscillating the restoring spring force is an oscillating force as well. The restoring spring force is experienced on the object until it reaches equilibrium. The restoring spring force is denoted as:

$$F_{res} = -c \cdot x \tag{2.33}$$

Rewriting equation (2.30) we get:

$$F_{add} + F_{rad} + F_{res} + F_{exc} = ma \tag{2.34}$$

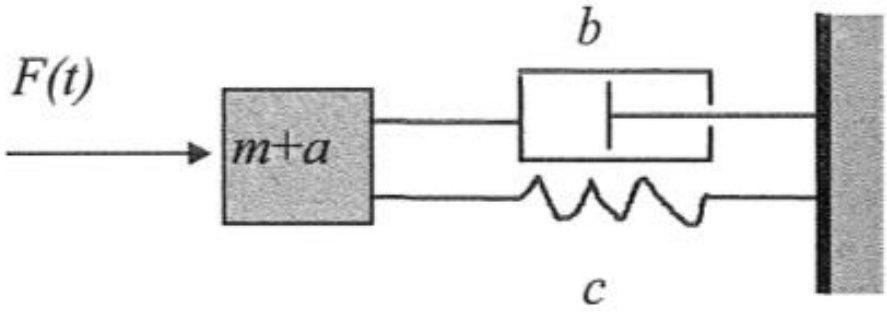

Figure 2-6 One Degree of Freedom Linear Mass Spring System [7]

Figure 2-5 shows a system with one degree of freedom, where:

$m = mass$

$a = added\ mass$

$b = damping\ coefficient$

$c = spring\ stiffness$

$x = displacement$

$\dot{x} = velocity$

$\ddot{x} = acceleration$

The harmonic motion response for displacement x, velocity $\dot{x}$ and acceleration $\ddot{x}$ in heave can be written as:

$$x = \hat{x}\cos(\omega t - \varepsilon) \tag{2.35}$$

$$\dot{x} = -\omega\hat{x}\sin(\omega t - \varepsilon) \tag{2.36}$$

$$\ddot{x} = -\omega^2\hat{x}\cos(\omega t - \varepsilon) \tag{2.37}$$

The equation of motion for the system can be written as:

$$(m + a)\ddot{x} + b\dot{x} + cx = F(t) \tag{2.38}$$

Equation (2.38) is then used to find the response amplitude operator (RAO), a transfer function expressing the amplitude of the harmonic response and the amplitude of disturbance. The RAO is commonly derived in complex notation to shorten the length of the equation, hence the harmonic functions can be rewritten using Euler's formula:

$$e^{i\theta} = \cos\theta + i\sin\theta \tag{2.39}$$

The RAO can then be derived in complex notation as in equation (2.40), this also allows the motion response to be calculated in the frequency domain instead of the time domain, for more detailed explanations see [11].

$$\frac{\eta_i}{\zeta_{amp}}(\omega) = \frac{F_{exc}}{(-(m+a)\omega^2 + ib\omega + c)} \tag{2.40}$$

For a six DOF system the six by six matrixes for added mass, radiation coefficient, spring coefficient and mass is denoted as in the following:

The added mass matrix *A* for 6 DOF can be written as:

$$A = \begin{bmatrix} A_{11} & 0 & 0 & 0 & A_{15} & 0 \\ 0 & A_{22} & 0 & A_{24} & 0 & 0 \\ 0 & 0 & A_{33} & 0 & 0 & 0 \\ 0 & A_{42} & 0 & A_{44} & 0 & 0 \\ A_{51} & 0 & 0 & 0 & A_{55} & 0 \\ 0 & 0 & 0 & 0 & 0 & A_{66} \end{bmatrix} \tag{2.41}$$

The radiation damping coefficient matrix *B* for 6 DOF is written as:

$$B = \begin{bmatrix} B_{11} & 0 & 0 & 0 & B_{15} & 0 \\ 0 & B_{22} & 0 & B_{24} & 0 & 0 \\ 0 & 0 & B_{33} & 0 & 0 & 0 \\ 0 & B_{42} & 0 & B_{44} & 0 & 0 \\ B_{51} & 0 & 0 & 0 & B_{55} & 0 \\ 0 & 0 & 0 & 0 & 0 & B_{66} \end{bmatrix} \tag{2.42}$$

For 6 DOF the restoring spring coefficient *C* can be written as:

$$C = \begin{bmatrix} 0 & 0 & 0 & 0 & 0 & 0 \\ 0 & 0 & 0 & 0 & 0 & 0 \\ 0 & 0 & C_{33} & 0 & C_{35} & 0 \\ 0 & 0 & 0 & C_{44} & 0 & 0 \\ 0 & 0 & C_{53} & 0 & C_{55} & 0 \\ 0 & 0 & 0 & 0 & 0 & 0 \end{bmatrix} \tag{2.43}$$

Where C_{33}, C_{44} and C_{55} are the spring coefficient for heave, pitch and roll. The spring coefficient for heave C_{33} is expressed as the sea water density p multiplited by gravity g and the waterline area A_w. Due to the symmetry of a Spar-Buoy $C_{44} = C_{55}$, and is expressed as the buoyancy force multiplied by the metacentric height:

$$A_w = \pi r^2 \tag{2.44}$$

$$C_{33} = pgA_w \tag{2.45}$$

$$C_{44} = C_{55} = pg\nabla \cdot \overline{GM} \tag{2.46}$$

Where the mass matrix *M* for a 6 DOF system can be written as:

$$M = \begin{bmatrix} m & 0 & 0 & 0 & 0 & 0 \\ 0 & m & 0 & 0 & 0 & 0 \\ 0 & 0 & m & 0 & 0 & 0 \\ 0 & 0 & 0 & I_{44} & 0 & -I_{46} \\ 0 & 0 & 0 & 0 & I_{55} & 0 \\ 0 & 0 & 0 & -I_{64} & 0 & I_{66} \end{bmatrix} \tag{2.47}$$

2.4.2 Natural Frequency and Viscous Damping

This subchapter gives a short introduction of the phenomenon of natural frequency and viscous damping.

Natural Frequency

The natural frequency, also called the eigenfrequency, is the specific frequency of the system where the system tends to oscillate in the absence of any distributing forces. Hence if a free decay test in undisturbed water would be performed, the system would oscillate with its natural frequency. This is important for motion behaviour, as the natural frequency of a floating structure is determined by the frequency dependant wave loads and added mass. The resonance is usually defined in the response amplitude operator (RAO) diagram as the local maximum. The natural frequency for a floating vessel is calculated by:

$$\omega_0 = \sqrt{\frac{c_{ij}}{m_{ij} + a_{ij}}} \tag{2.48}$$

Where *c* equals to the spring term, *m* equals to the mass term and *a* equal to the added mass term. For slender structures like the spar-buoy, pitch and heave natural frequencies are the important, and is calculated as, since this thesis does not take mooring lines into consideration, the natural frequency of pitch and heave are calculated as [7]:

$$\omega_{0,33} = \sqrt{\frac{c_{33}}{m_{33} + a_{33}}} \tag{2.49}$$

$$\omega_{0,55} = \sqrt{\frac{c_{55}}{m_{55} + a_{55}}} \tag{2.50}$$

Viscous Damping

In LWT, viscous forces are not considered, hence the hydrodynamic results based on computer programs using only LWT are not sufficient to calculate the proper vessel response. The viscous effects are especially important when working on slender structures such as semi-submersibles and spars. In hydrodynamic analysis several approaches can be applied to account for viscous effects. A common approach is to use an iterative process to linearize the non-linear damping. Another approach is to use a small percentage of the critical damping which is expressed as [12]:

$$b_{cr} = 2\sqrt{(m_{ij} + a_{ij}) \cdot c_{ij}} \tag{2.51}$$

Where m_{ij} is the mass term, a_{ij} is the added mass term and c_{ij} is the restoring spring term. Thus, due to the workload in the report, this simplified approach is applied. The non-hydrodynamic damping is calculated as a fraction of the critical damping b_{cr}. Using b_{cr} for the viscous damping terms, the RAO can be rewritten from equation (2.40) into:

$$\frac{\eta_i}{\zeta_{amp}}(\omega) = \frac{F_{exc}}{(-(m+a)\omega^2 + (ib + b_{cr})\omega + c)} \tag{2.52}$$

2.4.3 Response Spectrum

For harmonic motions, the superposition principle can be used to calculate the displacement, velocity and acceleration at a point P (x_p, y_p, z_p). The calculations are simple after the RAO is found, likewise when the equations are written in complex notations it is easy to apply for different sea states. In the equations below η_i is the complex motion response in i direction.

The displacement of a point (x_p, y_p, z_p) can be written as:

$$x = \eta_1 + z_p\eta_5 - y_0\eta_6 \tag{2.53}$$

$$y = \eta_2 - z_p\eta_4 + x_0\eta_6 \tag{2.54}$$

$$z = \eta_3 + y_p\eta_4 - x_0\eta_5 \tag{2.55}$$

Whereas the response spectrum can be written as:

$$S_r(\omega) = \left|RAO_\zeta(\omega)\right|^2 S_\zeta(\omega)d\omega \tag{2.56}$$

Once the response spectrum is known, the acceleration spectrum can be calculated by multiplying the response spectrum with frequency squared with the power of 4:

$$S_r(\omega) = \omega^4 \left|RAO_\zeta(\omega)\right|^2 S_\zeta(\omega) d\omega \tag{2.57}$$

The moments of the response spectrums are given by:

$$m_{n,m} = \int_0^\infty \left|RAO_\zeta(\omega)\right|^2 S_\zeta(\omega) d\omega \quad with: n = 0,1,2 \; and \; m = 0,1,2,3,4,5 \tag{2.58}$$

The root mean squared (RMS) value for displacement and acceleration is then found by taking the square root of the moment $m_{n,m}$ [7]:

$$\sigma_{0,m}^2 = m_{0,m} = \int_0^\infty \left|RAO_\zeta(\omega)\right|^2 S_\zeta(\omega) d\omega \tag{2.59}$$

$$\sigma_{2,m}^2 = m_{2,m} = \int_0^\infty \omega^4 \left|RAO_\zeta(\omega)\right|^2 S_\zeta(\omega) d\omega \tag{2.60}$$

$$RMS = \sigma_{n,m} = \sqrt{\sigma_{n,m}^2} \tag{2.61}$$

The most probable maximum response value is found by using the standard deviation of the response spectrum $\sigma_{n,m}$ in equation instead of the standard deviation of the wave spectrum σ_Ξ in equation (2.29). Hence the most probable maximum response value can be written as [10]:

$$\bar{c}_{3h\ Response} = \sigma_{n,m} \sqrt{2\ ln(\bar{n}_{3h})} \tag{2.62}$$

3 Numerical Method and Methodology

This chapter aims to describe the properties of the baseline design, how the design is modified and the environmental conditions. Moreover, the variables, constraints and objective functions are explained in detail. Also, the simplifications and assumptions used for the system design are described in detail. Lastly the numerical method, methodology and automated optimization procedure using open-source programs is described.

3.1 NREL 5 MW Reference Wind Turbine

In this thesis a scaled three bladed 5 MW reference offshore wind turbine, developed by the National Renewable Energy Laboratory (NREL) for the OC3-Spar-buoy study, is used. The model is used as a reference turbine for research in the offshore wind field in order to standardize offshore wind specifications [13].

Tower properties

The turbine tower has a height of 77.6 m, with the base of the tower is connected to the top of the floater at 10 m above SWL, hence the top of the tower is located at 87.6 m above SWL. The tower has a steel density of 8500kg/m^3. The wall thickness at the tower base (0.027 m) and radius (3.25 m) is assumed to be linearly tapered off to the top thickness (0.019 m) and top radius (1.935 m). In the OC3 study, the lower diameter (6.5 m) of the wind turbine tower matches the top diameter of the OC3 spar-buoy. However, in this study the structural parameters are fixed to simplify the calculations. The overall tower mass is 249 718 kg with the centre of mass of the tower (CM_{Tower}) located at 43.4 m above SWL which is derived from the overall tower length of 77.6 m. The undistributed tower properties are given in the table 3-1:

Elevation to tower base above SWL	10 m
Center of tower mass above SWL (CM_{Tower})	43.4 m
Elevation to tower top	87.6 m
Overall Tower length	77.7 m
Tower mass	249 718 kg

Table 3-1 Undistributed tower properties

Hub, Rotor and Nacelle properties

The nacelle mass is specified to be 240 000 kg with a height of 2.4 m, the hub is connected to the turbine tower thus the top of the nacelle is at 90 m above SWL, the hub and rotor mass is specified to 110 000 kg. In order to simplify the calculations, the centre of mass for the rotor, nacelle and hub is assumed to 1.2 m above the tower top, it is also assumed that the centre of mass coincides directly above the centre of gravity of the floater. Hence the centre of mass, $CM_{Hub,\ Rotor\ \&\ Nacelle}$ is assumed be 88.8 m above SWL. This also implies that the x and y coordinates of the $CM_{Hub,\ Rotor\ \&\ Nacelle}$ is located at x = 0 and y = 0. The Hub, Rotor and Nacelle properties are given in table 3-2:

Elevation to centre of mass above SWL	88.8 m
Nacelle height	2.4 m
Nacelle mass	240 000 kg
Hub and Rotor mass	110 000 kg

Table 3-2 Hub, Rotor and Nacelle undistributed properties

3.2 NREL OC3 Spar-Buoy

The OC3 Spar Buoy model is based upon Equinor's "Hywind" model, however the OC3 model is adjusted from the original design in order to fit the NREL 5-MW wind turbine[14]. The spar is 130 m high with a draft of 120 m, thus the height of the entire structure and the NREL wind turbine tower is 207.6 m. Furthermore, the structure is symmetric in the *xy- and xz-plane,* hence making it easier to calculate properties and develop mesh for the structure. Furthermore, the spar's geometry consists of an upper cylinder with a diameter of 6.5 m and a height of 14 m, with 10 m being above SWL, this develops into a tapered cylinder with a height of 8 m and a lower diameter of 9.4 m, then the bottom part of the spar is a 108 m high cylinder with a diameter of 9.4 m. The mass of the floater including the ballast was calculated to be 7 466 330 kg for the OC3. Properties of the full system are not stated in the original study, only the structural properties for the floater including the ballast are given, these are shown in table 3-3 [14]:

Elevation to tower base above SWL	10 m
Draft	120 m
Upper cylinder height	14 m
Depth to tapered cylinder from SWL	4 m
Tapered cylinder height	8 m
Lower cylinder height	108 m
Floater mass	7 466 330 kg
Total displacement	8029 m^3
Platform Roll Inertia	4 229 230 000 kgm^2
Platform Pitch Inertia	4 229 230 000 kgm^2

Table 3-3 OC3 Structural properties

Figure 3-1 OC3 & NREL 5 MW Illustration

3.3 Design Variables, Objective Functions and Constraints

In order to analyse and find the optimum design of the Spar-Buoy floater, the design is required to fulfil certain design criteria. These are based upon offshore standards such as DNV [15] and industry recommended values [16][4][17]. For the following optimization procedure the mathematical optimization problem can be written as [18]:

$$minimize: F_1(x) \tag{3.1}$$

$$maximize: F_2(x) \tag{3.2}$$

$$subjected\ to: g_i(x) < 0, \quad i = 1, \dots n;\ x^L < x < x^U \tag{3.3}$$

Where $F_1(x)$ and $F_2(x)$ is the objective functions to be minimized or maximized, $h_i(x)$ is the constraint function, $x^L < x < x^U$ are the constraint boundaries and x is the design variable vector. The objective functions present the optimums for each objective, however it is preferred to find the optimum geometry considering both objective functions. To do so, the weighted sum method is applied. The weighted sum method for two objective functions can be mathematically expressed as:

$$minimize: F(x) = w_1 f_1(x) + w_2 f_2(x), \qquad \sum_{i=1}^{M} w_i,\ \ w_i \in (0,1) \tag{3.4}$$

The implementation of the weighted sum method is further explained in chapter 3.3.3.

3.3.1 Description of the Spar-Buoy

The OC3 system can be separated into four separate parts, the wind turbine, the floater (platform), the mooring system and the ballast. In this thesis the mooring system is neglected, thus the weight of the mooring system is included as ballast in order to keep hydrostatic equilibrium. Also, the effects of the mooring system are not evaluated. This way the system in this thesis can be separated into three separate parts namely the wind turbine, the floater and the ballast. The wind turbine is described in chapter 3.1 and its properties are kept as a fixed values. The freeboard/elevation H_F from tower base to SWL is set as a fixed value of 10 m similar to the OC3 and OC4 floaters, it is also a recommended value for floating wind turbines [16] [19]. The height of the tapered part H_T is a set at a constant length of 8 m, this is also done for the upper cylinder height H_U, which is set to a fixed height of 4 m below SWL. The radius of the upper cylinder R_U is set to a fixed value of 3.25 m in order to fit the radius of the wind turbine tower. Hence the upper radius of the tapered cylinder equals to R_U, whereas the lower radius of the tapered cylinder is equal to R_L. To achieve a constant freeboard of 10 m, Archimedes is applied to keep equilibrium between the floater and the buoyancy force. Thus, in order to keep the mass force equal to the buoyancy force, the ballast volume needs to be changed accordingly. The ballast height is calculated as:

$$B_H = \frac{Ballast\ Volume}{\pi(r - W_t)^2} \tag{3.5}$$

Thus, the geometry of the floater and the ballast is shown in figure 3-2:

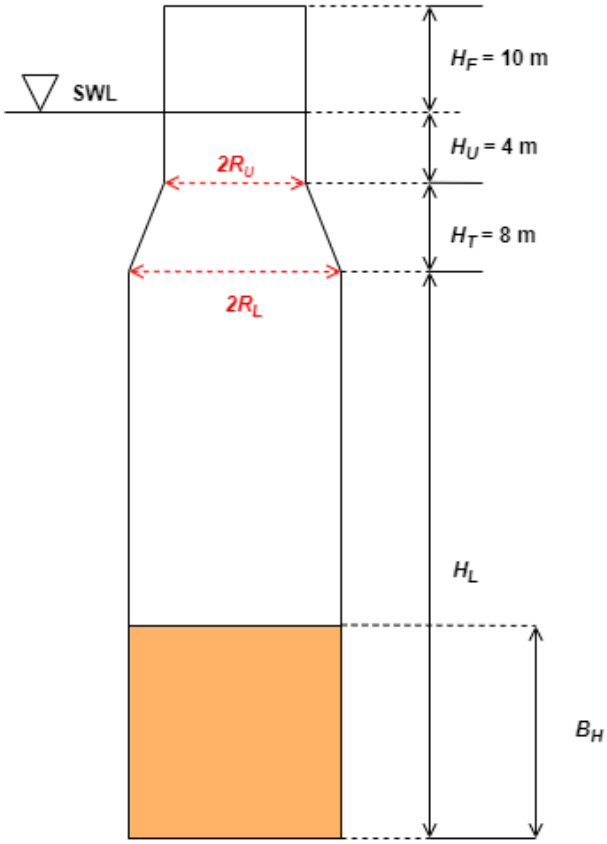

Figure 3-2 Geometry of the Spar-Buoy

3.3.2 Design Variables

The spar geometries in this study changes with two variables, namely the height (H_L) and the radius (R_L) of the lower cylinder as seen in figure 3-2. The design space is created such that a reasonable amount of geometries is analysed. H_L varies with 10 different heights, the lower bound of the height is set to 80 m and the upper bound is set to 120 m. The lower bound is chosen to keep the CoG low, the upper bound is set a little higher than the original OC3 in order to examine the performance of a higher spar than the OC3. The radius of the lower cylinder also varies with 10 different radiuses. The lower bound is set to 3.25 m as the lower part of the wind turbine tower is kept at a fixed value of 3.25 m as seen in figure 3-2. The upper bound is chosen to evaluate the performance of the spar with a wider structure. The design variables are shown in table 3-4.

Design Variables	Symbols	Lower bounds (m)	Upper bounds (m)
Height of lower cylinder	H_L	80	120
Width of lower cylinder	R_L	3.25	6

Table 3-4 Design Variables

3.3.3 Objective Functions

Objective Function nr.1

The first objective function is a cost function, where the goal is to minimize the price of the structure, hence; $minimize\ F_1(x)$. This is done by reducing the mass of the Spar-Buoy and the ballast. Hence the mass of the structure can be expressed as the sum of the combined volume of the Spar-Buoy V_{Steel} and the ballast volume $V_{Ballast}$, each multiplied by their respective material density ρ_{Steel} and $\rho_{Ballast}$. In this study the Spar-Buoy material is chosen to be steel and the ballast material is chosen to be Olivine. Hence the cost of each material is multiplied by a price coefficient for the respective material, namely a_{Steel} and $a_{Ballast}$. Hence the objective function can be expressed as:

$$minimize F_1 = f(H_{Li}, R_{Li}) \tag{3.6}$$

$$f(H_{Li}, R_{Li}) = V_{Steel} \cdot \rho_{Steel} \cdot a_{Steel} + V_{Ballast} \cdot \rho_{Ballast} \cdot a_{Ballast} \tag{3.7}$$

Objective Function nr.2

As mentioned, Spar-Buoys are *ballast stabilized* floaters, which means that a large volume of ballast causes the CoG to be centred far below the CoB. As the upper cylinder radius R_U is set to a fixed value for all the geometries that are simulated, the change in the metacentric radius $\overline{BM}$ is negligible due to a small waterline area A_w and a large submerged volume ∇. Hence the change in the metacentric height $\overline{GM}$ is mainly dependant on the CoG and the CoB of the structure. Due to this the $\overline{GM}$ is a good indicator for the stability of the Spar-Buoy. Thus, the second objective function is a stability function, where the goal is to maximize the $\overline{GM}$ of the structure hence; $maximize\ F_2(x)$. This is done by finding the geometry which equals the highest possible $\overline{GM}$. Hence the second objective function can be expressed as:

$$maximize\ F_2(x) = \overline{GM}(H_{Li}, R_{Li}) \tag{3.8}$$

Weighted sum method

In order to apply the weighted sum method, both objective functions need to have the goal of obtaining the minimum value. The method is described by the following steps:

1. First both objective functions are normalized with a value from 0 to 1.
2. The normalized values of objective function $F_2(x)$, can be expressed as $f_{2\,Normalized}(x)$ this is then converted into $f_{2\,Converted}(x) = 1 - f_{2\,Normalized}(x)$, this way the minimum value of $f_2(x)$ equals to the maximum objective, i.e. the largest $\overline{GM}$.

By applying the method described above, the combined objective function can be written as:

$$minimize: F(x) = w_1 f_1(x) + w_2 f_{2\,Converted}(x), \qquad \sum_{i=1}^{M} w_i, \;\; w_i \in (0,1) \tag{3.9}$$

Where:

$w_2 = 1 - w_1$.

3.3.4 Constraints

The Spar-Buoy is also subjected to some performance criterions. These are important in order to keep good hydrostatic and hydrodynamic performance and are applied as constraints. The performance criterions are explained in the section below:

1. Maximum inclination

Based on literature on floating offshore wind turbines, the total inclination angle should not exceed 10º during operational conditions [16] [20] [14] [21]. This refers to the maximum pitch or roll angle caused by both wind and waves. However, in this study only wave forces are taken into consideration for the hydrodynamic analysis, thus the results are considered as liberal estimates. Since linear wave theory is used, the most probable maximum pitch angle is found using short term conditions, this is usually referring to a stationary process. A stationary process is normally for 1-3 hours and is described in chapter 2.3.2. In this study a 3-hour stationary wave condition is used, and the most probable 3-hour maximum pitch angle is used as the maximum inclination. Thus the 3-hour most probable maximum pitch angle is derived from equation (2.62):

$$\alpha^{3h} = \sigma_{\text{pitch}} \sqrt{2 \ln(\bar{n}_{3h})} \tag{3.10}$$

The inequality constraint can be expressed as:

$$g_1 = \alpha^{3h} - 10° < 0 \tag{3.11}$$

2. Maximum acceleration

It is common in the industry to set the operational limit of acceleration at the nacelle to be 0.2-0.3 g i.e. 1.962 m/s^2-2.943 m/s^2. This is done in order to not cause any fatigue or damage on sensitive part's such as gearbox, bearings and the generator which is located at the nacelle [20]. It is uncertain how much the acceleration affects the sensitive parts at the nacelle, thus the maximum allowable acceleration at the nacelle is set to a conservative value of 0.2 g i.e. 1.962

m/s^2 as the wind effects of the platform motions are not taken into consideration in the hydrodynamic analysis [17]. The acceleration is calculated as the standard deviation of the acceleration spectrum σ_{acc} given in equation (2.61). The constraint can be expressed as:

$$g_2 = \sigma_{acc} - 1.962\ m/s^2 < 0 \tag{3.12}$$

3. Metacentric height

The metacentric height $\overline{GM}$ is an important property for Spar-Buoys. As described in chapter 2.1, the $\overline{GM}$ is an indicator of the structure's initial stability. Further in objective function nr.2 the objective is to maximize the $\overline{GM}$ to find a geometry with a large initial stability. However, if only objective function nr.1 is considered, requirements from industry standards apply. In order to ensure that the floater stays in stable equilibrium the floater needs to have a $\overline{GM}$ equal or greater than 1 m [15]. From equation (2.5) in chapter 2.1, the constraint can be expressed as:

$$g_3 = \overline{GM} - 2\ m < 0 \tag{3.13}$$

4. Pitch angle due to mean wind thrust

For floating offshore wind turbines, it is important to consider the stability effects of wind acting on the turbine. Steady state wind forces acting on the turbine causes a static heeling moment, which causes inclination of the wind turbine and a reduction in power production. Thus, the relationship of the maximum heeling moment and the inclination angle should be considered, this is referred to as "pitch angle due to mean wind thrust". If the forces are static, a simple one-dimensional model for the aerodynamic thrust can be applied. The thrust force can then be expressed as [22]:

$$F_{thrust} = \frac{1}{2} p_w \boldsymbol{\upsilon}^2 A c_t \tag{3.14}$$

Where p_w is the air density, $\boldsymbol{\upsilon}$ is the wind velocity and $A = \pi R^2$ is the wind turbine sweep area and c_t is the thrust coefficient. In this thesis, no calculations for wind is performed, thus the thrust force is not calculated from the site used in this thesis. However the thrust force is derived from the author of the NREL 5 MW reference wind turbine study, whereas the maximum thrust force obtained is 819.271 kN, this is the thrust force relative to rated wind speed [13]. This is done as a simplification, and it is assumed it the value is representative for the site chosen for this study. This thrust force from the rotor is used to calculate the thrust overturning moment about the CoG, deformation is neglected and the thrust moment can be expressed as[23]:

$$M_{thrust} = F_{thrust} \cdot d \tag{3.15}$$

Where d represents the vertical distance between the centroid of the nacelle and the CoB. The maximum static heeling angle $\alpha_{static\ heel}$ is then calculated by dividing the thrust moment M_{thrust} by the hydrostatic pitch stiffness C_{55}:

$$\alpha_{static\ heel} = \frac{M_{thrust}}{C_{55}} \tag{3.16}$$

From DNV, the heeling angle should not exceed 7º in operating conditions [15]. The heeling angle constraint can then be expressed as:

$$g_4 = \alpha_{static\ heel} - 7° < 0 \tag{3.17}$$

Constraints

The constraints should always take a value less or equal to zero.

Constraint	Expression	Description
g_1	$\alpha^{3h} - 10° < 0$	Allowable pitch angle due to waves
g_2	$\sigma_{acc} - 1.962\ m/s^2 < 0$	Allowable acceleration during operation
g_3	$\overline{GM} - 2\ m < 0$	Minimum Value for $\overline{GM}$
g_4	$\alpha_{static\ heel} - 7° < 0$	Allowable static heel angle due to wind

Table 3-5 Table of Constraints

3.3.5 Simplifications and Assumptions of the Spar-Floater

The objective of this thesis is to examine the performance of 100 different spar-buoys which are modified from the original OC3 design. However, there are properties of the spar structure which are not stated in the original study, based on relevant literature these are derived in the following matter.

Steel density

This thesis does not examine the local structural integrity of the Spar-Buoy, thus the steel density is derived from similar studies. Regular s355 steel with a density of $7850\ \mathrm{kg/m^3}$ is applied, this is the standard steel grade used for offshore structures. The same steel grade is also used in an advanced spar buoy optimization study [24]. However a steel density of $10\ 000\ \mathrm{kg/m^3}$have been suggested in another study by the same author [14]. Further, the steel with a lower steel density is applied as this causes a larger volume of ballast to be applied, thus lowering the CoG.

Wall thickness

In order to calculate a proper wall thickness, a representative value for the ratio between the spar structural mass and buoyancy mass is derived by *Bachynski.E*, the ratio is assumed to be 0.13 [25]. Using the OC3 as baseline, floater mass is calculated as:

$$0.13 \cdot Bouyancy\ mass = 0.13 \cdot \frac{80\ 708\ 100\ N}{9.81} = 1\ 069\ 526.3\ \ kg \tag{3.18}$$

From the floater mass, the wall thickness (W_t) can be calculated as:

$$W_t = \frac{\sum_i (H_i(2R_i))^2 - \sqrt{[\sum_i (H_i(R_i))]^2 - \frac{4}{\pi}\frac{spar\ mass}{steel\ density}\sum_i H_i}}{2\sum_i H_i} = 0.0372\ m \tag{3.19}$$

Where H_i and R_i is the height and radius of each element. Further referring to the OC4 [26], the main column in the study has a wall thickness of 0.03 m, hence a wall thickness of 0.0372 m is assumed to be ok. From the ratio derived by *Bachynski.E*, the floater mass should change when the geometry changes, however for simplicity the wall thickness is kept at a fixed value of 0.0372 m. Moreover, the wall thickness is only applied to the circumferential walls of the floater. The bottom and top cap are set to 0.001 m which is derived from a verification study [27].

Ballast density

One of the main pros of a spar-buoy is the stability, this is achieved by having the CoG far below the CoB. This is mainly achieved by applying a large volume of ballast at the bottom of the spar, thus ballast with a high material density is desirable. The main dry ballast component for Equinor's *Hywind Tampen* project is Olivine which has a mass density of 3220 kg/m^3. The same material is used as the only ballast component in this thesis [28].

3.4 Environmental Conditions

Figure 3-3 Location of Site 14

To study the response of floating offshore wind turbines, sufficient information about the environmental conditions is required. Joint data for wind and waves from the "Norway 5", site 14 is chosen for this analysis [29]. The site is located 30 km from shore, with an average water depth of 202 m, the location of the site is seen in figure 3-3. The environmental data is based on hourly samples from a hindcast model between 2001 and 2010. The long-term joint distribution of significant wave height (H_s), wave period (T_p) and mean wind speed (U_w) were estimated by fitting the sampled hindcast data with analytical distributions. The joint distribution of U_w, H_s and T_p consists of three different distributions, and the method for choosing the environmental conditions are:

1. A marginal distribution of mean wind speed U_w at 10 m above SWL, following a 2-parameter Weibull distribution, is used to estimate the most probable mean wind speed value.
2. A conditional distribution of significant wave height H_s, given mean wind speed U_w, following a 2-parameter Weibull distribution, is used to estimate the most probable significant wave height.

3. A conditional distribution of wave period T_p, given both mean wind speed U_w and significant wave height H_s following a lognormal distribution, is used to estimate the most probable wave period.

Based on the joint distribution, contour surfaces are applied in order to estimate the extreme conditions with a return period 50-years. The environmental data is used to calculate the hydrodynamic response for cut-in, rated, cut-out and extreme conditions for this thesis. Further information about the distribution parameters and fitting methods can be found in [29]. The conditions are listed in the table below:

EC	**Mean wind speed (m/s)**	**Significant wave height (m)**	**Wave period (s)**	**Operating status**
1 (Cut-in)	3	1.46	10.91	Operating
2 (Rated)	11.4	2.59	10.18	Operating
3 (Close to cut-out)	24	6.14	11.22	Operating
4 (Cut-out)	25	6.51	11.34	Parked
5 (Extreme)	31.2	15.6	14.5	Parked

Table 3-6 Environmental Conditions for Site 14

3.5 Numerical Method and Open-Source Program

This chapter aims to describe the numerical methods used to automate, sample and analyse the data used in this thesis. It is common to use a software like SESAM, a well-established software which includes different models for structural and hydrodynamic analysis of ships and offshore structures. The program comes with a well-established graphical user interface (GUI), thus modifications of the models are easy to perform. However due to the circumstances caused by the Covid-19 situation, which caused uncertain accessibility to the computer lab it was decided to implement open-source programs for this thesis. Thus, only open-source programs are used. Moreover, it is important to point out that all calculations are performed using self-made scripts which are run in Python. It is only the hydrodynamic coefficients which are calculated by another software, namely Nemoh. It should also be noted that Nemoh only calculates the hydrodynamic properties: added mass, linear damping, excitation force and phase angle. Hence the hydrostatic properties, hydrodynamic response, sea environment, optimization etc. are calculated using Python. Further the mesh model is created using Salome.

3.5.1 Mesh Modelling in Salome

Salome is an open-source software framework, used for modelling, mesh generation, pre and post processing simulation of physical problems. The software framework uses an open and flexible architecture made of reusable components. Furthermore, the software is a cross-platform solution which can be used on multiple hardware's. One of the core futures of Salome is that it supports interoperability between Computer Aided Design (CAD) modelling and computational software. This way Salome can be used as a standalone feature for the generation of CAD models in preparation for numerical calculations. Hence generated mesh models can be exported to the preferred format for pre or post processing. Salome also features an integrated Python Application Programming Interface (API) console which allows users to modify mesh properties from simple Python scripts [30].

Salome is used to generate the necessary mesh models for hydrodynamic simulation in Nemoh. Nemoh is a linear 3D diffraction theory, panel method solver, thus it is only dependant on the wetted surface of the structure. Due to this the mesh is created with a right-hand coordinate system such that the x and y-axis is located at the SWL i.e. z=0, whereas the z-axis is located at the centre of the structure.

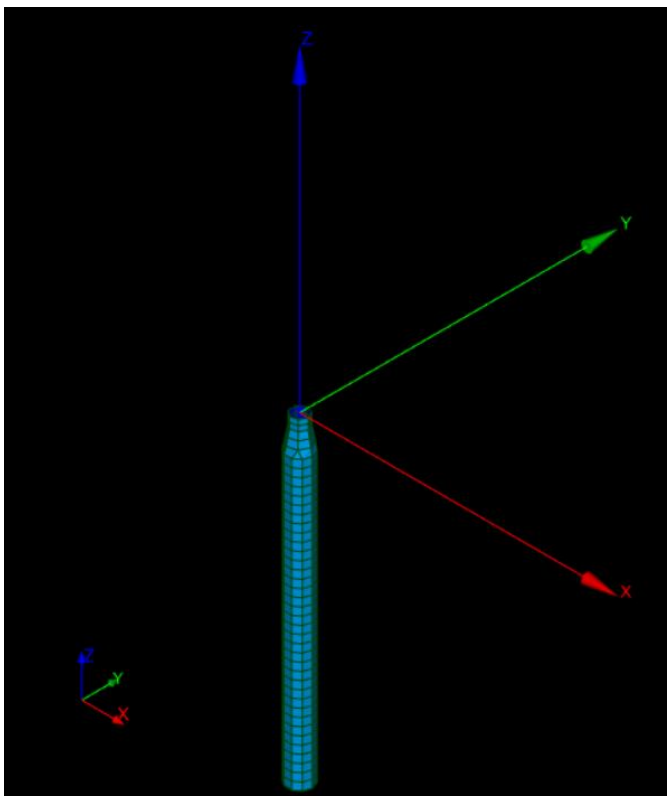

Figure 3-4 Mesh Model in Salome

As mentioned, Salome comes with a Python API console for Salome mesh, this allows the CAD model to be manipulated in a python script. First a script for a geometry is created, then the mesh is "dumped" (exported) to a python script. This script allows the user to manipulate the mesh without using the GUI, the script is also manipulated to always export the proper mesh file for Nemoh, namely a .dat file, a .dat file is similar to a normal .txt text file which contains the information about the number and coordinates of the nodes and panels of the mesh. Figure 3-4 is an example of a Spar-Buoy mesh model created in Salome.

3.5.2 Computation of First Order Wave Loads in Nemoh

Nemoh is an open-source Boundary Element Method (BEM) code used to calculate hydrodynamic properties such as added mass, damping, excitation force and phase angle for offshore structures. The program is based on linear *3-D diffraction-theory*, thus applying the same assumptions used for linear wave theory, for a detailed description, the reader can refer to chapter *7.4.1* in *Offshore Hydromechanics* by *Massie* [7]. Further the *3-D panel method* is applied, hence the geometry provided by Salome is divided into points and panels, where the centre of each panel has coordinated provided as input for Nemoh, for a detailed description the reader can refer to chapter *8.3.4* in *Offshore Hydromechanics* by *Massie* [7]. The code was developed at "*Ecole Centrale de Nantes"* in France for over 30 years and is the first BEM code available to the public since July 2014. Nemoh is commonly used to calculate the hydrodynamic response of floating structures or used for performance assessments for wave energy converters. A Matlab wrapper have also been developed for mesh creation and easy use of Nemoh in the Matlab environment, this feature includes properties such as the spring matrix to be calculated by Nemoh, however this is geometry dependent and the feature is only applicable in simple research cases [31]. Also, this study applies Python instead of Matlab in order to create an automated simulation tool connecting Salome and Nemoh.

Nemoh is the BEM code used for the computation of the first order hydrodynamic coefficients added mass, linear damping, excitation force and phase angle. In Nemoh all the calculations are performed in the frequency domain. The program also compute far field coefficients for the calculation of slow wave drift forces, moreover it should be noted that the program does not consider viscous effects or irregular frequencies [32]. Nemoh does not feature a graphical user interface (GUI) and is primarily run through the windows command line or an external coding

program such as Matlab or Spyder. The program is composed of three different sets of programs which should be run in the following order:

- pre-Processor: Read and prepare the mesh and calculation cases (set of body conditions).
- Solver: For each body condition, solve the linear BPV for the potential and calculate pressure field, hydrodynamic coefficients, far field coefficients and wave elevation.
- post-Processor: Post processing the results, i.e. hydrodynamic properties.

As mentioned, Salome is used for mesh generation, however the exported .dat file from Salome requires to be modified in order to be run by Nemoh, a script provided by supervisor Filippos Kalofotias allows for the correct conversion. The conversion relocated and structures the original .dat file into a .dat file that is compatible with Nemoh. The correct mesh file (.dat file) needs to be updated in the input file and it should also be located in the same folder as the Nemoh programs. Furthermore, an input file called "nemoh.cal" requires modifications in order to calculate the correct results. The "nemoh.cal" file can be seen as the User Interface (UI) of Nemoh, this file is also similar to a normal .txt text file. The following input is accessible for editing in the "nemoh.cal" file is similar to table 3-7:

Input	Default	Selected
Sea Water Density (kg/m^3)	1000	1025
Gravity (m/s^2)	9.81	9.81
Water Depth (m)	Infinite	200
Number of DoF	6	6
Name of mesh file	nemohMesh.dat	User defined mesh file name .dat
Number of points and panels	Derived automatically from the correlated mesh file	Derived automatically from the correlated mesh file
Coordinate System	User Defined	CoG
Min, Max, Frequency Range rad/s	0.05-2	0.05-1.2
Number of Wave Frequencies	41	140
Number of Wave Directions	1	1

Table 3-7 Nemoh input

Once the “nemoh.cal” file is modified to fit the user’s preferences and corresponding mesh, Nemoh is run and the hydrodynamic output is calculated. The calculated output is presented as .tec files, in two separate folders, named “mesh” and “results”, the “results” folder contains the hydrodynamic output which is used for post processing, the .tec files are also similar to a .txt file, whereas the .tec files contains the results structured in rows and columns. It should be noted that the input file, “results” and “mesh” folders should be located in the same folder as the set of Nemoh programs are located, also the “results” and “mesh” folders needs to have the correct names, namely results and mesh. Further the results are presented in the files:

- ExcitationForce.tec which contains the excitation forces which are a combination of the diffraction forces as well as the Froude-krylov forces, the file also contains the corresponding phase angle.
- RadiationCoefficients.tec which contains the added mass and linear damping for all DoF’s.

Nemoh is only a BEM solver, hence it does not provide any tools for post processing or reading tools for the results. As described in a Nemoh verification study the program is poorly documented with little to no guides or manuals [32]. However, a manual for the Salome-Nemoh interaction provided by supervisor Filippos Kalofotias established a better understanding of how the programs interact. However, the manual only describes how to solve the interaction for one single simple geometry, also the mesh creation, mesh file conversion and Nemoh input needs to be done manually. To solve this, an automated approach is created and described in chapter 3.6.

3.5.3 Post Processing in Python

In this thesis the open-source program Spyder is used. Spyder is an open-source scientific development environment written in Python programming language, using a combination of Python scientific plugins for data inspection, calculation, and analysis. The Spyder environment includes plugins such as SciPy, NumPy and Matplotlib which includes tools for interpolation, matrix calculations and data visualisation for advanced problems. As Spyder uses Python programming language, the Salome-Python console allows the mesh to be modified using scripts.

As mentioned, Nemoh does not provide tools for post-processing or analysis of the results, hence pre- and post-processing scripts are created in Python in order to calculate the results (see appendix A.4). Thus, the results from Nemoh, namely added mass, damping, excitation force and phase angle is read and structured such that it matches the corresponding matrix format while corresponding to the correct frequency. Similar scripts are created for the structural properties such as the spring matrix, mass matrix and CoG. This way calculations such as the RAO, response spectrums and wave spectrums can be calculated.

3.5.4 Simplifications in Salome and Nemoh

Mesh-size

As mentioned, the mesh provided from Salome is constructed with a number of points and panels. These numbers are related to the mesh-size, which can be changed in the Salome-Python script. A large number of points and panels requires a larger simulation time in Nemoh, thus the mesh size is set to 3.0 m. By doing this the simulation time is reduced, however the volume of the geometry reduces as the spar will not be a circle but rather a rectangular polygon as shown in figure 3-5. Thus, the modelled waterline area is not the same as presented in equation (2.44). This causes an imprecise relationship between the calculated excitation forces and the hydrodynamic stiffness matrix for heave motions shown in equation (3.51). However, this is only important for motions dominated by spring terms, i.e. for very low frequencies. Also, it should be noted that when the radius increases the inaccuracy decreases.

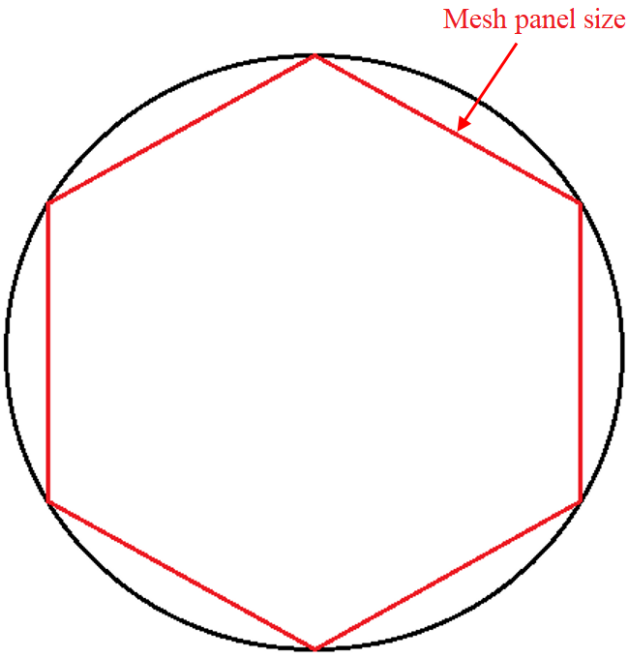

Figure 3-5 Illustration of Simplified Mesh Size

Number of wave frequencies

The number of wave frequencies decided for input in Nemoh is set to 140, while the min and max frequency range is set to 0.05-1.2 rad/s giving a frequency step of ca 0.083 rad/s. This is done in order to reduce the simulation time in Nemoh and post processing computation time in Python. However, by reducing the frequency step, the response frequency of the simulated geometry might not coincide with the natural frequency of the structure, hence giving lower or inaccurate peak values for the RAO's. Further, the RAO is interpolated such that the interpolated frequency step is 0.005, this is done in order to smoothen the curve and increase the accuracy of the results.

3.6 Integrated Design Optimization

3.6.1 Salome-Nemoh Automation

The Salome and Nemoh interaction is usually used for only one geometry, whereas in this thesis N simulations are required. As described in chapter 3.5.2 Nemoh allows for a number of modifications to be performed in the input file, however in this thesis only the mesh file and corresponding CoG needs to be updated in the Nemoh input file for each simulation. In order to simulate N geometries an automated modelling script was created, to the authors and supervisor's knowledge, as well as research based on Salome and Nemoh forums posts, manuals etc. no such automation have been created for Salome-Nemoh before. Previous attempts of automating the procedure have been slow or failed due to Nemoh not finishing the simulation before another geometry is run in Salome, however in this thesis this problem was solved using a python *subprocess(capture_output=True).stdout* command which requires the script to capture the output of each simulation before going to the next line. Thus, the script can serve as a basis for future iterative simulations using Salome and Nemoh, the script is given in appendix A-3.

The approach requires a number of calculations to be performed for each simulation. The simulation architecture is visualized in the figure below, and can be described in the following steps, the process is described in figure 3-6:

1. An initial geometry is created in the Salome GUI and is exported (dumped) as a python applicable file(see appendix A-1). The file is then modified such that the variables H_L and R_L can be changed for each iteration. The script is also manipulated such that when

the variables changes, the upper cylinder always intersects with $z = 0$ (SWL). Further the script is created such that when the file is run, it exports the corresponding .dat file for the geometry, i.e. the file containing the number of points and panels of the mesh.

2. The .dat conversion script mentioned in chapter 3.5.2 is then automated to convert the correct .dat file provided for each iteration(see appendix A-3).
3. A script calculating the hydrostatic properties and finally the CoG of the geometry is run.
4. The converted .dat file is then placed in the same folder as the nemoh.cal input file where the properties for the name of the meshfile, number of points and panels and the location of the CoG is changed accordingly for each iteration. Thus Nemoh is ready to run.
5. Nemoh is run, and the results are stored in folders with the name resultsN_n and meshN_n with respect to the n'th iteration, the Nemoh.cal file is also stored in the resultsN_n folder in order to be able to verify that the CoG and number of points and panels correspond to the correct geometry.
6. The simulations continue until N simulations are performed.

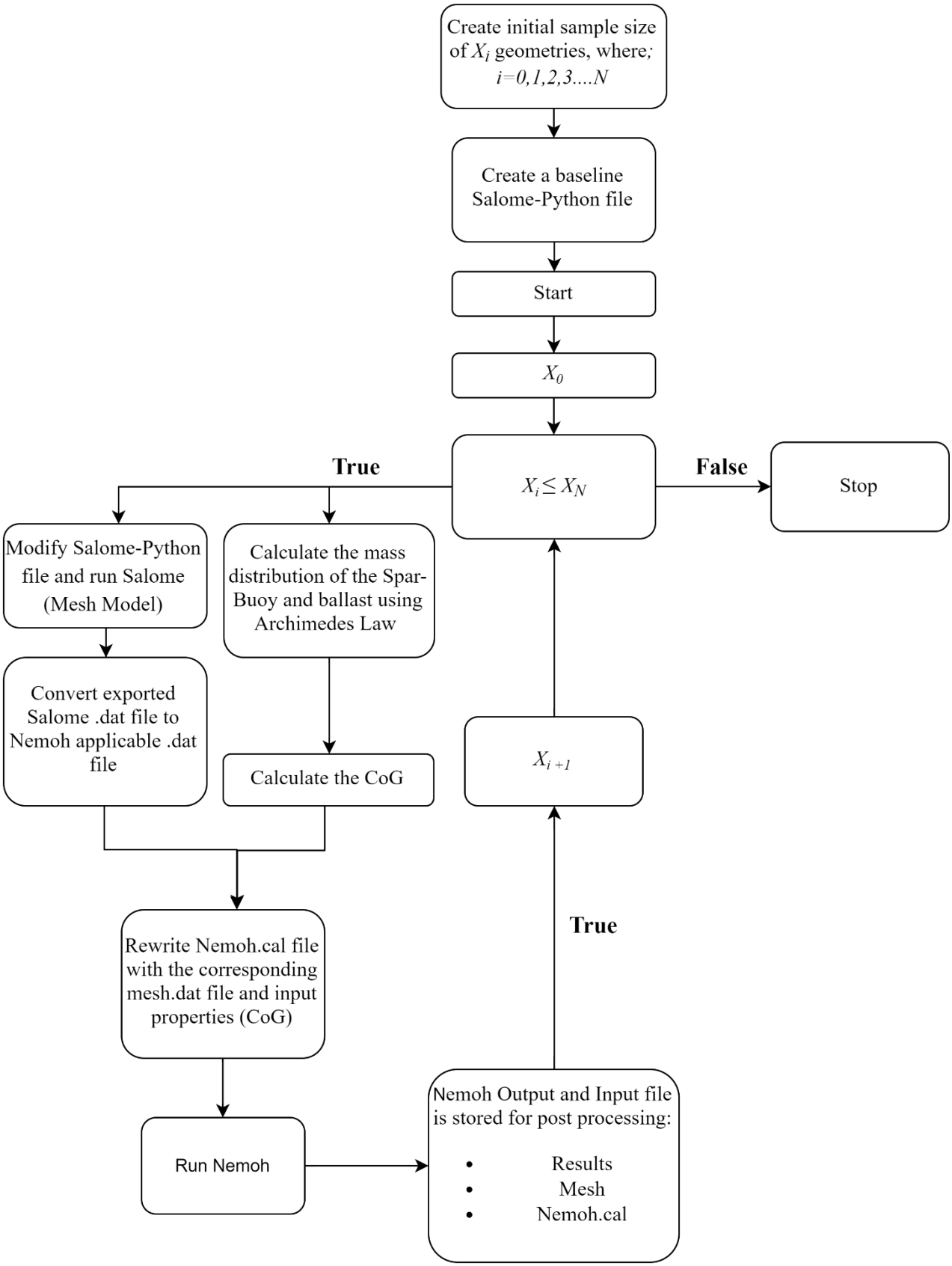

Figure 3-6 Automated Simulation Flowchart

Sampling method

In this thesis, a basic 2D-rectangular grid is used as sampling method. The sample consists of a sample size, with 10 samples n_H for the lower cylinder height H_L, and 10 samples for the lower cylinder radius R_L. Thus, a total of $n_H \cdot n_R = 100$ different geometries are used as the sample size. The sample domain is created such that a similar geometry as the OC3 baseline design is in the middle of the domain. The 2d-grid structure allows for easy visualization and analysis of the design space.

3.6.2 Optimization Procedure

The optimization procedure is performed by connecting the results from the hydrostatic calculations in Python as well as the results from the hydrodynamic simulations performed in Nemoh. The geometries are then subjected to the constraints (see chapter 3.3.4), whereas the geometries which not fulfil the criterions are eliminated. The weighted sum method is then applied to calculate the combined objective function. Lastly the set of optimum geometries are analysed manually. The optimization architecture is described in the figure 3-7:

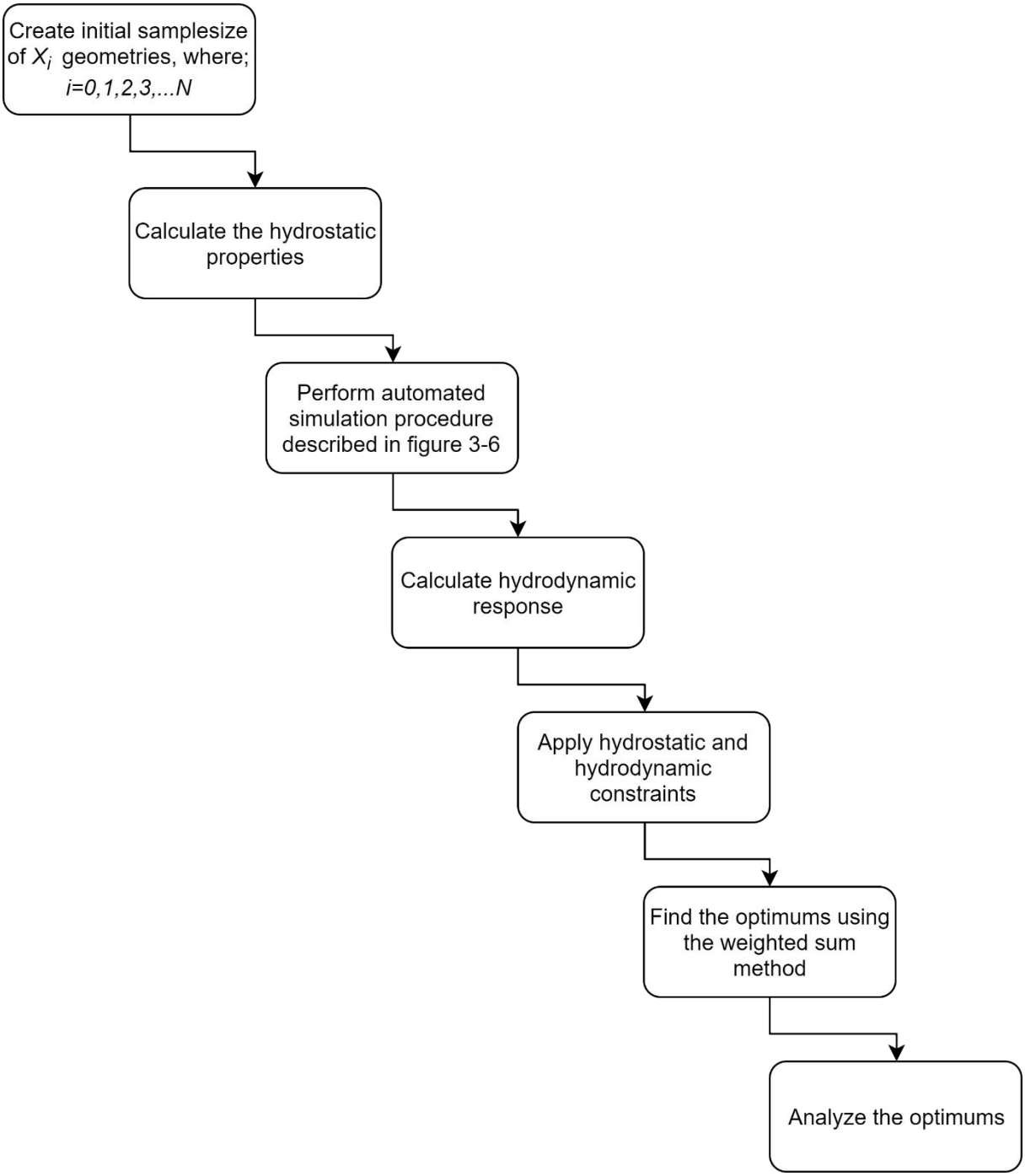

Figure 3-7 Optimization Architecture

4 Results and Discussions

100 different spar geometries have been simulated as a 10x10 grid where the radius of the lower cylinder ranges from 3.25 m – 6 m and the lower height ranges from 80 m – 120 m, whereas the properties such as the ballast and the tapered region changes accordingly.

This chapter presents the results from the hydrostatic and hydrodynamic analysis, the results will be further discussed in chapter 6. The results include:

- Comparison of the original OC3
- Hydrostatic properties; Displaced volume, buoyancy force, CoG, CoB, $\overline{GM}$, hydrostatic spring stiffness and static pitch angle.
- Hydrodynamic response; Response spectra for acceleration in heave and pitch. Response spectra for pitch angle and natural periods for heave and pitch.
- Analysis of the different objective functions.
- Analysis of the different optimums.
- Sensitivity studies which analyses the change in hydrodynamic properties while having either the height or radius as a fixed value. This includes the added mass, damping, excitation force and RAO's.

4.1 Hydrostatic Analysis

4.1.1 Hydrostatic Properties

In figure 4-1, 4-2 and 4-3 the buoyancy force, displaced volume and ballast mass are presented as colorplots giving the appropriate value for each point on the grid. As expected, the displaced volume, buoyancy force and ballast mass increases as the height and radius of the structure increases. Moreover, is can be seen that the values increase more rapidly as the radius increases compared with the height. It can be seen that the buoyancy force, displaced volume and ballast mass have an approximate increase of ten times the force, displacement and mass from the smalles geometry to the largest.

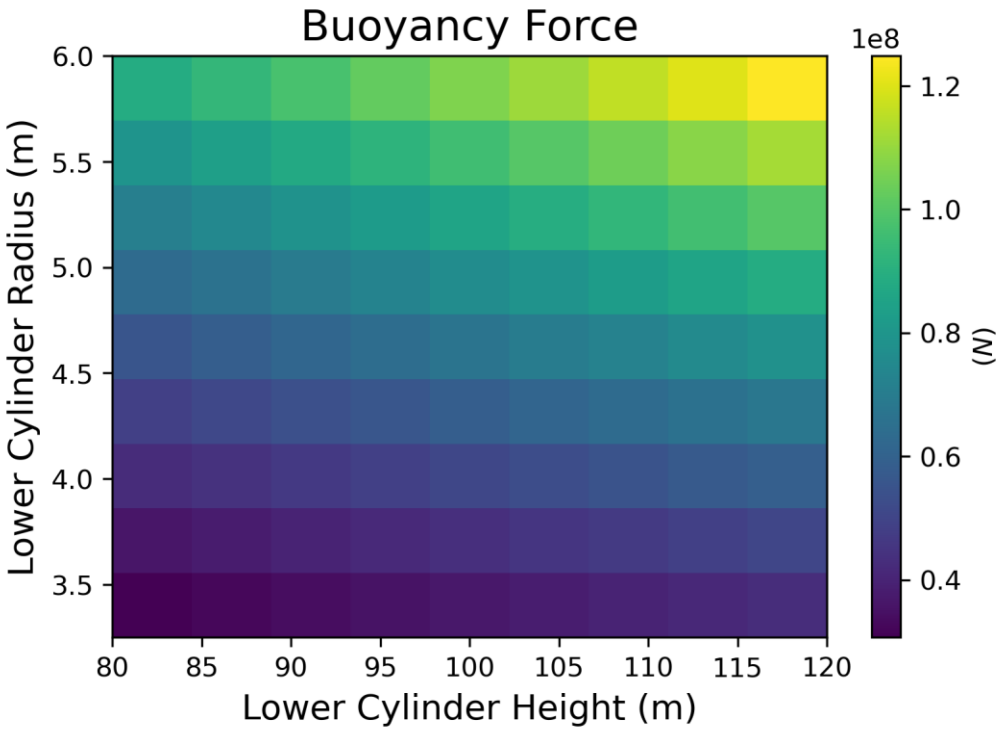

Figure 4-1 Buoyancy Force F_{∇}

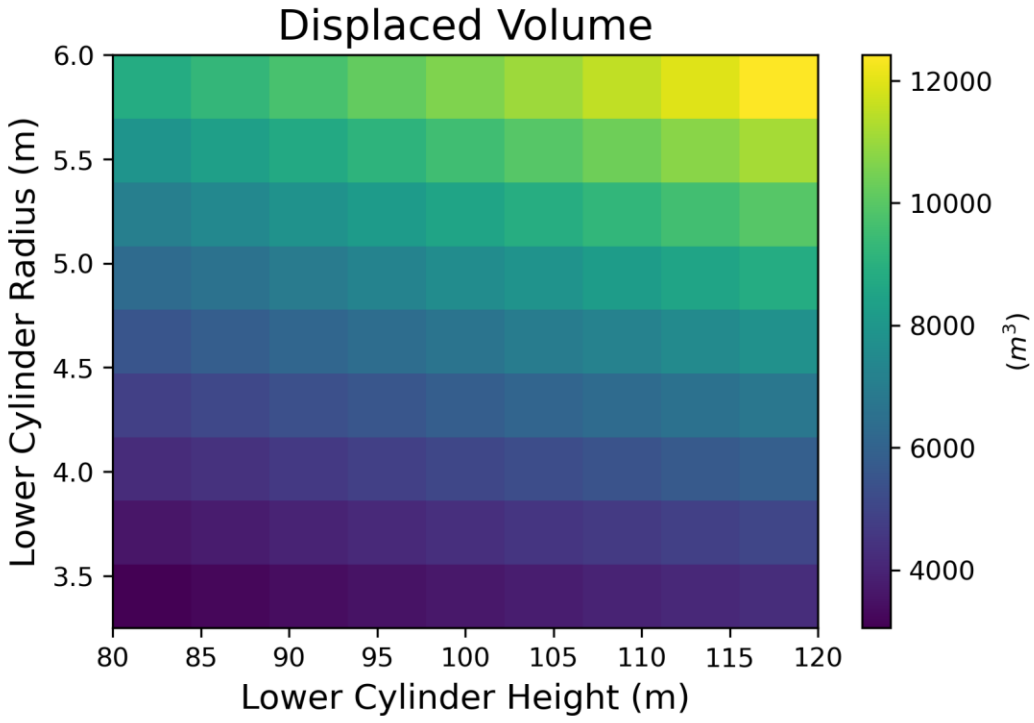

Figure 4-2 Displaced Volume ∇

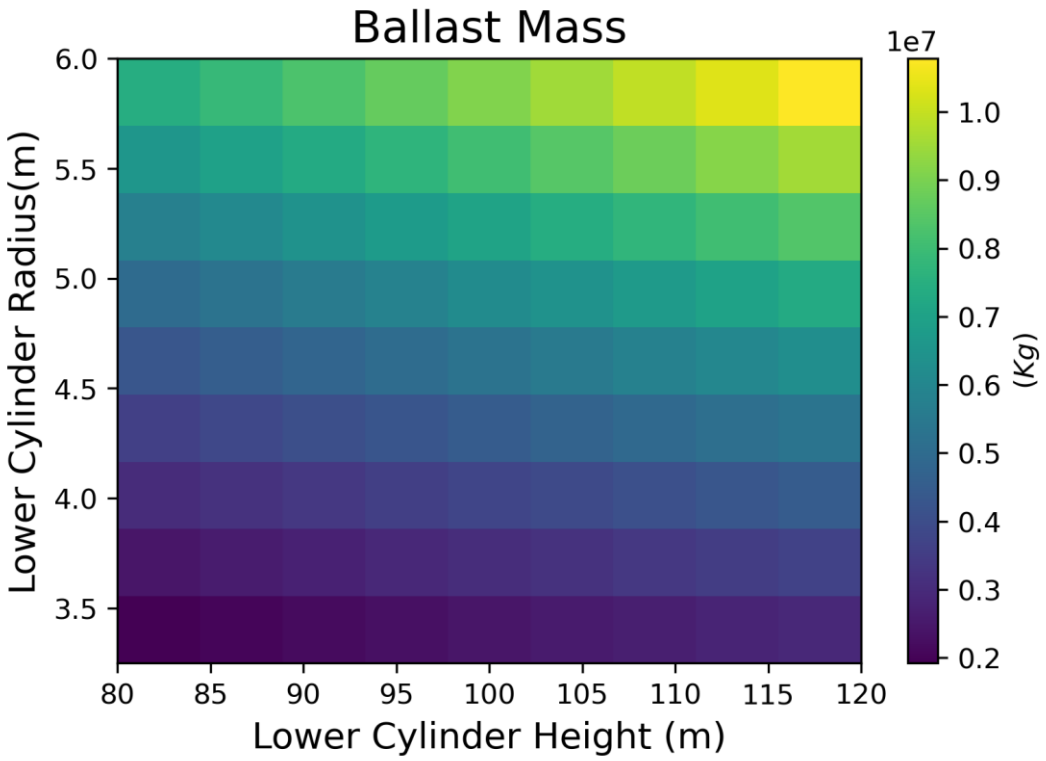

Figure 4-3 Ballast Mass

Further, in figure 4-4, 4-5 and 4-6 the Centre of Gravity CoG, Centre of Buoyancy CoB and metacentric height $\overline{GM}$ is plotted. As expected, an increase in submerged volume causes an increased value of the CoG bellow the sea water level SWL, this is due to more ballast which is placed at the bottom of the spar, as a result the CoG is lowered. Further the CoB also increases at a similar rate, the largest increase happens for the spar with a lower radius, this is because when the radius gets larger the tapered cylinder gets larger as well, thus decreasing the distance from the SWL to the CoB. The development of the $\overline{GM}$ is similar to the increased distance from the SWL to the CoG. For a geometries with a radius of 3.25 m and height of 80 m and 84.4 m the $\overline{GM}$ is below 1 m, this is because of the centroid of the ballast being located closer to the CoB, causing the CoG to be very close or above the CoB. As the waterline area defining the metacentric radius $\overline{BM}$ is negligible, a small or negative value of the $\overline{GM}$ is caused by the CoG's locations is slightly below or even above the CoB. This is related to the ballast density, a material with a larger density would increase the distance from the CoG to the SWL, whereas a material with a lower density would decrease the distance. In figure 4-6 for the $\overline{GM}$ it can be seen that two geometries are plotted with the colour white, this is because these geometries does not fulfil constraint g_3 for the $\overline{GM}$, and hence these are not applicable for a suitable design, thus these are not considered for the hydrodynamic calculations.

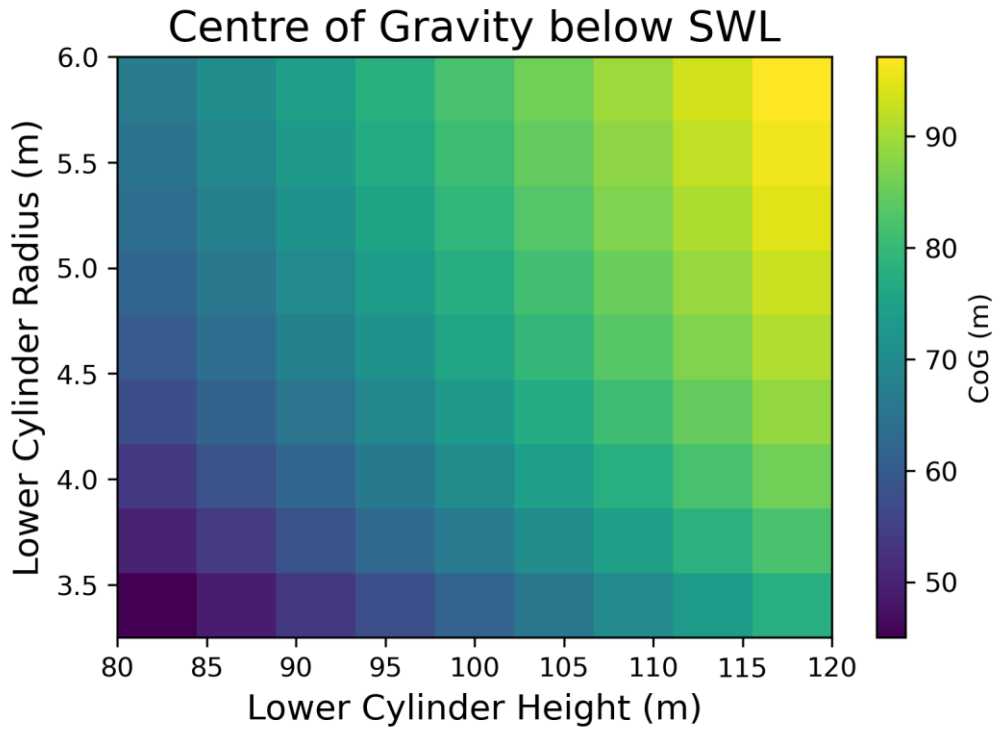

Figure 4-4 Centre of Gravity CoG

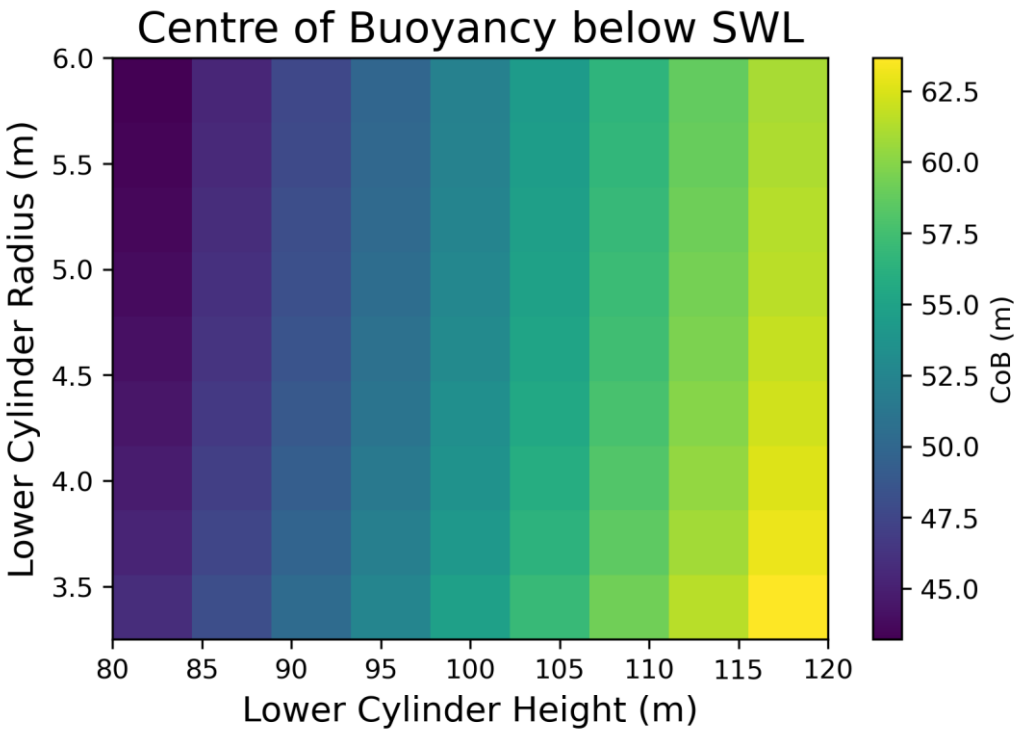

Figure 4-5 Centre of Buoyancy CoB

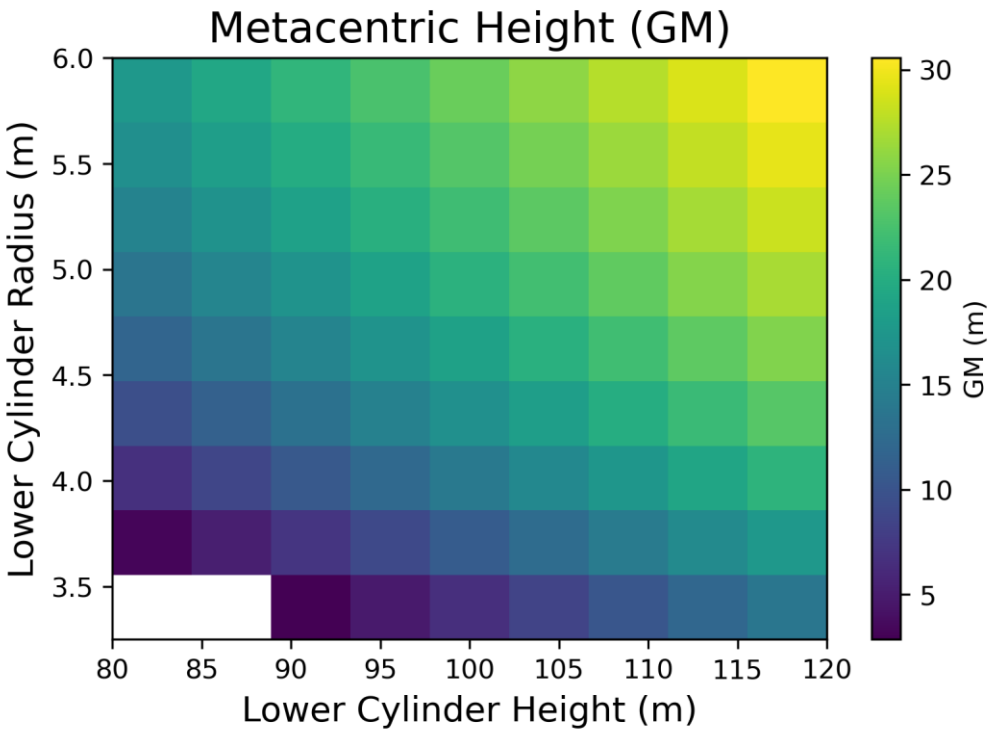

Figure 4-6 Metacentric Height $g_3 = \overline{GM} - 2\ m < 0$

Moreover in figure 4-7, 4-8 and 4-9 the total mass, pitch spring stiffness C_{55} and static heeling angle $\alpha_{static\ heel}$ is shown. As expected when the displaced volume (figure 4-2) increases so does the totalt mass in figure 4-7. This can also be seen for the pitch spring stiffness C_{55} in figure 4-8 . Hence when C_{55} increases the static pitch angle decreases. This is because of M_{thrust} in equation (3.16) is a fixed value whereas C_{55} is dependent on the structrual properties.. Thus, the correlation of mass and hydrostatic stiffness improves the static pitch angle, whereas the largest geometry has the lowest static pitch angle. Furthermore, it can also be seen that 39% of the geometries are not plotted, this is because these geometries do not fulfil constraint g_4, thus the static heeling angle exceeds 7 degrees.

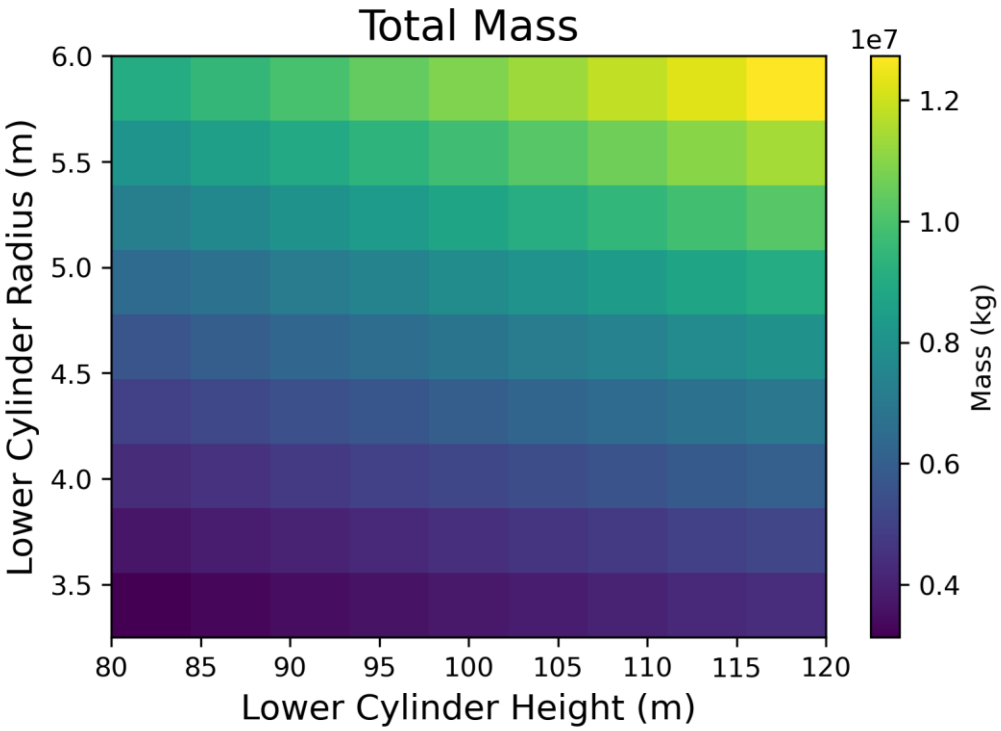

Figure 4-7 Total Mass (Spar-Buoy, Ballast and Wind Turbine)

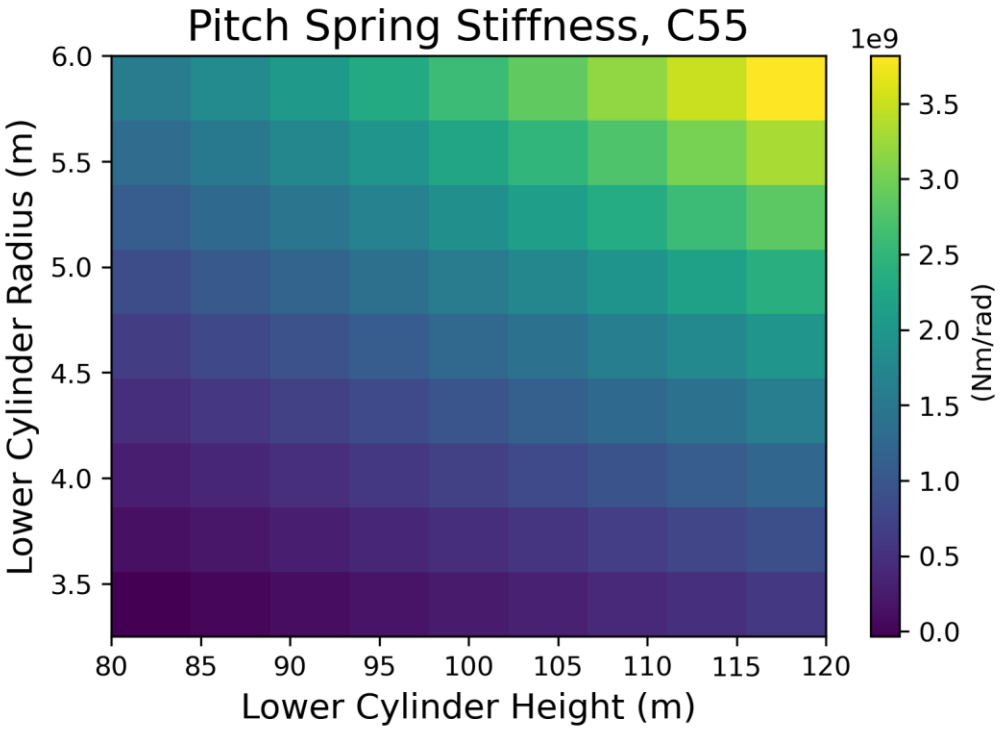

Figure 4-8 Pitch Spring Stiffness $C_{55} = \rho g \nabla \cdot \overline{GM}$

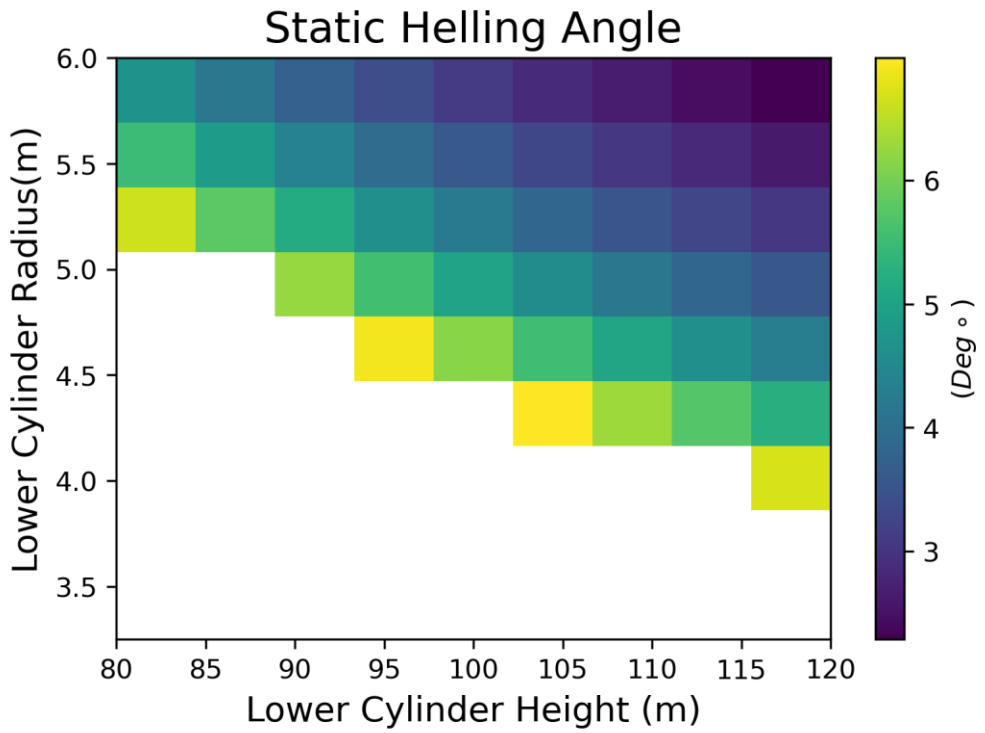

Figure 4-9 Static Heeling Angle $g_4 = \alpha_{static\ heel} - 7° < 0$

4.2 Hydrodynamic Analysis

4.2.1 Verification of Hydrodynamic Results in Nemoh

To compare the results and calculations, a geometry with the same dimensions as the OC3 Spar-buoy was modelled and simulated in Nemoh. The calculations are different as the wall thickness, ballast density and ballast mass are not given in the original OC3 study, and thus the results presented here are calculated using the same assumptions given in chapter 3.3.5. It should also be noted that the results in the original study refers to the SWL, while the results presented here refers to the CoG. Also, the results presented I this thesis are calculated using a simplified approach and using the BEM software Nemoh, whereas the original study applies the BEM software WAMIT. Furthermore the calculations in the original study are manually modified by the author, for more details the reader is referred to *Definition of the Floating System for Phase IV of OC3* by J. Jonkman, et.al [14]. Moreover, the original study includes mooring lines and damping matrices linked to turbine performance as well as viscous damping for the calculations of the RAO's. However, the results are assumed to be of similar nature. The hydrodynamic properties i.e. added mass, damping coefficient, spring coefficient, excitation

force and phase angle are given in the original OC3 study, while the RAO's and natural frequencies are given in an investigational study [14] [33].

Nemoh Output

Added Mass

As presented in figure 4-10 the added mass for translational motions are very similar to the results given in the original OC3 paper. However, the added mass for the rotational motions in figure 4-11 are different, this is assumed to be because of moments refers to the SWL and not the CoG. Furthermore, the mass distribution is not the same, thus the CoG is not the same in as in the original study. It should also be noted that due to the symmetry of the spar, surge and sway motions are identical as well as pitch and roll.

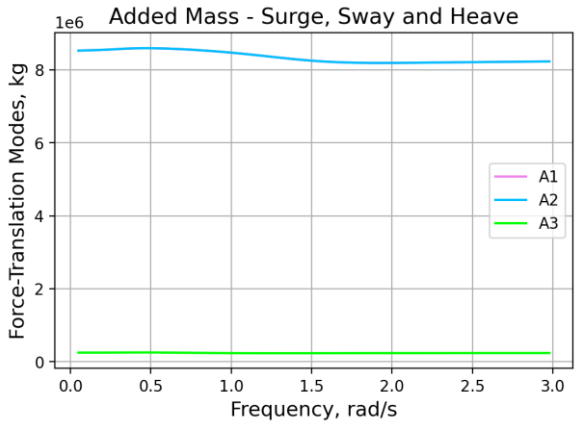

Figure 4-10 OC3: Added Mass for Rotational Model

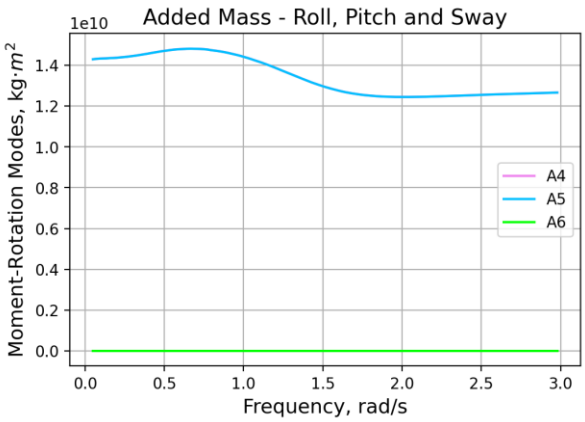

Figure 4-11 OC3: Added Mass for Translation Modes

Damping

The damping coefficients for translational modes in figure 4-12 are also very similar to the results in the original OC3 study, whereas the the rotational modes in figure 4-13 are different. As mentioned the refrence system is not the same, thus the values are expected to be different. However the peak of the damping coefficient is shifted to a higher frequency for the results given from Nemoh, as seen in figure 4-12 and 4-13 the peak of the linear damping occurs close to a freqency of 1.5 rad/s while in the the rerence damping occurs at a frequency of ca 0.5 rad/s. This is because of the viscous effect which are not acounted for in Nemoh.

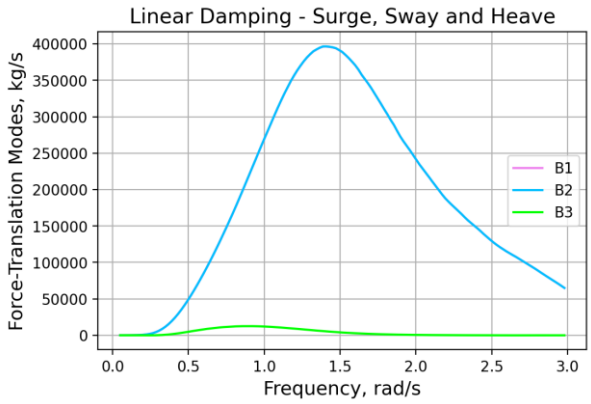

Figure 4-12 OC3: Linear Damping for Translation Modes

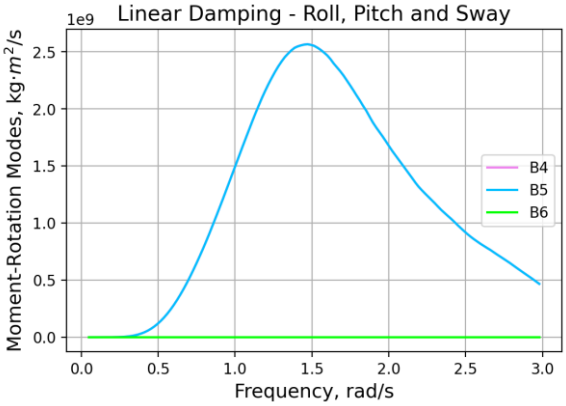

Figure 4-13 OC3: Linear Damping for Rotational Modes

Excitation Force

Again, the excitation forces for translational motions are very similar. However the same shift of frequency occurs when at the pitch excitation force, only this time the peak frequency is under 1 rad/s for both results. As mentioned this might be due to the use of another reference system or that other properties are taken into account (mooring, viscous forces etc).

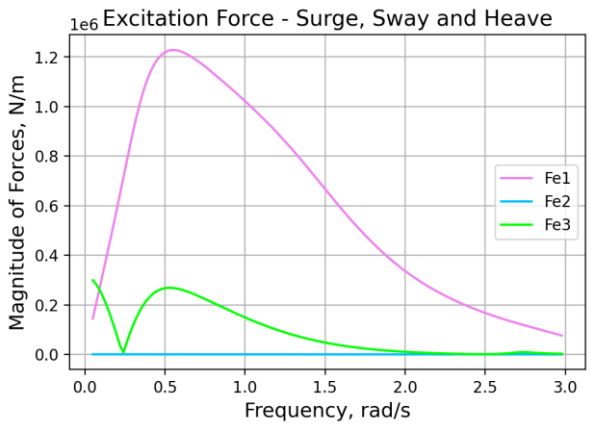

Figure 4-14 OC3: Excitation Force for Translation Modes

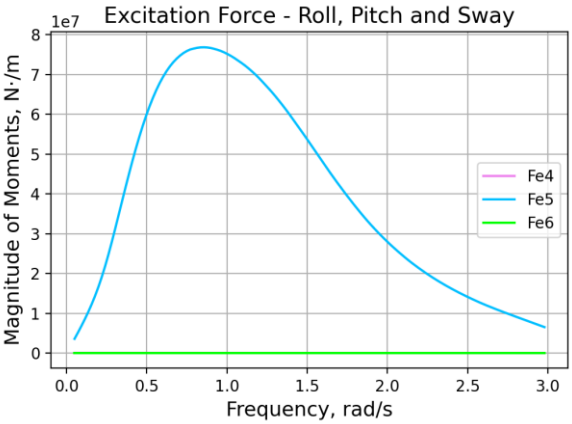

Figure 4-15 OC3: Excitation Force for Rotational Modes

Natural Frequencies & RAO's

As viscous effects are not considered in Nemoh, a small percentage of critical damping is used instead. Commonly a minimum of 2% is used to account for the viscous effects, but the percentage might be different depending on the motion. In this study the % of viscous damping is found by trial and error for both heave and pitch by comparing the RAO's with the reference RAO's. It was found that 4% is suitable for pitch, while 3.8% is suitable for heave. The natural frequency for heave is shown in figure 4-20 and is close to 0.199 rad/s, as expected this is where

the heave RAO has its peak value. The result is similar to the natural frequency of 0.201 rad/s given in the reference. Moreover, the natural frequency for pitch is close to 0.237 rad/s, and as expected this resides with the peak of the RAO. However, the pitch natural frequency is shifted from the reference value of 0.0214 rad/s. This might be explained due to a different mass distribution, mooring, viscous damping etc. It should also be noted that the previous results for excitation and damping had also where shifted to a higher frequency. The RAO's with and without critical damping are also shown in in figure 4-16 to 4-19.

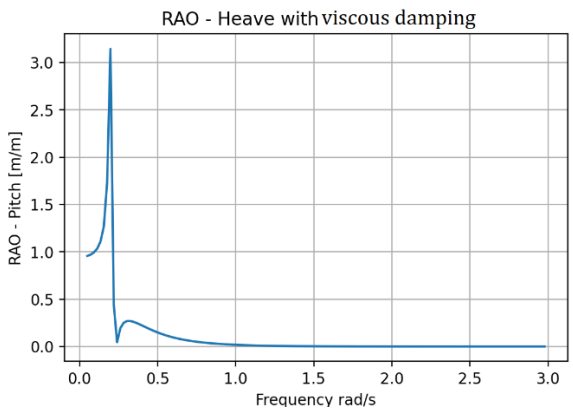

Figure 4-16 RAO Heave with Viscous Damping

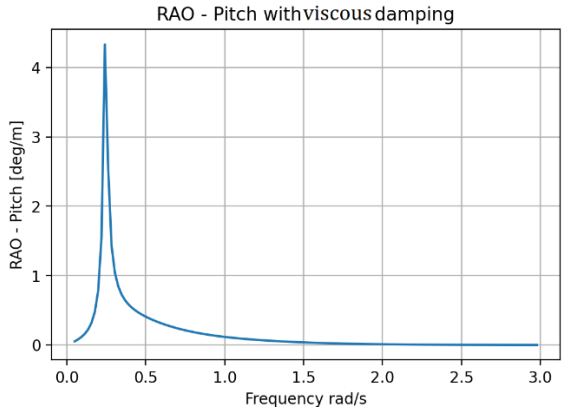

Figure 4-17 RAO Pitch with Viscous Damping

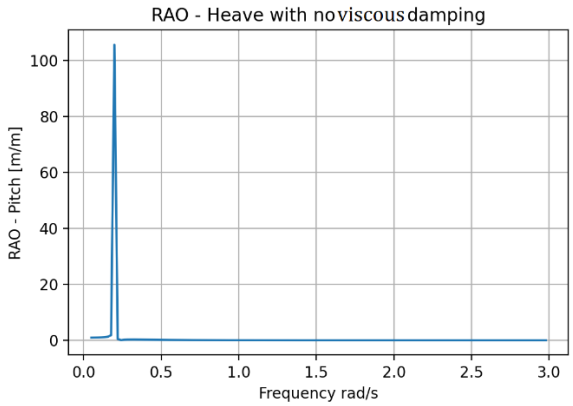

Figure 4-18 RAO Heave Without Viscous Damping

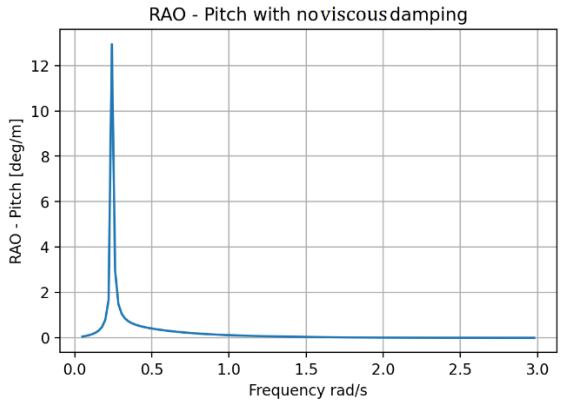

Figure 4-19 RAO Pitch Without Viscous Damping

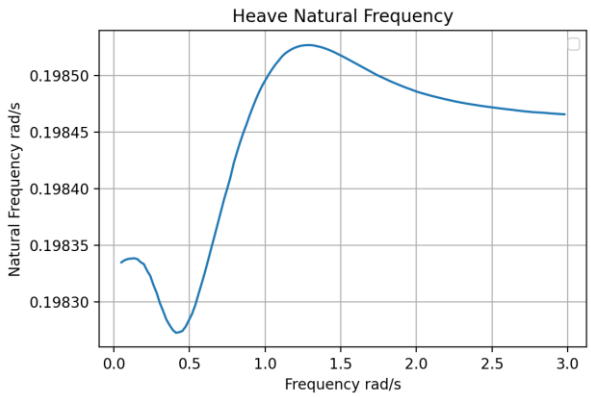

Figure 4-20 Heave Natural Frequency

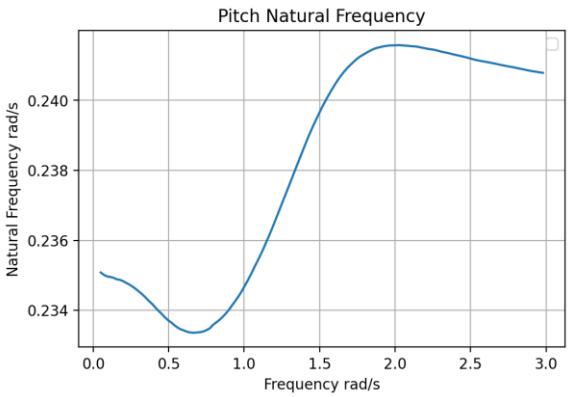

Figure 4-21 Pitch Natural Frequency

4.2.2 Results from Nemoh

In order to analyse the hydrodynamic responses for the geometries, the hydrodynamic results from Nemoh is plotted for the geometries with a fixed height at $H_L = 97.8m$ with radius R_L as a variable. The results show how the linear damping, added mass, phase angle and excitation force changes with varying radius. The RAO, natural frequency, viscous damping, and spring stiffness for the geometries are plotted. The results are plotted for the DoF's with the highest responses, namely for pitch and heave motions. The results are shown in figure 4-22 to 4-29, the results for pitch are discussed first, then the results for heave afterwards.

Pitch

When the radius increases the hydrodynamic properties increases as well. The spring stiffness C55 changes with the radius due to a larger displaced volume and a larger metacentric height $\overline{GM}$. This is because an increase in radius causes an increase in the ballast mass, further this increases the depth to the CoG from the SWL. Further, as H_L is fixed the CoB barely changes its position, hence the $\overline{GM}$ is also getting larger as the radius increases. From the calculations a higher radius increases the pitch RAO, whereas the peak of the RAO corresponds to the natural frequency (see figure 4-29).

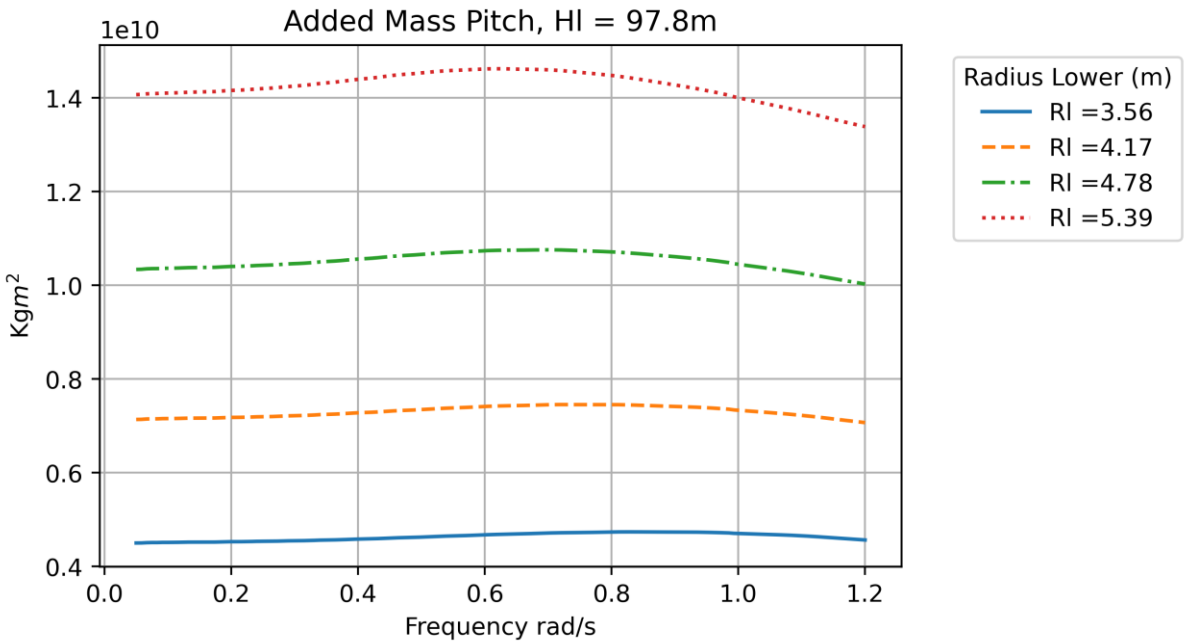

Figure 4-22 Added Mass for Pitch, Hl=97.8 m

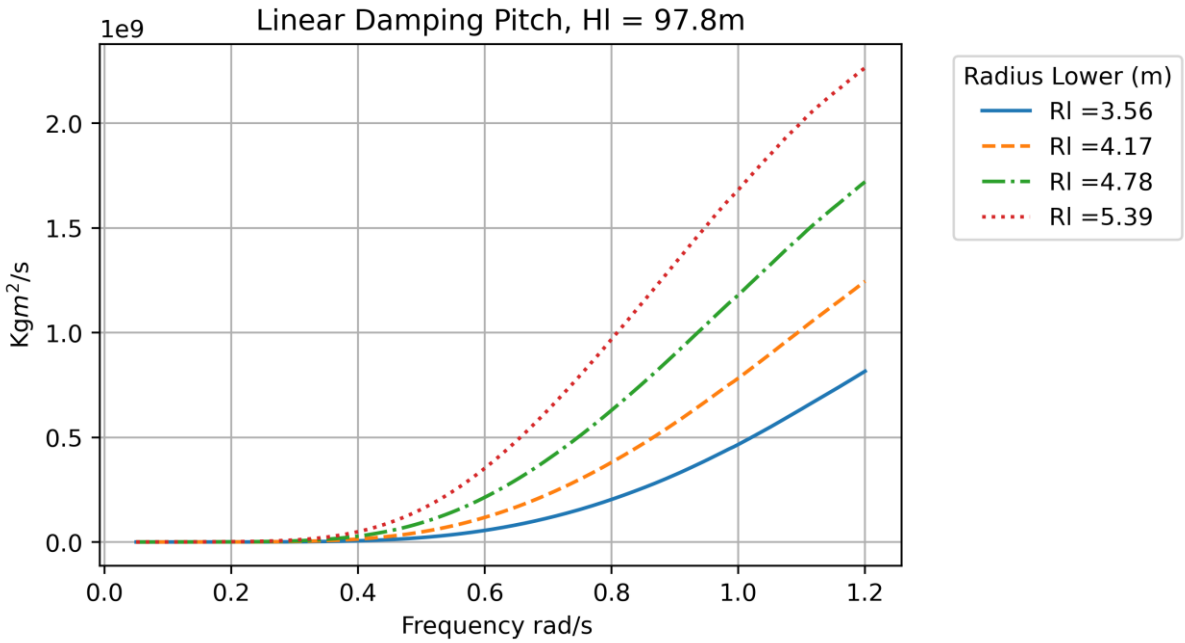

Figure 4-23 Linear Damping Pitch, Hl=97.8 m

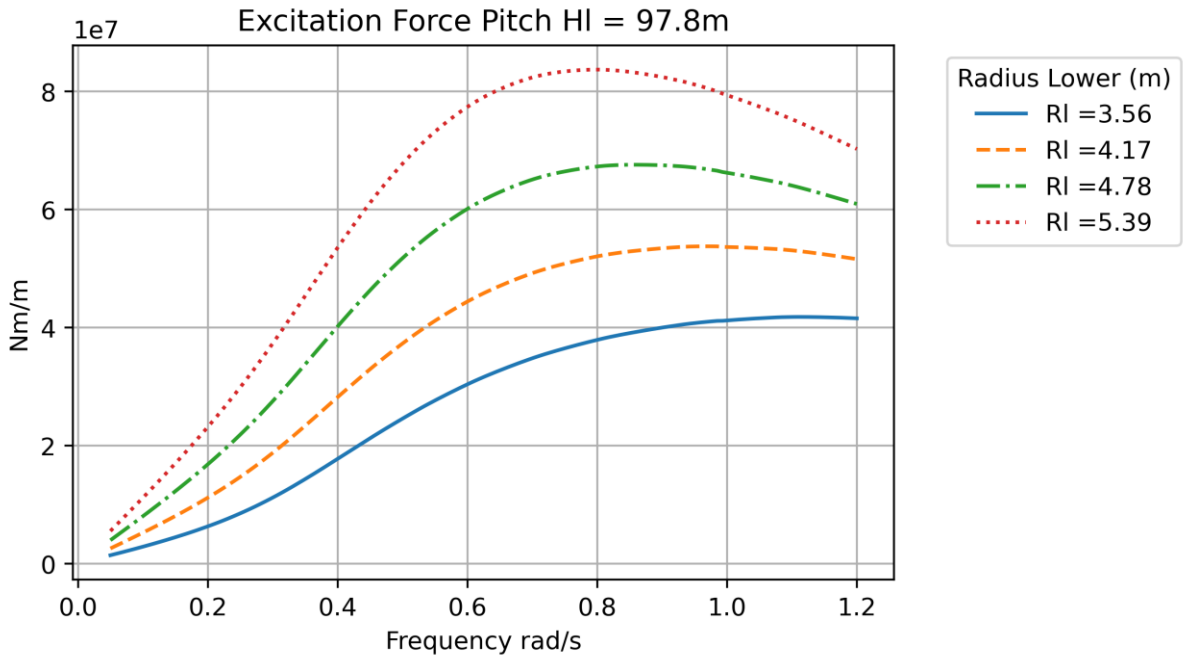

Figure 4-24 Excitation Force Pitch, Hl = 97.8 m

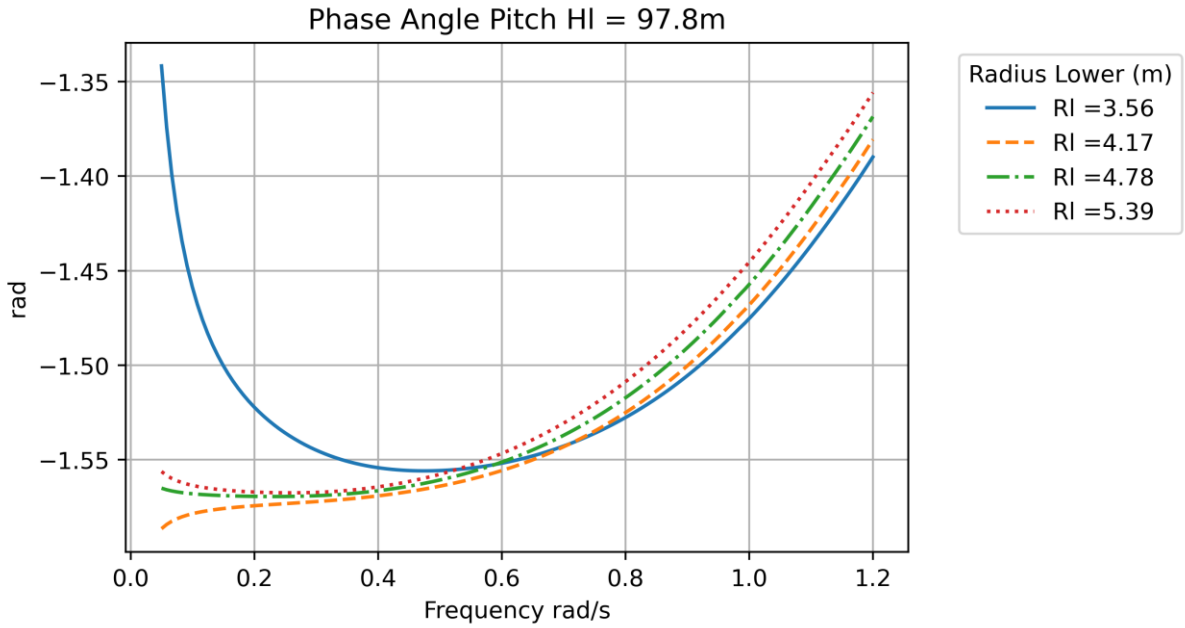

Figure 4-25 Phase Angle Pitch, Hl=97.8 m

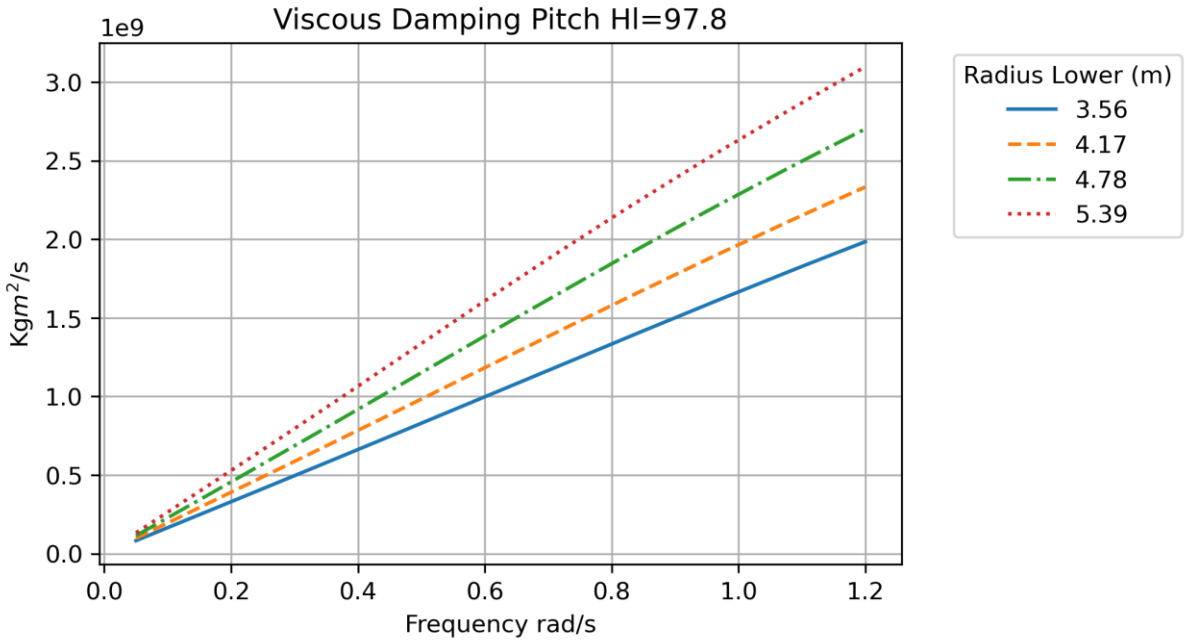

Figure 4-26 Viscous Damping Pitch, Hl=97.8 m

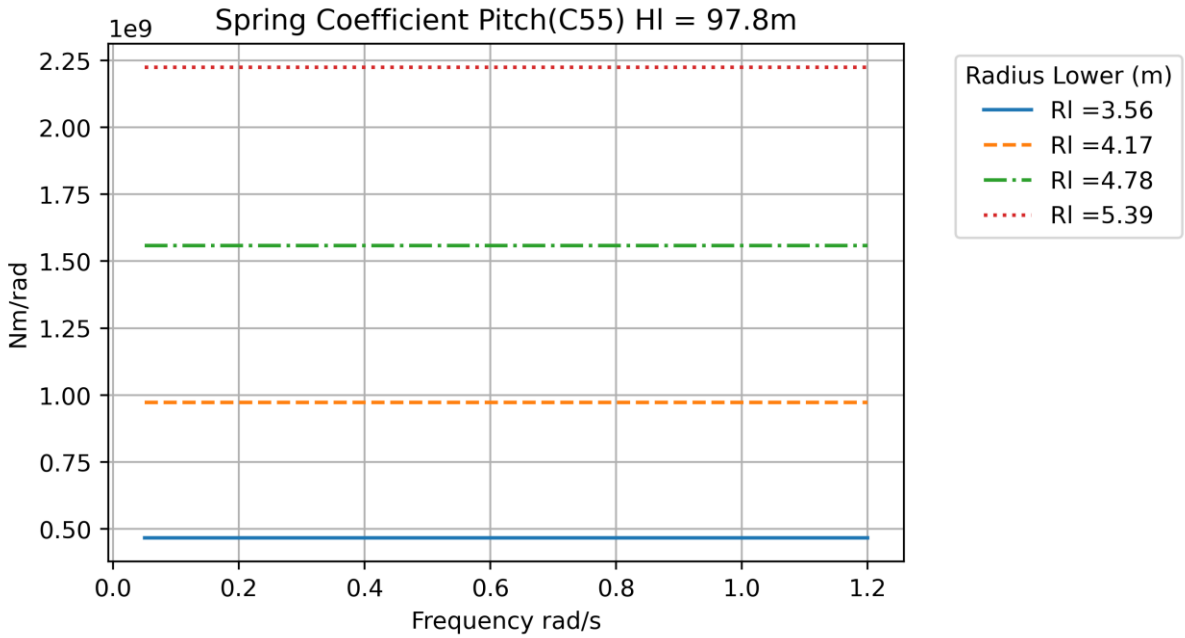

Figure 4-27 Spring Coefficient Pitch, , Hl=97.8 m

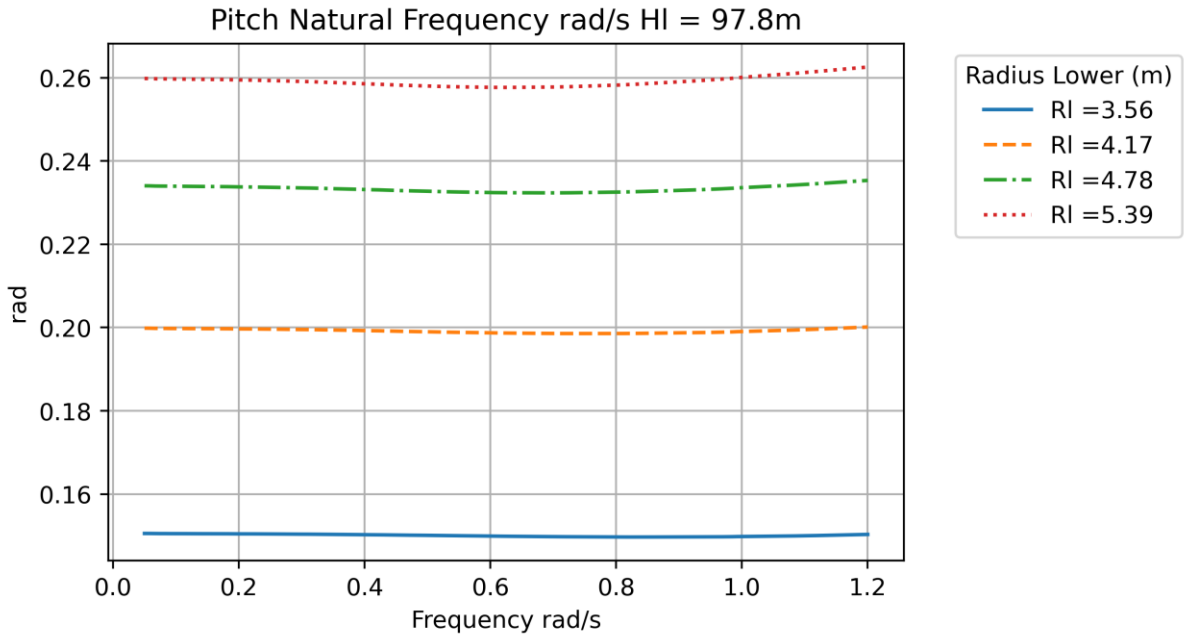

Figure 4-28 Pitch Natural Frequency, Hl=97.8 m

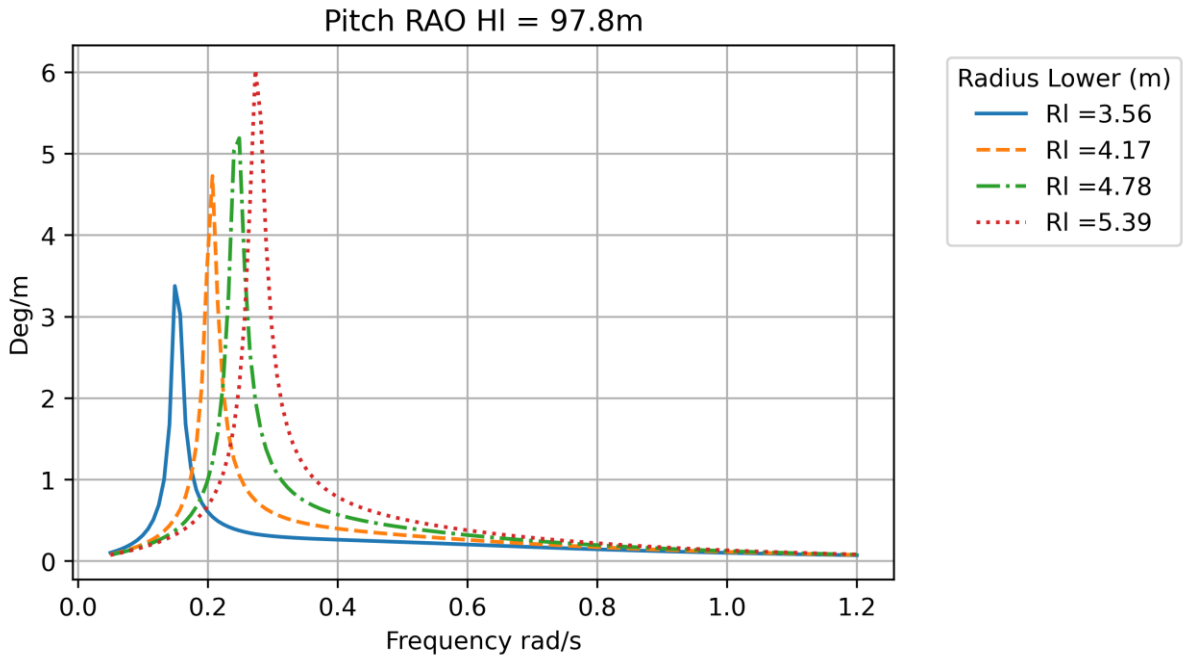

Figure 4-29 Pitch Rao, Hl=97.8 m

Heave

Figure 4-30 to 4-37. shows how the hydrodynamic properties for heave changes with respect to a change in radius. It should be noted that the spring stiffness C33 is the same for all geometries as the water plane area remains the same, thus the assumed viscous damping, i.e. the amount of critical damping does not increase at the same rate as it does for pitch. This causes the RAO for heave to be lower for a geometry with a larger radius than with a lower radius, it should also be noted that the natural frequencies correspond to the peaks of the RAO's.

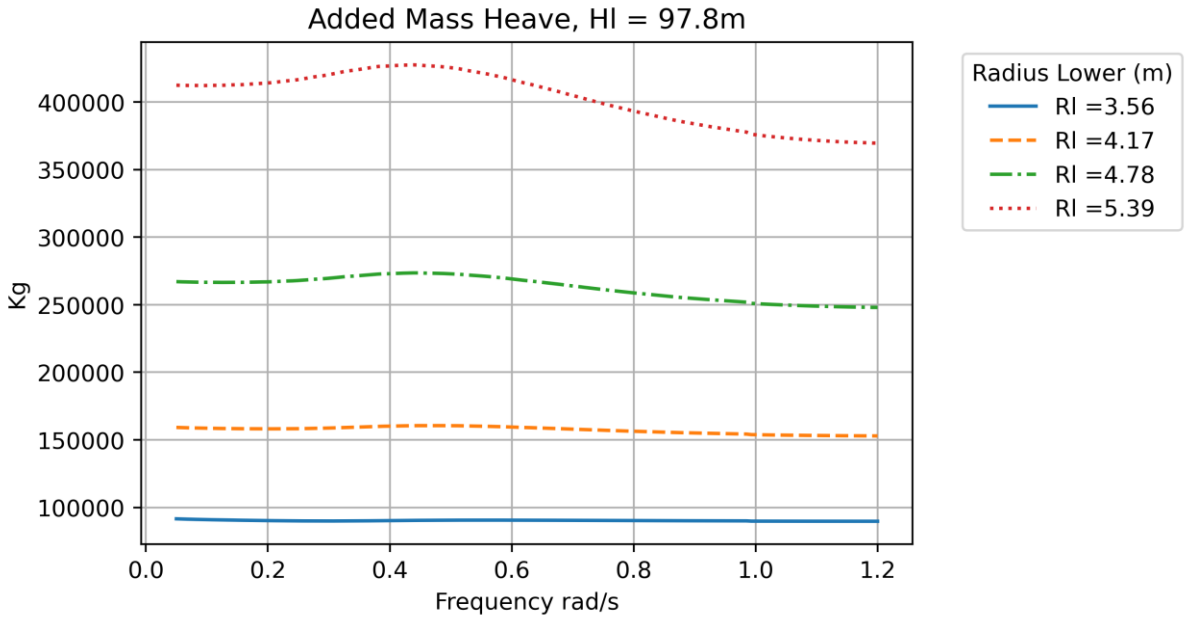

Figure 4-30 Added Mass Heave, Hl=97.8 m

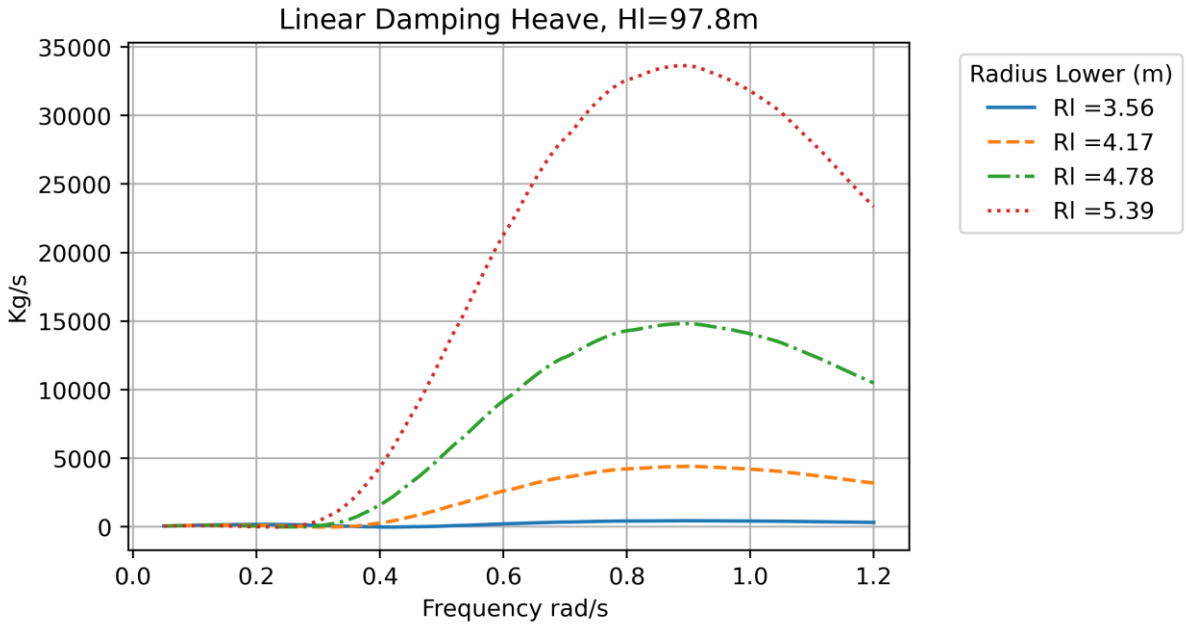

Figure 4-31 Linear Damping Heave, Hl=97.8 m

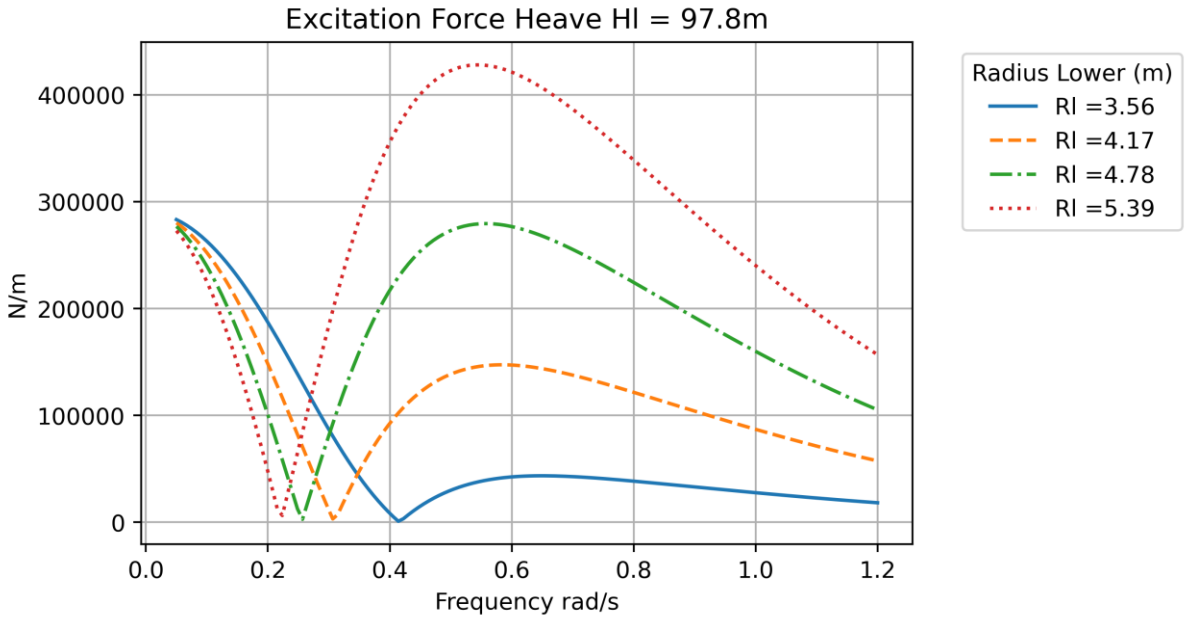

Figure 4-32 Excitation Force Heave, Hl=97.8 m

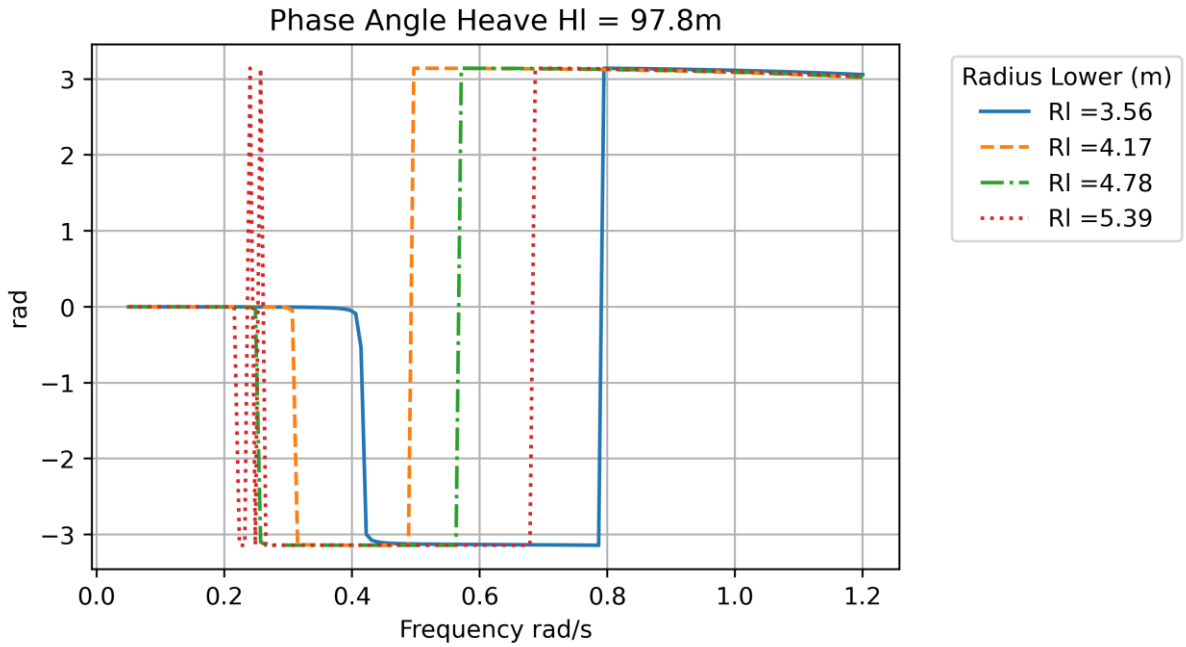

Figure 4-33 Phase Angle Heave, Hl=97.8 m

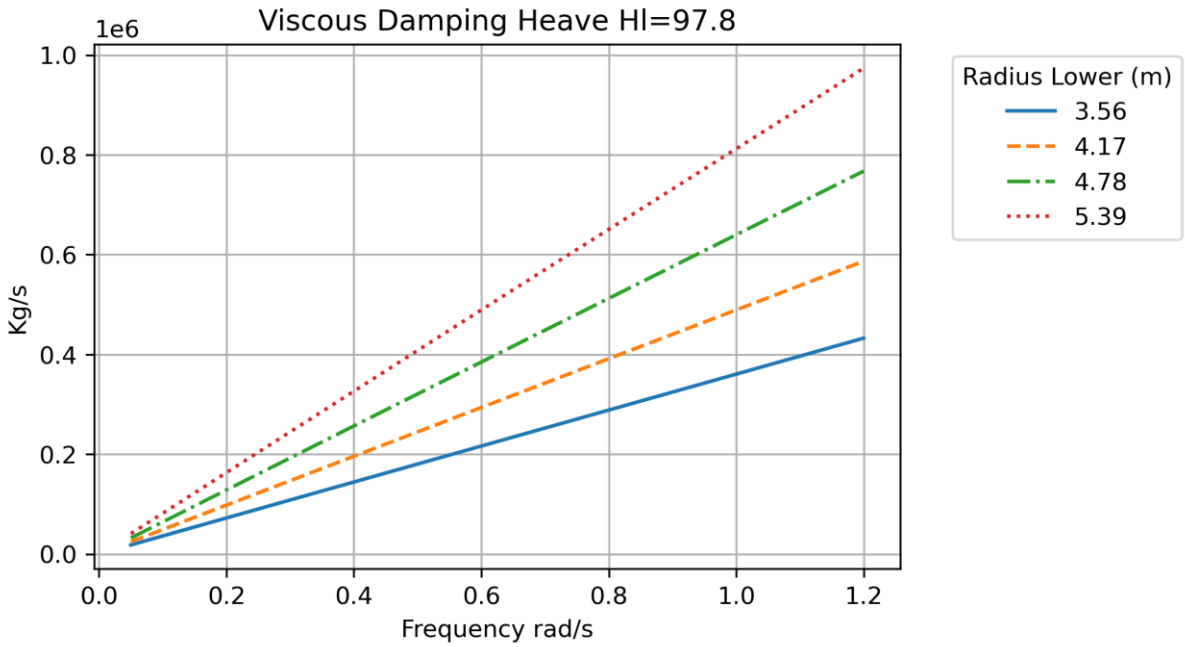

Figure 4-34 Viscous Damping Heave, Hl=97.8 m

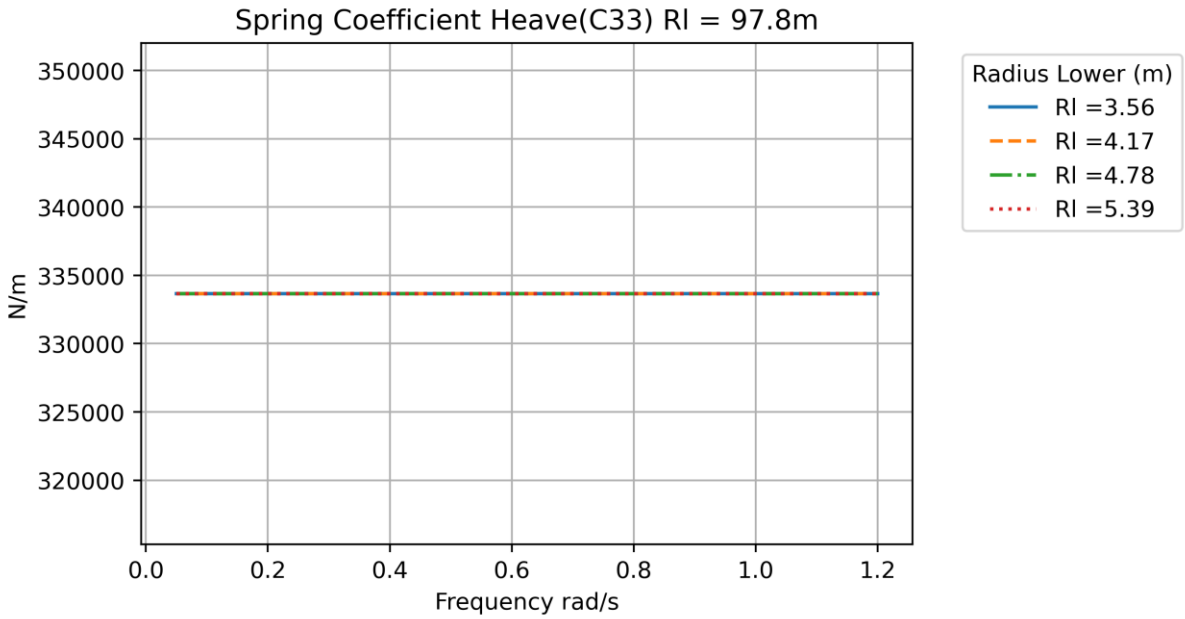

Figure 4-35 Spring Coefficient Heave, Hl=97.8 m

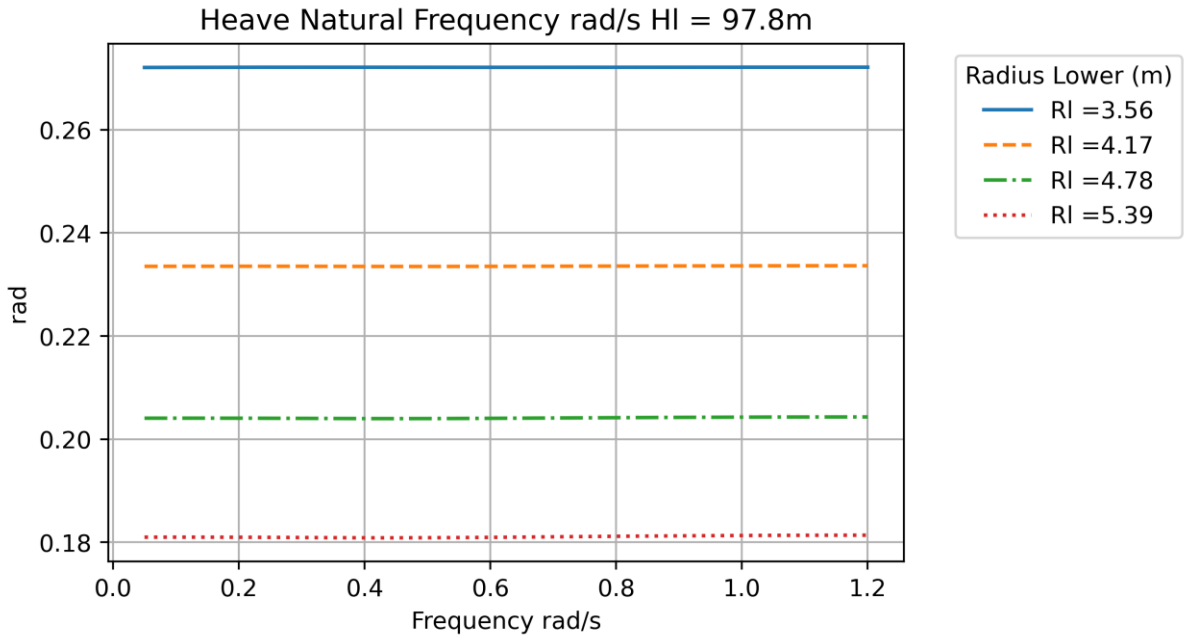

Figure 4-36 Heave Natural Frequency, Hl=97.8 m

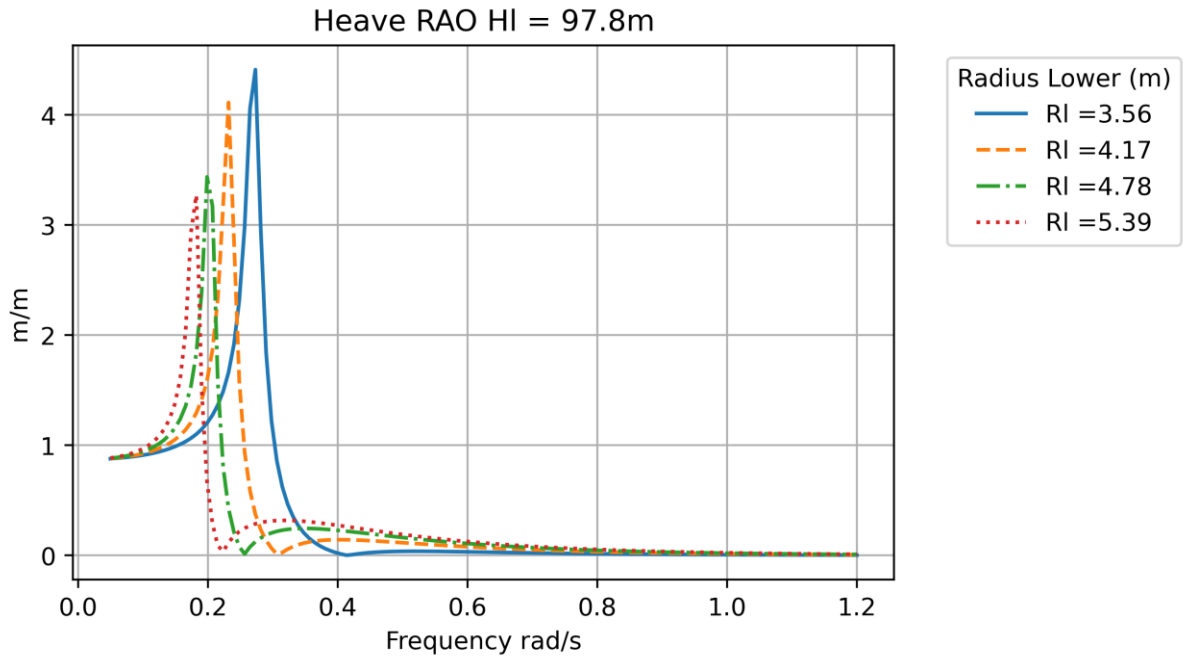

Figure 4-37 Heave Rao, Hl=97.8 m

The results show that as the radius gets larger, the RAO and the natural frequency for pitch increases. However, for the heave RAO it is the opposite, the RAO, and the natural frequency decreases. This is due to the fact that the spring stiffness for pitch is dependent on the displaced volume and the $\overline{GM}$, hence as for heave it is only dependant on the water plane area A_w. This affects the viscous damping equation (2.51) and the spring term in the RAO equation (2.52), which gives different results for the heave and pitch RAO.

4.2.3 Response Spectrums

The results from Nemoh are used to calculate the hydrodynamic responses for the sea states given in chapter 3.5. The longitudinal and vertical acceleration is calculated for the nacelle by applying equation (2.59) as written in chapter 2.4.3. Further, the most probable maximum pitch angle is calculated using equation (2.60). The results for the most significant responses, i.e. most probable maximum pitch angle for a 3-hour sea state, longitudinal acceleration as well as the standard deviation for pitch are plotted. The results displayed a similar trend for all the environmental conditions, thus the results for Environmental Condition 3 EC-3 and Environmental Condition 5 EC-5 are discussed in the following section.

EC3 and EC5

The results for the geometries calculated with EC-3 and EC-5 are as expected, considering the results from chapter 4.2.2, the results for EC-3 and EC-5 are plotted in figure 4-38 to 4-43. The MPM 3-hour pitch angle and longitudinal acceleration increases as the radius gets larger, however for EC-3 neither constraint g_1 for maximum pitch angle or g_2 for maximum acceleration is exceeded. However, it should be noted that the maximum values appear at the maximum radius but not with the maximum height, this is because of the natural frequency of the structures with the highest response is closer to the peak values of the wave spectrum. However, for extreme conditions in EC-5 constraint g_1 and g_2 are both exceeded, it is also seen that the maximum responses correspond to the largest structures. Further, as the constraints only apply for operating conditions, the geometries are still accounted for during the optimization procedure.

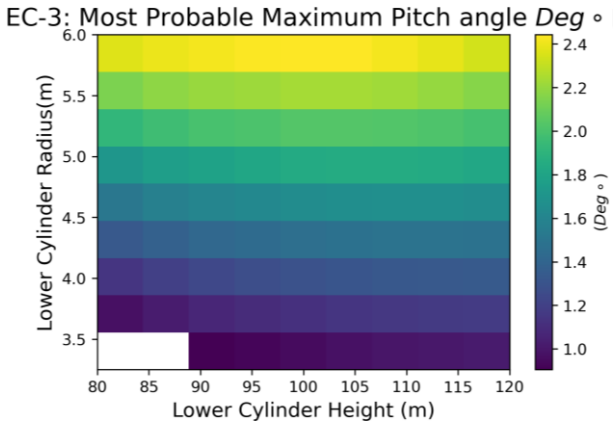

Figure 4-38 EC-5 Most Probable Maximum Pitch Angle

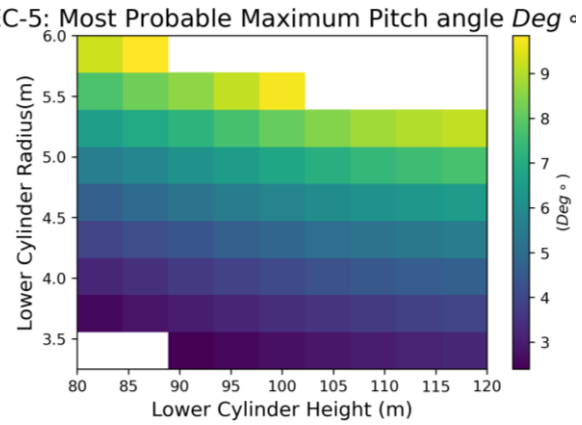

Figure 4-39 EC3: Most Probable Maximum Pitch Angle

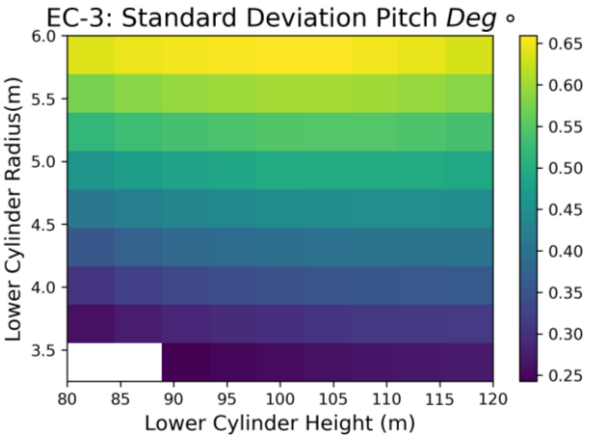

Figure 4-40 EC-5 Standard Deviation Pitch

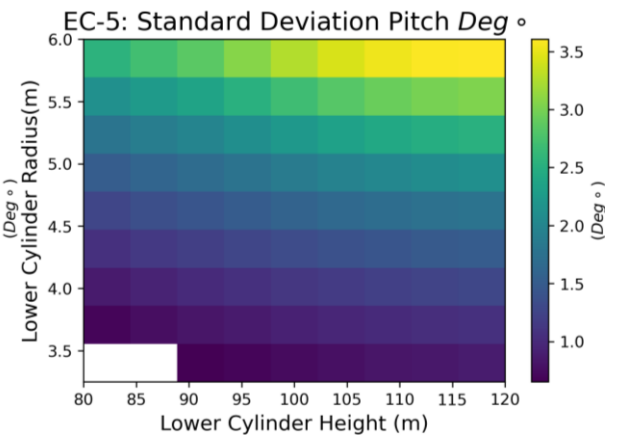

Figure 4-41 EC-3 Standard Deviation Pitch

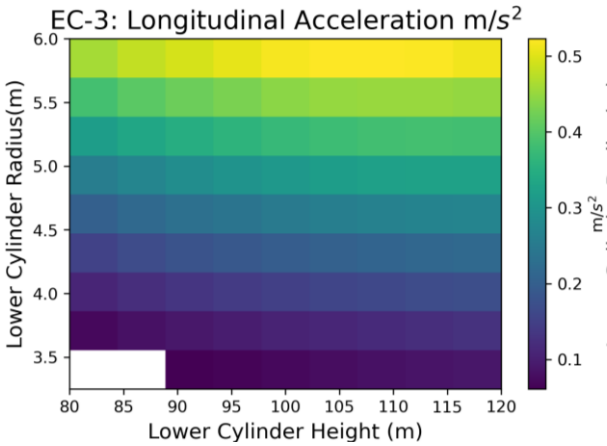

Figure 4-42 EC-5 Longitudinal Acceleration

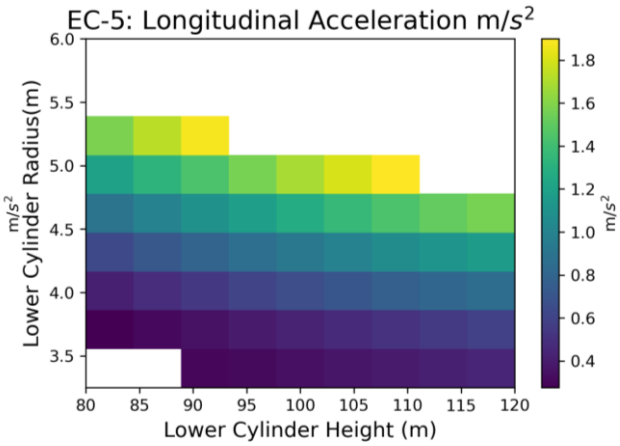

Figure 4-43 EC-3 Longitudinal Acceleration

4.3 Optimization Process

For the optimization process the price coefficients for steel and ballast are $a_{Steel} = 0.99$ and $a_{Ballast} = 0.01$. This is because of the complexity and manufacturing of steel, thus the price is assumed to be a lot larger than the price for the ballast. During conversations with the construction manager's at Equinors Hywind Tampen the price for one ton of Olivine is 95 kr. But as Hywind Tampen is a concrete structure the price for steel was not given, however it is assumed to be dominating and a lot larger than 95 kr each ton.

For the optimization procedure 6 different weights are assigned between 0 and 1, the objective function is then expressed as, with the results presented in figure 4-22:

$$minimize: F(x) = w_1 f_1(x) + (1 - w_1) f_{2\,Converted}(x) \quad (4.1)$$

$$For: w_1 = [0, 0.2, 0.4, 0.6, 0.8, 1]$$

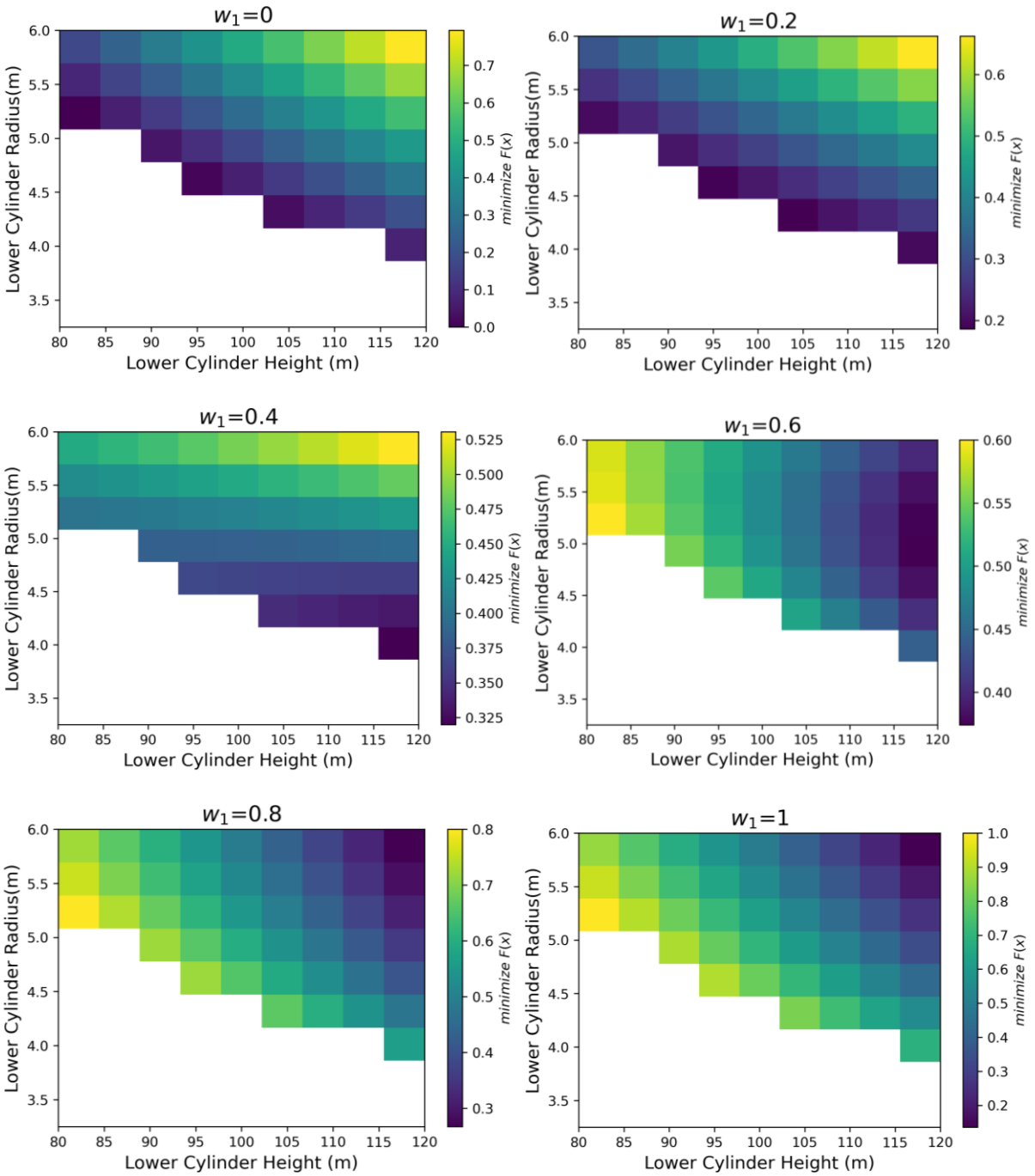

Figure 4-44 minimize: $F(x) = w_1 f_1(x) + (1 - w_1) f_{2\,Converted}(x)$, *For:* $w_1 = [0, 0.2, 0.4, 0.6, 0.8, 1]$

From the results, five different optimum geometries are found as $w_1 = 0.8$ and $w_1 = 1$ corresponds to the same geometry. Whereas $w_1 = 1$ equals to the optimum geometry for objective function $F_2(x)$ corresponding to the maximum metacentric height $\overline{GM}$, i.e. the most stable geometry and, $w_1 = 0$ corresponds to objective function $F_1(x)$ corresponding to the cheapest geometry. The optimum geometries, weights, normalized cost and $\overline{GM}$ are presented

in table 4-1, the optimum geometries with respect to their performance criteria's for operational conditions in Environmental Condition 3 are presented in table 4-2:

w_1	$Optimum\ Geometry\ [H_L, R_L]$	$Normalized\ Cost$	$\overline{GM}\ (m)$
0	$[80\ m, 5.08\ m]$	0	15.22
0.2	$[102.2\ m, 4.16m]$	0.026	18.33
0.4	$[120m, 3.86m]$	0.12	22.44
0.6	$[120m, 4.77m]$	0.49	28.57
0.8 and 1	$[120m, 6m]$	1	32.96

Table 4-1 The optimum geometries, Normalized Cost of the geometry and $\overline{GM}$ with respect to different weights

w_1	$Optimum\ Geometry$ $[H_L, R_L]$	$g_1 = \alpha^{3h}$ (Deg)	$g_2 = \sigma_{acc}$ $(\frac{m}{s^2})$	$g_4 = \alpha_{static\ heel}$ (Deg)
0	$[80\ m, 5.08\ m]$	1.91	0.32	6.63
0.2	$[102.2\ m, 4.16m]$	1.48	0.21	6.99
0.4	$[120m, 3.86m]$	1.33	0.18	6.12
0.6	$[120m, 4.77m]$	1.79	0.33	3.31
0.8 and 1	$[120m, 6m]$	2.46	0.57	1.89

Table 4-2 Performance criteria's for the optimum geometries for operational conditions in EC3

The results presented in table 4-1 shows a significant increase in normalized cost, relative to the relation between the lower cylinder radius R_L. The largest increase appears from $w_1 = 0.6$, $[H_L, R_L] = [120m, 4.77m]$ to $w_1 = 0.8$ or $w_1 = 1$, $[H_L, R_L] = [120m, 6m]$, where the difference in normalized cost is 51%. This is because of a large increase in steel and ballast volume, for the same change in geometry the metacentric height $\overline{GM}$ is only improved by 4.46 m. Further there is an increase in performance criteria's $g_1 = \alpha^{3h}$ and $g_2 = \sigma_{acc}$ (see table 4-2), however these are well within the range of acceptable values. Moreover performance criteria $g_4 = \alpha_{static\ heel}$ is almost reduced by ca 43% (see table 4-2), this is because of the larger submerged volume ∇ and $\overline{GM}$ causing an increase of the pitch spring stiffness C_{55}. From $w_1 = 0.4$, $[H_L, R_L] = [120m, 3.86m]$ to $w_1 = 0.6$, $[H_L, R_L] = [120m, 4.77m]$, there is also a large increase of normalized cost of 37% (see table 4-2), whereas the increase in $\overline{GM}$ is 6.13 m (see

table 4-1), thus there is a larger increase in $\overline{GM}$ and a smaller increase in normalized cost compared with the changes from $w_1 = 0.6$ to $w_1 = 0.8$ or $w_1 = 1$. However, there is a large improvement of performance criteria $g_4 = \alpha_{static\ heel}$, with a reduction of 2.81 degrees. Thus, the initial stability is a lot better for the optimum weighted with $w_1 = 0.6$, $[H_L, R_L] = [120m, 4.77m]$.

The objective functions consider cost and stability $\overline{GM}$, where all the performance criteria's are fulfilled, hence the combined objective function weighted with $w_1 = 0$, $[H_L, R_L] = [80\ m, 5.08\ m]$ being the cheapest structure, where the stability $\overline{GM} = 15.22\ m$ is assumed to be acceptable, as it is larger than $\overline{GM} = 11.32\ m$ for the optimum Spar-Buoy derived from Ghigo et.al [34]. However, as the aerodynamic effects on the wind turbine are not taken into consideration in this thesis, a more conservative optimum would be to choose the optimum weighted with $w_1 = 0.4$, $[H_L, R_L] = [120m, 3.86m]$. Where the structure gives the best trade-off between objective functions for cost and $\overline{GM}$, where all the performance criterions are fulfilled, it is also the structure which has the lowest response for performance criteria's $g_1 = \alpha^{3h}$ and $g_2 = \sigma_{acc}$, hence it is assumed to have a better aerodynamic response as well.

5 Conclusion and Future Work

5.1 Conclusion

In this thesis, a hydrostatic and hydrodynamic analysis on Spar-Buoy foundations using open-source programs is performed, in order to estimate the hydrodynamic performance of Spar-Buoy geometries with varying height H_L and radius R_L of the lower cylinder of the structure. To do so an automated simulation procedure is created using the open-source programs Salome, Nemoh and Python. The automated procedure simulates the hydrodynamic properties with respect to the hydrostatic and structural properties. After the simulations are performed an analysis procedure is performed in the following manner. First the hydrostatic properties are analysed using colorplots. The results are as expected, and shows that an increase in the lower cylinder height H_L and radius R_L, increases the Spar-Buoys properties such as the CoG, CoB, $\overline{GM}$, ballast mass, pitch spring stiffness C_{55} and displaced volume ∇. Further, performance constraints g_3 and g_4 concerning the hydrostatic stability of the Spar-Buoy is analysed, the results show's that 39% of the geometries does not fulfil the one or both of the stability constraints (see chapter 4.1.1).

Secondly a comparison of the first order wave loads simulated in Nemoh, for a geometry with the same dimensions as the OC3 baseline geometry is performed. The results are very similar for translational motions, however the rotational motions have similar values but at a different frequency. The results are assumed to be different due to not implementing viscous effects, as well differences in the structural properties such as the ballast material, wall thickness and coordinate systems (see chapter 4.2.1). The results are used to calculate a percentage of critical damping which is substituted as the viscous damping for further analysis.

Lastly a hydrodynamic analysis is performed, where the hydrodynamic response for five environmental condition's is calculated and the performance criterions for pitch angle and acceleration at the nacelle is analysed. The results imply that an increase in H_L and R_L increases the motion response, more so for an increase in R_L than an increase in H_L. Lastly an optimization procedure is implemented, where the geometries which does not fulfil the hydrostatic and hydrodynamic constraints are eliminated. Further, a combined objective function concerning cost and stability is applied to the remaining structures. The optimum

geometry is then chosen with variables $[H_L, R_L] = [120m, 3.86m]$, the results imply that this is the optimum geometry given the trade-off between cost and stability also fulfilling all the constraints, the normalized cost is 0.12 whereas the $\overline{GM} = 22.44\, m$ respectfully. Also, the results for response of the pitch angle $g_1 = \alpha^{3h}$ and acceleration $g_2 = \sigma_{acc}$ is the lowest for this structure compared to the other optimums.

5.2 Recommendations for Future Work

The automated simulation and optimization procedure created and utilized in thesis is based on simplifications and assumptions (see chapter 3.3.5). Whereas the automated simulation procedure developed in this thesis can be used as the foundations for future work using Salome, Nemoh and Python. The recommendations for future work would be the following:

- Implement numerical estimation of viscous effects using ITTC's recommended procedure for numerical estimation of viscous effects [35].
- Implement aerodynamic effect using an open-source program such as OpenFAST and analyse the coupled hydrodynamic and aerodynamic effects on the structure.
- Introduce mooring lines and their effects on the structure.
- Use the results from the automated simulation procedure to create a metamodel-based simulation optimization procedure.
- Increase the number of design variables, example for the upper cylinder or tapered section.
- Increase the number of constraints, example drift forces or suspension of mooring lines.

6 References

[1] IRENA, 2018. “Future of wind: Deployment, investment, technology, grid integration and socio-economic aspects,” Abu Dhabi, 2019b. [Online]. Available: https://www.irena.org/publications/2019/Oct/Future-of-wind

[2] “How Hywind works” [Online.] Available: https://www.equinor.com/en/what-we-do/floating-wind/how-hywind-works.html

[3] IRENA, 2019. “Global energy transformation: A roadmap to 2050 (2019 edition)” Abu Dhabi, 2019a. [Online]. Available: https://www.irena.org/publications/2019/Apr/Global-energy-transformation-A-roadmap-to-2050-2019Edition

[4] W. Musial, Sandy Butterfield, and A. Boone, 2004. “Feasibility of Floating Platform Systems for Wind Turbines,” presented at the 42nd AIAA Aerospace Sciences Meeting and Exhibit, Reno, Nevada. doi: 10.2514/6.2004-1007.

[5] M. Leimeister, A. Kolios, and M. Collu, 2018. “Critical review of floating support structures for offshore wind farm deployment,” J. Phys. Conf. Ser., vol. 1104, p. 012007. doi: 10.1088/1742-6596/1104/1/012007.

[6] P. Sclavounos, C. Tracy, and S. Lee, 2008. “Floating Offshore Wind Turbines: Responses in a Seastate Pareto Optimal Designs and Economic Assessment,” in Volume 6: Nick Newman Symposium on Marine Hydrodynamics; Yoshida and Maeda Special Symposium on Ocean Space Utilization; Special Symposium on Offshore Renewable Energy, Estoril, Portugal, pp. 31–41. doi: 10.1115/OMAE2008-57056.

[7] J.M.J. Journée and W.W. Massie, 2001. Offshore Hydrodynamics. Delft University of Technology.

[8] C. Y. A and C. J. M, 2018. Fluid Mechanics, Fundamentals and Applications, Fourth Edition in SI Units. Mc Graw Hill.

[9] D. Manley St and P. Willard J, 1953. “On the motions of ships in confused seas,”.

[10] S. Haver, 2018. Metocean Modeling and Prediction of Extremes. UiS, NTNU.

[11] L. Bergdahl, 2009. Wave-Induced Loads and Ship Motions. Goteborg, Sweden: Chalmers University of Technology.

[12] O. Faltinsen, 1993. Sea Loads on Ships and Offshore Structures. Trondheim, Norway: Cambridge.

[13] J. Jonkman, S. Butterfield, W. Musial, and G. Scott, 2009. "Definition of a 5-MW Reference Wind Turbine for Offshore System Development," National Renewable Energy Lab. (NREL), Golden, CO (United States), NREL/TP-500-38060,2009. doi: 10.2172/947422.

[14] J. Jonkman, 2010. "Definition of the Floating System for Phase IV of OC3," National Renewable Energy Lab, Golden, CO (United States), NREL/TP-500-47535, 979456. doi: 10.2172/979456.

[15] A. L. H. Hopstad, K. Argyriadis, A. Manjock, J. Goldsmith, and K. O. Ronold, 2018. "DNV GL Standard for Floating Wind Turbines,". doi: 10.1115/IOWTC2018-1035.

[16] M. Borg and M. Collu, Jan. 2016. "Design of floating offshore wind turbines," Offshore Wind Farms, pp. 359–385. doi: 10.1016/B978-0-08-100779-2.00011-8.

[17] A. Rasekhi Nejad, E. E. Bachynski, and T. Moan, 2017. "On Tower Top Axial Acceleration and Drivetrain Responses in a Spar-Type Floating Wind Turbine," in Volume 9: Offshore Geotechnics; Torgeir Moan Honoring Symposium, Trondheim, Norway, p. V009T12A009. doi: 10.1115/OMAE2017-62314.

[18] L. Li, Z. Jiang, M. C. Ong, and W. Hu, 2019. "Design optimization of mooring system: An application to a vessel-shaped offshore fish farm," Eng. Struct., vol. 197, p. 109363, doi: 10.1016/j.engstruct.2019.109363.

[19] C. Ng and L. Ran, 2016 "Offshore Wind Farms - 1st Edition,", https://www.elsevier.com/books/offshore-wind-farms/ng/978-0-08-100779-2

[20] M. Leimeister, A. Kolios, M. Collu, and P. Thomas, 2020. “Design optimization of the OC3 phase IV floating spar-buoy, based on global limit states,” Ocean Eng., vol. 202, p. 107186, doi: 10.1016/j.oceaneng.2020.107186.

[21] B. Bulder et al., 2002 “Study to feasibility of and boundary conditions for floating offshore wind turbines,”.

[22] M. Hansen, 2015. “One-dimensional momentum theory for an ideal wind turbine,” in Aerodynamics of Wind Turbines, 3rd ed., Routledge.

[23] A. Ghigo, L. Cottura, R. Caradonna, G. Bracco, and G. Mattiazzo, 2020. “Platform Optimization and Cost Analysis in a Floating Offshore Wind Farm,” J. Mar. Sci. Eng., vol. 8, no. 11, Art. no. 11, doi: 10.3390/jmse8110835.

[24] M. Leimeister, M. Collu, and A. Kolios, 2020. “A fully integrated optimization framework for designing a complexgeometry offshore wind turbine spar-type floating support structure,” Design methods, reliability and uncertainty modelling, preprint. doi: 10.5194/wes-2020-93.

[25] E. Bachynski, 2018. “Fixed and Floating Offshore Wind Turbine Support Structures,”, pp. 103–142. doi: 10.1002/9781119097808.ch4.

[26] L. Lang, H. Zhiqiang, J. Wange, and H. Quihao, 2014 . “Dynamic responses of a semi-type offshore floating wind turbine during normal state and emergency shutdown,”. https://www.researchgate.net/publication/271197957_Dynamic_responses_of_a_semi-type_offshore_floating_wind_turbine_during_normal_state_and_emergency_shutdown

[27] M. Leimeister, A. Kolios, and M. Collu, 2020. “Development and Verification of an Aero-Hydro-Servo-Elastic Coupled Model of Dynamics for FOWT, Based on the MoWiT Library,” Energies, vol. 13, no. 8, Art. no. 8, doi: 10.3390/en13081974.

[28] R. Hegyessy, 2016. “Classification of Olivin 02,” NIVA, p. 23.

[29] L. Li, Z. Gao, and T. Moan, 2015. “Joint Distribution of Environmental Condition at Five European Offshore Sites for Design of Combined Wind and Wave Energy Devices,” J. Offshore Mech. Arct. Eng., vol. 137, no. 031901, doi: 10.1115/1.4029842.

[30] “Salome Webpage.” https://www.salome-platform.org/

[31] G. Parisella and T. P. Gourlay, 2016. “Comparison of open-source code Nemoh with Wamit for cargo ship motions in shallow water,” CMST, p. 39.

[32] E. Andersson, 2018. Application of the open sourcecode Nemoh for modelling ofadded mass and damping in shipmotion simulations. [Online]. Available: http://urn.kb.se/resolve?urn=urn:nbn:se:kth:diva-239044

[33] G. K. V. Ramachandran, A. Robertson, J. M. Jonkman, and M. D. Masciola, 2013. “Investigation of Response Amplitude Operators for Floating Offshore Wind Turbines: Preprint,” National Renewable Energy Lab. (NREL), Golden, CO (United States), NREL/CP-5000-58098. [Online]. Available: https://www.osti.gov/biblio/1087800-investigation-response-amplitude-operators-floating-offshore-wind-turbines-preprint

[34] A. Ghigo, L. Cottura, R. Caradonna, G. Bracco, and G. Mattiazzo, 2020. “Platform Optimization and Cost Analysis in a Floating Offshore Wind Farm,” J. Mar. Sci. Eng., vol. 8, p. 835, doi: 10.3390/jmse8110835.

[35] ITTC, 2011. “ITTC – Recommended Procedures, Numerical Estimation of Roll Damping.” ITTC, [Online]. Available: https://ittc.info/media/4182/75-02-07-045.pdf

Appendix A

A.1 Baseline Spar-Buoy Salome-Python

```
#!/usr/bin/env python

###
### This file is generated automatically by SALOME v9.6.0 with dump python
###



import sys
import salome


salome.salome_init()
import salome_notebook
notebook = salome_notebook.NoteBook()
sys.path.insert(0, r'C:/Users/Torstein/Desktop/SALOME-9.6.0/twodim')

###
### GEOM component
###

import GEOM
from salome.geom import geomBuilder
import math
import SALOMEDS



Hl =
Rl =
Hu =
Ru =
Rl =

Ht = 8

geompy = geomBuilder.New()

O = geompy.MakeVertex(0, 0, 0)
OX = geompy.MakeVectorDXDYDZ(1, 0, 0)
OY = geompy.MakeVectorDXDYDZ(0, 1, 0)
OZ = geompy.MakeVectorDXDYDZ(0, 0, 1)
Cylinder_1 = geompy.MakeCylinder(O, OZ, Ru, Hu)
Cone_1 = geompy.MakeConeR1R2H(Rl, Ru, Ht)
Cylinder_2 = geompy.MakeCylinderRH(Rl, Hl)
geompy.TranslateDXDYDZ(Cylinder_1, 0, 0, -Hu)
geompy.TranslateDXDYDZ(Cone_1, 0, 0, -(Hu+8))
geompy.TranslateDXDYDZ(Cylinder_2, 0, 0, -(Hu+Hl+8))
Fuse_1 = geompy.MakeFuseList([Cylinder_1, Cone_1, Cylinder_2], True, True)
[Face_1,Face_2,Face_3,Face_4,Face_5] = geompy.ExtractShapes(Fuse_1,
                                                geompy.ShapeType["FACE"], True)
geompy.addToStudy( O, 'O' )
geompy.addToStudy( OX, 'OX' )
geompy.addToStudy( OY, 'OY' )
geompy.addToStudy( OZ, 'OZ' )
geompy.addToStudy( Cylinder_1, 'Cylinder_1' )
geompy.addToStudy( Cone_1, 'Cone_1' )
geompy.addToStudy( Cylinder_2, 'Cylinder_2' )
geompy.addToStudy( Fuse_1, 'Fuse_1' )
```

```
geompy.addToStudyInFather( Fuse_1, Face_1, 'Face_1' )
geompy.addToStudyInFather( Fuse_1, Face_2, 'Face_2' )
geompy.addToStudyInFather( Fuse_1, Face_3, 'Face_3' )
geompy.addToStudyInFather( Fuse_1, Face_4, 'Face_4' )
geompy.addToStudyInFather( Fuse_1, Face_5, 'Face_5' )

###
### SMESH component
###

import  SMESH, SALOMEDS
from salome.smesh import smeshBuilder

smesh = smeshBuilder.New()
#smesh.SetEnablePublish( False ) # Set to False to avoid publish in study if
#                                  not needed or in some particular situations:
# multiples meshes built in parallel, complex and numerous mesh edition
#(performance)

Mesh_1 = smesh.Mesh(Face_1)
Regular_1D = Mesh_1.Segment()
Local_Length_1 = Regular_1D.LocalLength(3,None,1e-07)
RadialQuadrangle_1D2D = Mesh_1.Quadrangle(algo=smeshBuilder.RADIAL_QUAD)
Mesh_2 = smesh.Mesh(Face_2)
status = Mesh_2.AddHypothesis(Local_Length_1)
Regular_1D_1 = Mesh_2.Segment()
Quadrangle_2D = Mesh_2.Quadrangle(algo=smeshBuilder.QUADRANGLE)
Mesh_3 = smesh.Mesh(Face_3)
status = Mesh_3.AddHypothesis(Local_Length_1)
Regular_1D_2 = Mesh_3.Segment()
Quadrangle_2D_1 = Mesh_3.Quadrangle(algo=smeshBuilder.QUADRANGLE)
Mesh_4 = smesh.Mesh(Face_4)
status = Mesh_4.AddHypothesis(Local_Length_1)
Regular_1D_3 = Mesh_4.Segment()
Quadrangle_2D_2 = Mesh_4.Quadrangle(algo=smeshBuilder.QUADRANGLE)
isDone = Mesh_1.Compute()
isDone = Mesh_2.Compute()
isDone = Mesh_3.Compute()
isDone = Mesh_4.Compute()
Compound_Mesh_1 = smesh.Concatenate( [ Mesh_1.GetMesh(), Mesh_2.GetMesh(),
                    Mesh_3.GetMesh(), Mesh_4.GetMesh() ], 1, 1, 1e-05, False )


## Set names of Mesh objects
smesh.SetName(Regular_1D.GetAlgorithm(), 'Regular_1D')
smesh.SetName(Quadrangle_2D.GetAlgorithm(), 'Quadrangle_2D')
smesh.SetName(RadialQuadrangle_1D2D.GetAlgorithm(), 'RadialQuadrangle_1D2D')
smesh.SetName(Local_Length_1, 'Local Length_1')
smesh.SetName(Mesh_1.GetMesh(), 'Mesh_1')
smesh.SetName(Mesh_3.GetMesh(), 'Mesh_3')
smesh.SetName(Mesh_2.GetMesh(), 'Mesh_2')
smesh.SetName(Compound_Mesh_1.GetMesh(), 'Compound_Mesh_1')
smesh.SetName(Mesh_4.GetMesh(), 'Mesh_4')


if salome.sg.hasDesktop():
  salome.sg.updateObjBrowser()

try:
```

```
  Compound_Mesh_1.ExportDAT( r'C:/Users/Torstein/Desktop/SALOME-9.6.0/
                             twodim/Functions/DatFromSalome/Spar.dat' )
  print('ExportDat() Success')
  pass
except:
  print('ExportDAT() failed. Invalid file name?')
```

Appendix A

A.2 Automated Salome-Nemoh

```
import os
import time
import subprocess
import numpy as np
import matplotlib.pyplot as plt
import shutil

from Functions.DatFromSalome.CenterOF import *

from Functions.DatFromSalome.Variables import *


hl = np.linspace(80, 120, num = 10)
rl = np.linspace(3.25, 6, num = 10)

Hl = []
Rl = []
for i in hl:
    for j in rl:
        Hl.append([i,j])

Hlnew = np.array(Hl)

num = 100
i = 0
for i in range(num):
    os.chdir(r'C:\\Users\\Torstein\\Desktop\\SALOME-9.6.0\\twodim')

    Hl = str(Hlnew[i][0])
    Rl = str(Hlnew[i][1])
    Hu = str(4)
    Ru = str(3.25)
    Hll= Hlnew[i][0]
    Rll= Hlnew[i][1]
    Huu= 4
    Ruu= 3.25
    cog= str(-(Hll+Huu+Ht)+(center_of_mass(Hll, Rll, Huu, Ruu, Ht, t)))

#Changes the geometry variables to the i index of the sample size with N=num
    if i == i:
        a_file = open("Sparl.py", "r")
        print('File Opened')
        list_of_lines = a_file.readlines()
        list_of_lines[33] = "Hl = " + Hl + "\n"
        list_of_lines[33] = "Rl = " + Rl + "\n"
        list_of_lines[31] = "Hu = " + Hu + "\n"
        list_of_lines[32] = "Ru = " + Ru + "\n"

        a_file = open("Sparl.py", "w")
        a_file.writelines(list_of_lines)
        a_file.close()

#Changes directory, so the new geometry can be runned in SALOME
#and creates a .dat"
```

```
        os.chdir(r'C:\\Users\\Torstein\\Desktop\\SALOME-9.6.0')

        print ('Salome Start')
        output = subprocess.run("run_salome.bat -t twodim\\Spar1.py"
                                , capture_output=True).stdout
        print (output)

        subprocess.run("kill_salome.bat", shell=False)

#Checks if the new dat file is created,then changes the name to "Name(num).dat"
        if os.path.exists('twodim\Functions\DatFromSalome\Spar.dat'):
            os.rename('twodim\Functions\DatFromSalome\Spar.dat'
                      ,'twodim\Functions\DatFromSalome\Spar'
                      + str(i+33) + ".dat")
            print("First Finished")

#Changes directory in order to refresh the .cal fil for NEMOH
#simulation as well as updates the properties in the .cal file so that
#the cog and frequency are correct
        os.chdir(r'C:\\Users\\Torstein\\Desktop\\SALOME-9.6.0\\twodim\
                 \Functions\\DatFromSalome')
        if i == i:
            a_file = open("s2n.py", "r")
            list_of_lines = a_file.readlines()
            list_of_lines[14] = "Hl = " + Hl + "\n"
            list_of_lines[15] = "Rl = " + Rl + "\n"
            list_of_lines[16] = "Hu = " + Hu + "\n"
            list_of_lines[17] = "Ru = " + Ru + "\n"

            a_file = open("s2n.py", "w")
            a_file.writelines(list_of_lines)
            a_file.close()

        print('Starting s2n')
        from s2n import salome2Nemoh
        filename = "Spar" + str(i) + ".dat"
        symmetryXZ = "no"
        nodesNPanels = salome2Nemoh(filename, symmetryXZ,cog)

        # Checks if the nemoMesh.dat file is created from salome2nemohscript
        if os.path.exists('nemohMesh.dat'):
            print ('Salome2Nemoh Finished')
            print ('Nemoh Start')

            # Runs Nemoh calculation for "Name(num)" file
            runpreProcessor = subprocess.run("preProcessor.exe"
                                             , capture_output=True).stdout
            print(runpreProcessor)
            print('PreProcess')
            runSolver = subprocess.run("Solver.exe"
                                       , capture_output=True).stdout
            print(runSolver)
            print('Process')
            runpostProcessor = subprocess.run("postProcessor.exe"
                                              , capture_output=True).stdout
            print(runpostProcessor)
            print('PostProcess')


            # Calculates the hydrodynamic responses from NEMOH output files
```

```
if os.path.exists('Results/RadiationCoefficients.tec'):
    print('Salome2Nemoh Finished!')
    os.rename("Results",("Results" + str(i)))
    os.rename("Mesh",("Mesh" + str(i)))

    # Creates new directories for the next NEMOH calculation
    if os.path.isdir("Results" + str(i)):
        os.mkdir("Results")
        os.mkdir("Mesh")


        shutil.move("Normalvelocities.dat",
                    "Results" + str(i) + "/Normalvelocities.dat")

        shutil.move("nemohMesh.dat",
                    "Results" + str(i) + "/nemohMesh.dat")

        shutil.move("Spar" + str(i+33) + ".dat",
                    "Results" + str(i) + "/Spar" + str(i) + ".dat")

        shutil.copyfile("Nemoh.cal", "Results"
                            + str(i) + "/Nemoh" + str(i) + ".cal")
```

Appendix A

A.3 Salome-Nemoh .dat convertion

```
# -*- coding: utf-8 -*-

# Function for converting Salome mesh .dat file to Nemoh mesh file
# INPUT:
# meshFileName = string with the name of the Salome filename including
# .dat extension
# symmetry = input argument for XZ-symmetry, 'yes' or 'no'

from Variables import freq
from CenterOF import *

f = freq



Hl =
Rl =
Hu =
Ru =



symmetryXZ = "no"
def salome2Nemoh(meshFilename, symmetry, cog):
    print('Åpnefil')
    # Reads the Salome mesh .dat file and saves all lines in a list as strings
    readFile = open(meshFilename, 'r')
    readFileList = readFile.readlines()
    readFile.close()
    print('Ferdig')

    # Creates and writes a nemohMesh.dat file ready to use in Nemoh
    writeFile = open('nemohMesh.dat', 'w')

    # Controls XZ symmetry, 'yes' or 'no' input argument in the function
    if symmetryXZ == 'yes':
        writeFile.write('2  1' + '\n')
    elif symmetryXZ == 'no':
        writeFile.write('2  0' + '\n')
    else:
        print('Symmetry Input Error')

    # Writes nodes part of the nemohMesh.dat file and counts the number of
    # nodes for entry in NNemoh.cal
    auxString = readFileList[0]
    auxList = auxString.split()
    nbNodes = int(auxList[0])

    for ii in range(1, nbNodes + 1):
        writeFile.write(readFileList[ii])

    writeFile.write('0 0.0 0.0 0.0' + '\n')

    auxString = readFileList[0]
    auxList = auxString.split()
    nbElements = int(auxList[1])

    # Writes panels part of nemohMesh.dat file and counts the number of panels
    nbPanels = 0
    for ii in range(nbNodes + 1, nbNodes + nbElements + 1):
```

```
    auxString = readFileList[ii]
    auxList = auxString.split()
    # Triangles
    if len(auxList) == 5:
        node1 = auxList[2]
        node2 = auxList[3]
        node3 = auxList[4]
        node4 = auxList[2]
        writeFile.write(node1 + ' ' + node2 + ' ' + node3 + ' '
                        + node4 + '\n')
        nbPanels = nbPanels + 1
    # Quadrangles
    if len(auxList) == 6:
        node1 = auxList[2]
        node2 = auxList[3]
        node3 = auxList[4]
        node4 = auxList[5]
        writeFile.write(node1 + ' ' + node2 + ' ' + node3 + ' '
                        + node4 + '\n')
        nbPanels = nbPanels + 1

writeFile.write('0 0 0 0')
writeFile.close()

# Writes and updates Nemoh.cal file for correct name of mesh
# file and number of nodes and panels
readFile = open('Nemoh.cal', 'r')
readFileList = readFile.readlines()
readFile.close()

writeFile = open('Nemoh.cal', 'w')

for item in readFileList:

    if 'Name of mesh file' in item:
        writeFile.write('nemohMesh.dat' + '  ! Name of mesh file' + '\n')
    elif 'RHO' in item:
        writeFile.write('1025.0' +
                        '! RHO ! KG/M**3 ! Fluid specific volume' + '\n')
    elif '! Number of points and number of panels' in item:
        writeFile.write(str(nbNodes) + ' ' + str(nbPanels) + '
                        ! Number of points and number of panels' + '\n')
    elif 'Roll about CdG' in item:
        writeFile.write('2 1. 0. 0. 0. 0.' + ' ' + cog + '
                        ' + '       ! Roll about CdG' + '\n')
    elif 'Pitch about CdG' in item:
        writeFile.write('2 0. 1. 0. 0. 0.' + ' ' + cog + '
                        ' + '       ! Pitch about CdG' + '\n')
    elif 'Yaw about CdG' in item:
        writeFile.write('2 0. 0. 1. 0. 0.' + '
                        ' + cog + ' ' + '       ! Yaw about CdG' + '\n')
    elif 'Moment force in x direction about CdG' in item:
        writeFile.write('2 1. 0. 0. 0. 0.' + ' ' + cog + ' ' +
                        '! Moment force in x direction about CdG' + '\n')
    elif 'Moment force in y direction about CdG' in item:
        writeFile.write('2 0. 1. 0. 0. 0.' + ' ' + cog + '
                        ' + !Moment force in y direction about CdG' + '\n')
    elif 'Moment force in z direction about CdG' in item:
        writeFile.write('2 0. 0. 1. 0. 0.' + ' ' + cog + ' ' +
```

```
                    '! Moment force in z direction about CdG' + '\n')
    elif 'Number of wave frequencies, Min, and Max (rad/s)' in item:
        writeFile.write(str(f) + '  0.05  1.2
                ! Number of wave frequencies, Min, and Max (rad/s)' + '\n')

    else:
        writeFile.write(item)



writeFile.close()

return
```

Appendix A

A.4 Read Nemoh into Python (Added Mass)

```
from DatFromSalome.Variables import freq

import numpy as np
def addedMass(i):
    with open("DatFromSalome/Results%d/RadiationCoefficients.tec" %i, "r") as fil:
        DOF = 0
        total = freq
        listMatrix = list()
        listFrequencies = list()
        arrayFrequencies = np.zeros(total)
        correction = 8

        for i in range(freq*2):
            matrix = np.zeros((6, 6))
            listMatrix.append(matrix)

        for linjeIndex, line in enumerate(fil):
            index = (linjeIndex - correction) % (freq+1)
            if linjeIndex < 8:
                continue
            if index == total:
                DOF += 1
                continue

            nAddedMass = 0
            nDamping = 0
            for i, element in enumerate(line.split()):
                if i == 0:
                    listFrequencies.append(element)
                    arrayFrequencies[index] = float(element)
                else:
                    if i % 2 == 1:
                        # Added mass
                        listMatrix[index][DOF][nAddedMass] = float(element)
                        nAddedMass += 1
                    else:
                        # Damping
                        listMatrix[index+total][DOF][nDamping] = float(element)
                        nDamping += 1

        listeAddedMass = list()
        listeDamped = list()

        listeAddedMass = listMatrix[:total]
        listeDamped = listMatrix[total:]


    return listeAddedMass
```